Cell Reports

Article

RAB3GAP2 is a regulator of skeletal muscle endothelial cell proliferation and associated with capillary-to-fiber ratio

Graphical abstract

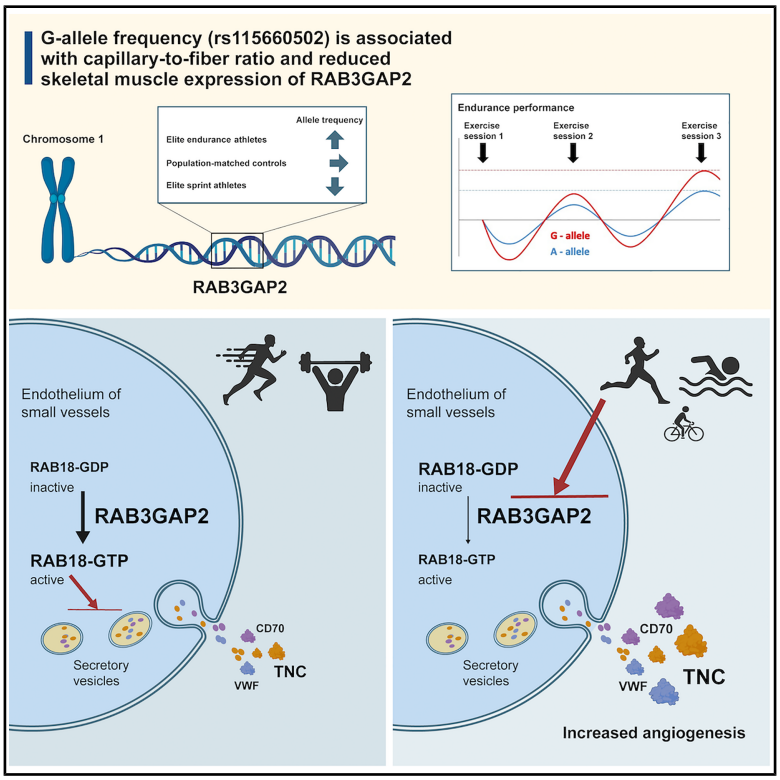

Highlights

- rs115660502 in *RAB3GAP2* associates with increased skeletal muscle capillarization
- RAB3GAP2 is predominantly expressed in endothelial cells and capillaries
- Reduced RAB3GAP2 enhances endothelial proliferation and angiogenic remodeling
- Low RAB3GAP2 expression promotes TNC release and exercise-like adaptations

Authors

Kristoffer Ström, Nikolay Oskolkov, Tugce Karaderi, ..., Cecilia M. Lindgren, Paul W. Franks, Ola Hansson

Correspondence

kristoffer.strom@med.lu.se

In brief

Ström et al. identify the rs115660502 variant in *RAB3GAP2* associated with increased skeletal muscle capillary-to-fiber ratio and enriched in endurance athletes. This variant reduces RAB3GAP2 expression, enhancing endothelial proliferation, tube formation, and TNC secretion, thereby promoting exercise-like angiogenesis and microvascular remodeling in skeletal muscle.

Ström et al., 2026, Cell Reports *45*, 116961
February 24, 2026
https://doi.org/10.1016/j.celrep.2026.116961

CellPress

Cell Reports

CellPress
OPEN ACCESS

Article

RAB3GAP2 is a regulator of skeletal muscle endothelial cell proliferation and associated with capillary-to-fiber ratio

Kristoffer Ström,[1,2,43,45,*] Nikolay Oskolkov,[1,43] Tugce Karaderi,[3,4,44] Sebastian Kalamajski,[5,44] Bilal A. Mir,[1] Ola Ekström,[1] Eri Miyamoto-Mikami,[6] Claes Ladenvall,[1,7] Ellen Kakulidis,[1] Steven Reid,[8] Anna-Maria Dutius Andersson,[9] Dmytro Kryvokhyzha,[9] Enming Zhang,[10] Joao Fadista,[1] Manonanthini Thangam,[1] Motoyuki Iemitsu,[11] Ekaterina A. Semenova,[12,13] Andrey K. Larin,[12] Rinat I. Sultanov,[12] Konstantin A. Babalyan,[12] Andrey V. Zhelankin,[12] Nikolay A. Kulemin,[12] Edward V. Generozov,[12] Michael Hultström,[14,15] Robert Frithiof,[14] Hugo Zeberg,[16]

(Author list continued on next page)

[1]Department of Clinical Sciences Malmö, Lund University Diabetes Center, Lund University, Malmö, Sweden
[2]Swedish Winter Sports Research Centre, Department of Health Sciences, Mid Sweden University, Östersund, Sweden
[3]The Wellcome Centre for Human Genetics, University of Oxford, Oxford, UK
[4]Center for Health Data Science, Faculty of Health and Medical Sciences, University of Copenhagen, Copenhagen, Denmark
[5]Department of Clinical Sciences, Genetic and Molecular Epidemiology Unit, Lund University Diabetes Center, Lund University, Helsingborg, Sweden
[6]Graduate School of Health and Sports Science, Juntendo University, Chiba, Japan
[7]Clinical Genomics Uppsala, Department of Immunology, Genetics and Pathology, Science for Life Laboratory, Uppsala University, Uppsala, Sweden
[8]Division of Translational Cancer Research, Department of Laboratory Medicine, Lund University Cancer Center, Lund University, Medicon Village, Lund, Sweden
[9]Department of Clinical Sciences, Diabetic Complications Unit, Lund University Diabetes Center, Lund University, Malmö, Sweden
[10]Department of Clinical Sciences, Diabetes Islet Pathophysiology Unit, Lund University Diabetes Center, Lund University, Malmö, Sweden
[11]Faculty of Sport and Health Science, Ritsumeikan University, Shiga, Japan

(Affiliations continued on next page)

SUMMARY

Skeletal muscle capillary density is correlated with physical performance and whole-body metabolic properties. Thus, we performed a genome-wide association study of skeletal muscle capillary-to-fiber ratio (C:F) (n = 603 males) and found that the rs115660502 G allele was associated ($p < 5 \times 10^{-8}$) with increased C:F and reduced skeletal muscle expression of RAB3 GTPase-activating non-catalytic protein subunit 2 (*RAB3GAP2*). The capillary-increasing G allele was more prevalent in elite endurance athletes than in power athletes and non-athlete controls in two independent cohorts. Low-muscle-expressing RAB3GAP2 expression quantitative trait locus (eQTL) alleles were associated with muscle damage in athletes. In healthy individuals, *RAB3GAP2* expression was reduced by high-intensity intermittent training. RAB3GAP2 protein was not uniformly expressed in muscle but predominantly expressed in the endothelium and capillaries. *RAB3GAP2* expression was lower in endurance compared with power athletes and was negatively associated with type I (oxidative) muscle fiber density. Experimental reduction of RAB3GAP2 in human endothelial cells led to (1) increased proliferation and tube formation *in vitro*, (2) regulation of secreted factors (e.g., CD70 and TNC) promoting angiogenesis and T cell activation, and (3) increased *in vivo* endothelial cell density in mice. *RAB3GAP2* expression in skeletal muscle was negatively correlated with exercise-induced release of TNC *in vivo* in humans. In conclusion, RAB3GAP2 is expressed in the microvascular endothelium and is suggested to be a negative regulator of angiogenesis through a decrease in endothelial cell proliferation, possibly mediated by RAB18, with its low-expressing variant associated with higher muscle C:F and elite endurance performance.

INTRODUCTION

One of the most pervasive threats to contemporary human health is the sedentary nature of our lifestyles. The WHO reports that one in four adults do not meet the global recommended levels of physical activity. Skeletal muscle adaptations to exercise include hypertrophy, improvements in substrate utilization, fiber-type switching (from type IIx to type IIa), and increased

Miklos Lipcsey,[14] Anders Larsson,[17] Anubha Mahajan,[3] Emma Ahlqvist,[1,29] Rashmi B. Prasad,[1,29] Kay Prüfer,[18] CHARGE Hemostasis Working Group, Maria Sabater-Lleal,[19,20,21] Nicholas L. Smith,[22,23,24] Abbas Dehghan,[25] Lars Lind,[17,26] Kerry McGawley,[2] Andrew P. Morris,[3,27] Johan P.A. Andersson,[28] Mikko Lehtovirta,[1,29] Łukasz Szczerbiński,[30] Adam Kretowski,[30] Ildus I. Ahmetov,[12,31,32,33] Guan Wang,[34,35] Yannis Pitsiladis,[36] Alejandro Santos-Lozano,[37,38] Alejandro Lucia,[38,39] Noriyuki Fuku,[6] Hans-Christer Holmberg,[40,41] Maria F. Gomez,[9] Karl-Fredrik Eriksson,[1] Kristian Pietras,[8] Cecilia M. Lindgren,[3] Paul W. Franks,[5,42] and Ola Hansson[1,29]

[12]Department of Molecular Biology and Genetics, Lopukhin Federal Research and Clinical Center of Physical-Chemical Medicine of Federal Medical Biological Agency, Moscow, Russia
[13]Research Institute of Physical Culture and Sport, Volga Region State University of Physical Culture, Sport and Tourism, Kazan, Russia
[14]Anaesthesiology and Intensive Care Medicine, Department of Surgical Sciences, Uppsala University, Uppsala, Sweden
[15]Integrative Physiology, Department of Medical Cell Biology, Uppsala University, Uppsala, Sweden
[16]Department of Physiology and Pharmacology, Karolinska Institute, Stockholm, Sweden
[17]Department of Medical Sciences, Uppsala University, Uppsala, Sweden
[18]Department of Archaeogenetics, Max Planck Institute for Evolutionary Anthropology, Leipzig, Germany
[19]Unit of Genomics of Complex Diseases, Institut de Recerca Sant Pau (IR SANT PAU), Barcelona, Spain
[20]Centre for Biomedical Network Research on Rare Diseases (CIBERER), Instituto de Salud Carlos III, Madrid, Spain
[21]Cardiovascular Medicine Unit, Department of Medicine Solna, Karolinska Institute, Stockholm, Sweden
[22]Department of Epidemiology, University of Washington, Seattle, WA, USA
[23]Department of Veterans Affairs, Seattle Epidemiologic Research and Information Center, Office of Research and Development, Seattle, WA, USA
[24]Kaiser Permanente Washington Health Research Institute, Kaiser Permanente Washington, Seattle, WA, USA
[25]Department of Epidemiology and Biostatistics, School of Public Health, Imperial College London, London, UK
[26]Department of Medical Sciences, Molecular Epidemiology and Science for Life Laboratory, Uppsala University, Uppsala, Sweden
[27]Centre for Genetics and Genomics Versus Arthritis, Centre for Musculoskeletal Research, The University of Manchester, Manchester, UK
[28]Department of Experimental Medical Science, Integrative Physiology Unit, Lund University, Lund, Sweden
[29]Institute for Molecular Medicine Finland (FIMM), Helsinki University, Helsinki, Finland
[30]Clinical Research Centre, Medical University of Bialystok, Białystok, Poland
[31]Research Institute for Sport and Exercise Sciences, Liverpool John Moores University, Liverpool, UK
[32]Laboratory of Molecular Genetics, Kazan State Medical University, Kazan, Russia
[33]Department of Physical Education, Plekhanov Russian University of Economics, Moscow, Russia
[34]School of Sport and Health Sciences, University of Brighton, Brighton, UK
[35]Centre for Regenerative Medicine and Devices, University of Brighton, Brighton, UK
[36]Centre for Stress and Age-Related Disease, University of Brighton, Brighton, UK
[37]i+HeALTH, Department of Health Sciences, European University Miguel de Cervantes, Valladolid, Spain
[38]Instituto de Investigación Hospital 12 de Octubre (imas12), Madrid, Spain
[39]Faculty of Sport Sciences, Universidad Europea de Madrid, Madrid, Spain
[40]Division of Machine Elements, Luleå University of Technology, Luleå, Sweden
[41]Department of Physiology and Pharmacology, Biomedicum C5, Karolinska Institute, Stockholm, Sweden
[42]Precision Healthcare University Research Institute, Queen Mary University of London, London, UK
[43]These authors contributed equally
[44]These authors contributed equally
[45]Lead contact
*Correspondence: kristoffer.strom@med.lu.se
https://doi.org/10.1016/j.celrep.2026.116961

capillary density, which leads to increased blood flow and perfusion. Skeletal muscle is highly vascularized, with capillaries comprising 2%–3% of total muscle mass. Capillary-to-fiber ratio (C:F) is correlated with fiber-type distribution but may also vary depending on the intensity and frequency of exercise. In sedentary men and women, on average, ~4 capillaries surround type I and IIa fibers and ~3 surround type IIx fibers.[1] In endurance-trained athletes C:F is higher (~5 or 6 surround type I and IIa fibers and ~4 surround type IIx fibers).[1] One less-recognized consequence of exercise is infiltration of skeletal muscle by immune cells and an acute inflammatory response within endothelial cells and macrophages that is evident in both metabolically healthy and diseased states.[2] Similar inflammatory responses are seen independent of exercise in people with insulin resistance, type 2 diabetes, and other cardiometabolic diseases.[3–5]

The heritability of C:F is not known, but related phenotypes, such as fiber-type distribution, are highly heritable.[6–8] A limited number of gene candidate studies linking genetic variation to angiogenesis-related phenotypes have been published, and a few studies have investigated how genetic variation influences exercise-induced angiogenesis in humans.[9–11] Examples are genetic variation in the angiotensin-converting enzyme[10,11] and tenascin C (TNC),[9] two genes that have been associated with C:F and capillary density.

However, genetics has proven powerful for the discovery of disease pathways and processes across many conditions. Such knowledge has been exploited in drug development, where information about genetic perturbations can help narrow the search for druggable targets.[12] Exercise is increasingly viewed as a therapeutic adjunct or alternative to drugs.[13] As with drug development, it is plausible that, by identifying genetic perturbations influencing pathways through which exercise impacts human health, discoveries might be made that broaden therapeutic options, either by facilitating the

Table 1. Variants showing association with capillary-to-fiber ratio

SNP	Reference allele	Non-reference allele	Chr	Genome position (build 37)	Effect estimate (β)	SE (β)	Nearest gene	Direction of effect (ULSAM and MM)	MAF	*N*	*p* value
rs115660502	G	A	1	220291773	0.77	0.14	IARS2	+ +	0.05	603	2.73×10^{-8}
rs191465330	A	G	1	220101936	1.92	0.35	SLC30A10	+ +	0.01	603	2.90×10^{-8}

"++" indicates direction of effect for the non-reference allele. SNP, single-nucleotide polymorphism; MAF, minor allele frequency; ULSAM, Uppsala Longitudinal Study of Adult Men; MM, Malmö Men study. nr/fiber

development of exercise mimetics or by individualizing exercise interventions.

The current study was designed to identify genetic variants associated with C:F in skeletal muscle and to use this information to elucidate the molecular mechanisms underlying the health-promoting effects of exercise.

RESULTS

The rs115660502 variant is associated with C:F, and its allele frequency differs between elite athletes and the general population

Skeletal muscle phenotypes, such as fiber-type distribution, are highly heritable[6–8] and, together with environmental factors, influence energy metabolism and performance capacity.[14–16] However, the specific genetic loci underpinning muscle phenotypes are largely undefined.

We began by undertaking a genome-wide association study (GWAS) for C:F in two independent cohorts, the Uppsala Longitudinal Study of Adult Men (ULSAM, n = 482, Table S1)[17] and the Malmö Men study (MM, n = 128, Table S2),[18] in which a correlation between C:F and fiber-type distribution was shown (Tables S3 and S4). We identified one genome-wide significant locus (0.77 [0.14] β [SE], $p = 2.73 \times 10^{-8}$). The signal for C:F was mapped to two variants (rs115660502 and rs191465330) within the same chromosome 1 (chr1) haplotype and probably reflects one signal captured by the rs115660502 variant after assessment by conditional analyses (Table 1; Figures 1A–1D and S1).

The minor (major) G (A) allele at rs115660502 (associated with increased C:F) is prevalent at 3%–5% in European-ancestry populations but lower or absent in African- and Asian-ancestry populations (Figure S2), indicating that the mutation occurred relatively recently (50,000–100,000 years ago). The capillary-increasing G allele at rs115660502 had a frequency of 4.8% and 3.3% in Swedish and Spanish non-athlete population controls, respectively, but was at 10% and 6.3% in Swedish cross-country skiers and Spanish triathletes, respectively. By contrast, the G allele had a 1.1% frequency in non-athlete Jamaican population controls, which was significantly higher than the 0.4% frequency in Jamaican sprinters (p = 0.03). Athletes of non-extreme or mixed sports had a similar G-allele frequency compared with their corresponding population controls (see STAR Methods). The combined ratios of the frequencies of the capillary-increasing G allele between athletes and population-matched controls are shown in Figure 1E. We defined athletes competing in cross-country skiing and triathlon as extreme endurance athletes (i.e., disciplines with >1.5 h of total uninterrupted physically demanding performance time) and athletes competing in sprint running as extreme power athletes (i.e., disciplines with <60 s of total performance time). Other disciplines were defined as not being extreme in their physical profile, e.g., skating, basketball, and judo. This difference in frequency was replicated in an independent cohort (Figure 1F; Table 2), with the G allele having a frequency of ∼9% and ∼0.7% in elite endurance ($p_{Fisher} < 0.05$) and power sport ($p_{Fisher} < 0.001$) athletes, respectively, compared with ∼3% in ethnicity-matched general population controls.

The rs115660502 variant is associated with RAB3GAP2 gene expression and the protein is localized to the endothelium and capillaries

Having identified non-coding variants associated with C:F, we examined whether genetic variation at or near the rs115660502 variant is associated with the expression of proximal genes (±1 Mb window). The only significant expression quantitative trait locus (eQTL) found in the meta-analysis was RAB3 GTPase-activating protein subunit 2 (RAB3GAP2) (Table S5; Figure S3). rs115660502 is proximal to the transcriptional start site of *RAB3GAP2* (∼20 kb upstream) and in two ENCODE cell lines (Huh7 and Medullo)[19] within a DNase-hypersensitive region. Several transcription factors implicated in angiogenesis (e.g., STAT3, FOSL1, SIRT6, TAL1, and GATA2) bind in close proximity (500–1,000 bp) to rs115660502 according to the ENCODE database.[19] We found that the G allele of the rs115660502 variant was associated with a modest ∼6% and ∼4% lower *RAB3GAP2* expression in human skeletal muscle in the MM ($p_{Mann\text{-}Whitney}$ = 0.006, n = 33 vs. 5) and Malmö Exercise Intervention (MEI) ($p_{Mann\text{-}Whitney}$ = 0.002, n = 36 vs. 3) cohorts, respectively, and a non-significant ∼23% lower expression in the Malmö Satellite Cell (MSAT) ($p_{Mann\text{-}Whitney} > 0.05$, n = 34 vs. 5) cohort (Figure 2A; Table S3). The G allele was associated with lower *RAB3GAP2* expression also when including publicly available datasets, i.e., GTEx (GTEx Portal, accessed June 19, 2024) and Fusion,[20] in a meta-analysis (−0.55 [−0.10 – 0.00] β [95% CI], $p < 0.05$, n_{tot} = 1,123; Figure S3). Both expression and C:F were available only in the MM cohort, and the *RAB3GAP2* mRNA expression was inversely correlated with C:F (ρ = −0.38, p = 0.03, n = 32) (Figure 2B). High-intensity intermittent training (HIIT; four times per week for 6 week) was associated with lower *RAB3GAP2* mRNA expression in human skeletal muscle by approximately −10%[21] ($p_{Wilcoxon}$ = 0.002, n = 11) (Figure 2C). The changes in VO_{2max} (ΔVO_{2max}) and the changes in muscle *RAB3GAP2* expression, comparing before vs. after the 6-week training period, were correlated (ρ = −0.66, $p_{Spearman}$ = 0.034, n = 11). Furthermore, when participants were divided into high responders (median or higher ΔVO_{2max})

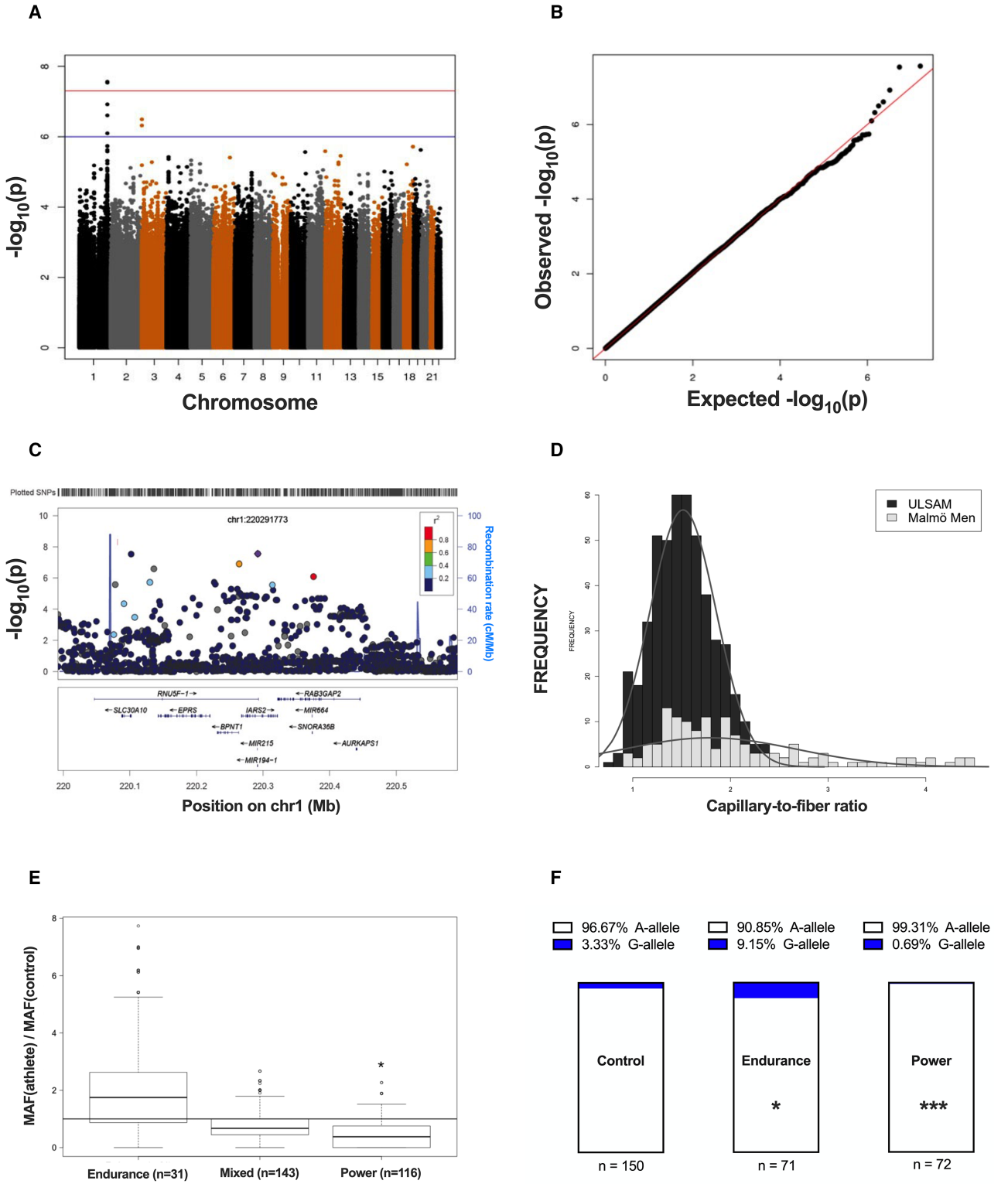

Figure 1. Genetic analysis of variants associated with capillary-to-fiber ratio identifying rs1156660502 as a candidate

(A and B) (A) Manhattan plot showing the (−log10) *p* values by genomic position for capillary-to-fiber ratio and (B) QQ plot of associations with capillary-to-fiber ratio from the meta-analysis of the Malmö Men study and the Uppsala Longitudinal Study of Adult Men (ULSAM) (n_{tot} = 603). The blue and red lines in (A) indicate the thresholds for suggestive ($p < 1 \times 10^{-6}$) and genome-wide ($p < 5 \times 10^{-8}$) significance, respectively.

(legend continued on next page)

Table 2. Replication of the association between rs115660502 and elite athlete status in an independent cohort

		RAB3GAP2 genotype							
Group	*n*	AA	AG	GG	G allele (%)	Odds ratio	*p* value (Fisher's)	*p* value (χ^2)	Comment
Endurance athletes	71	59	11	1	9.1	–	–	–	–
Power athletes	72	71	1	0	0.7	14.4	0.0007	0.0024	endurance vs. power
Non-athlete population-matched controls	150	141	8	1	3.3	2.9	0.0194	0.0191	endurance vs. controls

and low responders (below median ΔVO_{2max}), the reduction in *RAB3GAP2* expression was more pronounced (~14% vs. ~3%) in the high responders ($p_{Mann\text{-}Whitney}$ = 0.0043, n = 5–6), i.e., high responders to HIIT in terms of VO_{2max} increase had more reduced expression of *RAB3GAP2*, while low responders had less changed expression of *RAB3GAP2*. The reduction in *RAB3GAP2* expression after HIIT was replicated in a meta-analysis of eight datasets with acute (15 min–2 h) HIIT (approximately −7%, $p_{meta} = 2.9 \times 10^{-3}$, n = 54) and in three datasets with prolonged (3–12 weeks) HIIT (approximately −6%, $p_{meta} = 1.5 \times 10^{-3}$, n = 34) in MetaMEx.[22] Furthermore, endurance athletes had ~22% lower skeletal muscle *RAB3GAP2* expression compared with power sport athletes ($p_{Mann\text{-}Whitney} = 5.0 \times 10^{-4}$, n = 12 and 7) (see STAR Methods, section "Experimental model and study participant details," subsections "Athlete cohorts" and "Replication cohort."

The RAB3GAP2 protein is widely expressed in human tissues, including skeletal muscle (Figure S4). *RAB3GAP2* expression was negatively associated with the proportion of type I (oxidative) muscle fibers in both *m. vastus lateralis* (p = 0.0001, r = −0.19, n = 291) and *m. gastrocnemius* (p < 0.0001, r = −0.28, n = 791), based on data extracted from the FUSION and GTEx muscle biopsy studies (see STAR Methods, section "muscle biopsy studies"). Using a publicly available single-nucleus RNA sequencing (RNA-seq) dataset from skeletal muscle biopsies,[23] *RAB3GAP2* was found to be predominantly expressed in vascular endothelial cells, with both higher expression levels and higher fraction of positive cells than those measured in skeletal muscle myocytes or satellite cells (Figure 2D). Immunohistochemistry in sections of human skeletal muscle tissue identified RAB3GAP2 protein expression primarily in skeletal muscle capillaries and very low expression in muscle fibers (Figures 2E–2G). Confocal immunofluorescence images confirmed the presence of RAB3GAP2 protein in CD31-positive endothelial cells (Figures 2H–2K). RAB3GAP2 was clearly detected in 46% of cultured human microvascular endothelial cells (HMECs), but it was not detected in cultured human endothelial cells from macrovascular origin (HUVECs) or in the wall of larger vessels in sections from skeletal muscle biopsies (Figure S5).

Reduced expression of RAB3GAP2 in human endothelial cells replicates the GWAS association with C:F, whereby knockdown of RAB3GAP2 leads to a gain of function with increased cell growth rate and tube formation *in vitro* and increased cell density *in vivo* in mice

To test whether *RAB3GAP2* expression is causally related to capillary formation, *RAB3GAP2* was knocked down in HMECs using CRISPR-Cas9 (mRNA by ~70%–80%, with corresponding protein reduction) (Figure S6). The level of knockdown was stable and sustained over 12 passages (Figure S6A). We then undertook an *in vitro* tube-formation assay using HMECs, where *RAB3GAP2* knockdown led to a 2.8-fold increase in number of loops (i.e., ring structures) at 6 h of differentiation and a 2.9-fold increase at 24 h ($p_{Mann\text{-}Whitney} = 8.0 \times 10^{-7}$ and $p_{Mann\text{-}Whitney} = 7.1 \times 10^{-5}$, respectively, n = 11 and 13). The number of branching points increased by ~30% in *RAB3GAP2*-knockdown cells compared with wild type at 6 h of differentiation ($p_{Mann\text{-}Whitney} = 8.8 \times 10^{-6}$, n = 11) and increased by ~32% at 24 h ($p_{Mann\text{-}Whitney} = 7.6 \times 10^{-4}$, n = 13). The total tube length formed was ~22% longer in *RAB3GAP2*-knockdown cells compared with wild type at 6 h of differentiation ($p_{Mann\text{-}Whitney} = 8.0 \times 10^{-7}$, n = 11) and ~27% longer at 24 h ($p_{Mann\text{-}Whitney} = 2.4 \times 10^{-5}$, n = 13). Quantification and example images of tube formation in HMECs from the different conditions are shown in Figures 3A–3D. More variables, i.e., median loop area, median loop perimeter, total loop area, median tube length, and total tubes, are shown in Figures S7A–S7E. In 34 independent experiments, *RAB3GAP2* knockdown led to a median 19% increased growth rate per day ($p_{Wilcoxon} = 6.0 \times 10^{-4}$, n = 34; Figure 3E), a result

(C) Enlarged view of genetic locus (LocusZoom) plot of the region on chromosome 1 harboring genetic variants associated with capillary-to-fiber ratio. The purple circle represents the genetic variant (rs115660502) with the lowest p value (left y axis) in the region. Other variants (circles) are colored according to their linkage disequilibrium with this variant, i.e., from highest (red) to lowest (dark blue). Estimated recombination rates are shown on the right y axis.
(D) Distribution of capillary-to-fiber ratio in the Malmö Men and ULSAM cohorts.
(E) Ratio of the frequencies of the capillary-increasing G allele in elite athletes compared with population-matched controls. The ratios were calculated in randomly drawn samples of individuals from the population-matched controls with n equal to the corresponding athlete cohort (significance tested with 10^5 bootstraps). Disciplines with >1.5 h of total uninterrupted physically demanding performance time were defined as endurance and disciplines with <60 s of total performance time as power. Other disciplines were defined as not being extreme in their physical profile and defined as mixed. $n_{endurance}$ = 31, n_{mixed} = 143, and n_{power} = 116. Data are represented as boxplots showing the median (center line), interquartile range (box), and minimum to maximum values (whiskers).
(F) Replication of the athletes vs. population-matched controls. $n_{control}$ = 150, $n_{endurance}$ = 71, and n_{power} = 72.
Significance was tested using Fisher's exact test. *p < 0.05 and ***p < 0.001.
See also Figures S1–S3.

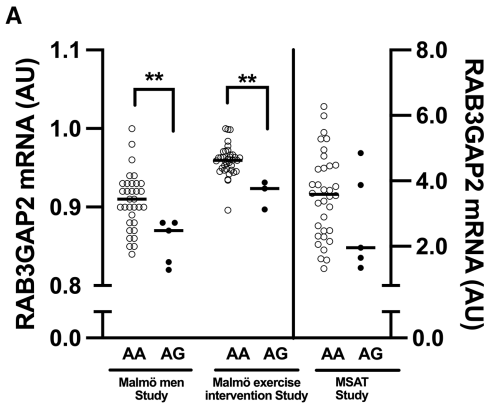

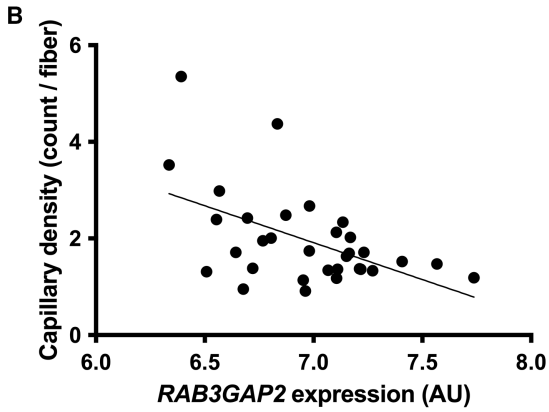

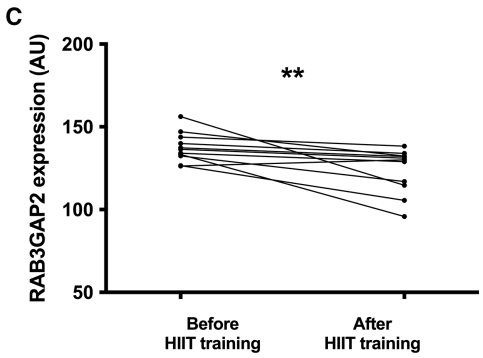

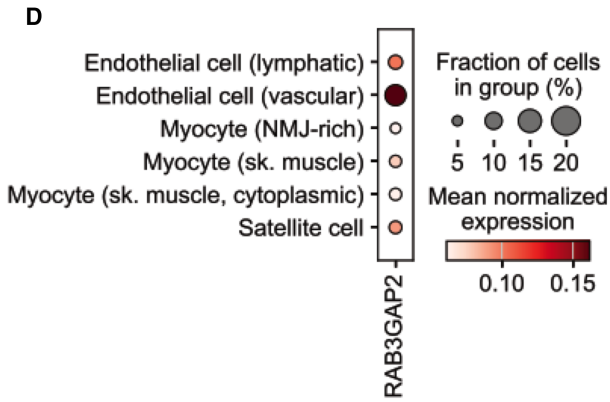

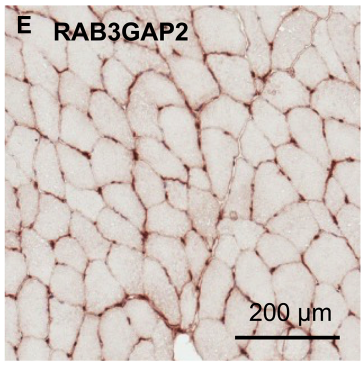

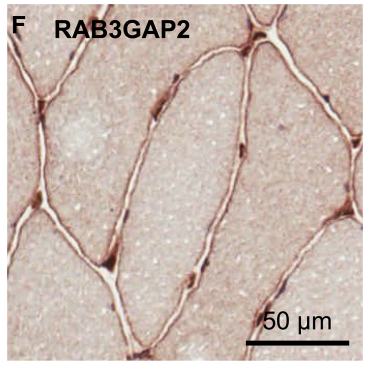

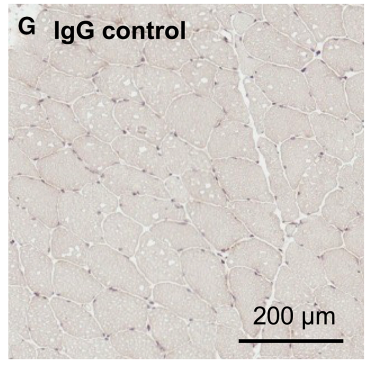

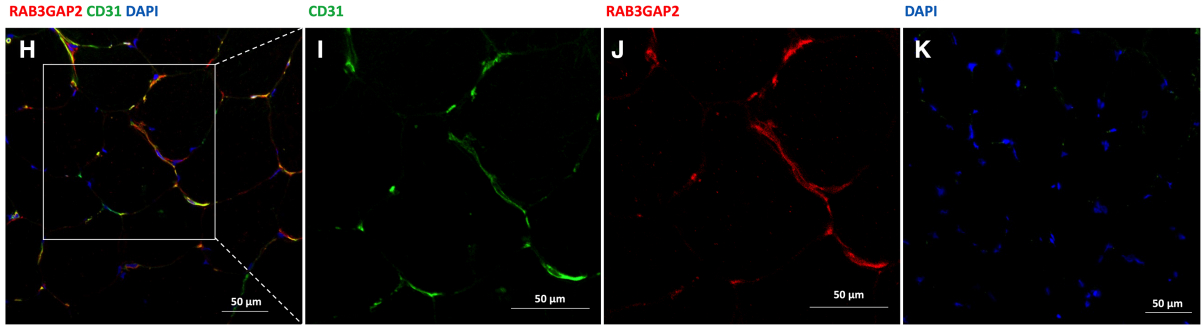

(legend on next page)

that was strengthened by a time course of live-cell imaging of HMEC growth in three additional experiments (Figures 3F and S8A–S8C). To characterize migratory activity, we did the basic cell culture wound healing assay in HMECs. However, we did not observe any major difference between *RAB3GAP2*-knockdown and wild-type cells (Figure S9).

To screen for candidates mediating the downstream effects of reduced RAB3GAP2 activity, expression levels of *RAB3A-D* and *RAB18* were investigated in HMEC RNA-seq data. The expression levels of *RAB3A* and *RAB3D* were low (∼0.5 and ∼12.5 cpm, respectively), and *RAB3C* expression was not detected. However, *RAB3B* had an expression level of ∼120 cpm and *RAB18* of ∼72 cpm. Furthermore, *RAB3B* had slightly reduced expression in *RAB3GAP2*-knockdown HMECs compared with wild-type cells (∼11%, p_{adj} = 0.047, n = 8). The other genes showed no tendency for differential expression. Subsequently, RAB3B and RAB18 were further investigated in HMECs using small interfering RNAs (siRNAs) targeting these two genes. Using siRNA, a knockdown of *RAB3B* or *RAB18* of 85%–90% was obtained. Next, the cell growth rate was investigated in wild-type and *RAB3GAP2*-knockdown cells. When *RAB3B* was knocked down, the same increased growth rate (∼20%) between *RAB3GAP2*-knockdown and wild-type cells was observed. Thus, RAB3B is not likely mediating the described effect of an increased proliferation with reduced *RAB3GAP2* expression. In contrast, knockdown of *RAB18* attenuated the increased growth rate observed with *RAB3GAP2* knockdown, i.e., no difference in proliferation between *RAB3GAP2*-knockdown and wild-type cells when *RAB18* was simultaneously knocked down (Figure 3G). *RAB18* knockdown in cells with wild-type levels of RAB3GAP2 showed an ∼15% increased growth rate. RAB18 could thus be a candidate mediator of the described effects on proliferation stimulated by RAB3GAP2 guanine nucleotide exchange factor (GEF) activity.

In an *in vivo* angiogenesis plug assay, Matrigel containing HMECs with or without *RAB3GAP2* knockdown was injected into the groin region of NGS mice. The resulting gel plugs were harvested after 7 day, sectioned, and stained using Masson's trichrome. The total HMEC area was ∼50% larger in *RAB3GAP2*-knockdown cells compared with wild type ($p_{Mann\text{-}Whitney}$ = 0.036, n = 3–5). Quantification and example images of cell density of HMECs are shown in Figures 3H and 3I.

RAB3GAP2 regulates the secretion of proteins in an angiogenesis-promoting direction, i.e., TNC, IGFBP3, tPA, CCL2, TNX, COL1A1, TFPI2, and CD70

RAB3GAP2 is known to regulate vesicle trafficking.[24] To identify secreted proteins regulated by RAB3GAP2 and possibly driving the effects described above, we performed an RNA-seq screen in HMECs with or without CRISPR-Cas9-mediated knockdown of *RAB3GAP2* expression (n = 8). We identified 496 and 993 genes with lower and higher expression, respectively, in *RAB3GAP2*-knockdown cells at a false discovery rate (FDR) of 5% (Table S6). In addition, 154 secreted proteins were screened in the medium of HMECs using four Olink panels with or without knockdown of *RAB3GAP2* (n = 6, Table S7). Combining these results, *RAB3GAP2* knockdown influenced the secretion of eight factors regulated in the same direction on both the RNA and the protein levels (Figures 4A–4D and S10A–S10E). Five of these factors are known to stimulate angiogenesis, i.e., T cell activating protein cluster of differentiation 70 (CD70), TNC, insulin-like growth factor binding protein 3 (IGFBP3), plasminogen activator tissue type or tPA (PLAT), and C-C motif chemokine ligand 2/MCP-1 (CCL2), and all had higher concentrations in *RAB3GAP2*-knockdown cells. For example, CD70 had an ∼3-fold higher RNA expression in *RAB3GAP2*-knockdown cells ($p_{FDR5\%} = 1.4 \times 10^{-40}$, n = 8; Figure S10E) and ∼2.5-fold higher protein concentration in the medium from *RAB3GAP2*-knockdown cells compared with wild type ($p_{Wilcoxon}$ = 0.03, n = 6; Figure 4A). Three (tenascin X [TNX]; collagen, type I, alpha 1 [COL1A1]; and tissue factor pathway inhibitor 2 [TFPI2]) of the eight factors are known to inhibit angiogenesis, and all had lower concentrations in medium from *RAB3GAP2*-knockdown cells.

RAB3GAP2 influences exercise-induced secretion of TNC *in vivo*, and carriers of low-RAB3GAP2-expressing alleles are more susceptible to muscle injury

Of the eight proteins identified, all with pro-angiogenic regulation by RAB3GAP2, TNC has the most-well-documented role in exercise-induced angiogenesis.[9,25–29] TNC levels are increased by exercise[25–28] and correlate with post-exercise strength loss.[28] Moreover, genetic variation at *TNC* is associated with exercise-induced angiogenesis.[9] To test whether *RAB3GAP2* expression correlates with exercise-induced TNC secretion

Figure 2. Functional follow-up of rs115660502 identifying RAB3GAP2 as the effector gene

(A) Expression of *RAB3GAP2* mRNA across rs115660502 genotypes in the Malmö Men (MM) study (n = 33 vs. 5), Malmö Exercise Intervention (MEI) study (n = 36 vs. 3), and Malmö Satellite Cell (MSAT) study (n = 34 vs. 5); $p_{Mann\text{-}Whitney}$ = 0.006, 0.002, and >0.05, respectively. Horizontal lines show median values.

(B) Plot of *RAB3GAP2* mRNA expression vs. capillary-to-fiber ratio in the MM study. r = 0.38, $p_{Spearman}$ = 0.03, n = 32.

(C) Expression of *RAB3GAP2* mRNA in skeletal muscle after 6 week of high-intensity intermittent training (HIIT).[21] $p_{Wilcoxon}$ = 0.002, n = 11.

(D) GTEx single-nucleus RNA sequencing data showing predominant expression of *RAB3GAP2* in vascular endothelial cells (both higher expression and higher fraction of positive cells).

(E and F) (E) Lower and (F) higher magnifications of RAB3GAP2 expression in human skeletal muscle as detected using immunohistochemistry (brown) (scale bars, 200 and 50 μm, respectively).

(G) Negative control using non-immune rabbit IgG. Sections were counterstained with Mayers hematoxylin and experiments were performed three times (scale bar, 200 μm).

(H–K) (H) Confocal immunofluorescence image showing colocalization of RAB3GAP2 to CD31-positive endothelial cells; nuclei are stained with DAPI. (I and J) Zoom-in of the inset in (H) with CD31 (green) and RAB3GAP2 (red) staining, respectively. (K) IgG control counterstained with DAPI. Experiments were performed twice. Scale bars for (H–K), 50 μm.

Skeletal muscle sections were from biopsies from n = 11.

See also Figure S5 and Table S5.

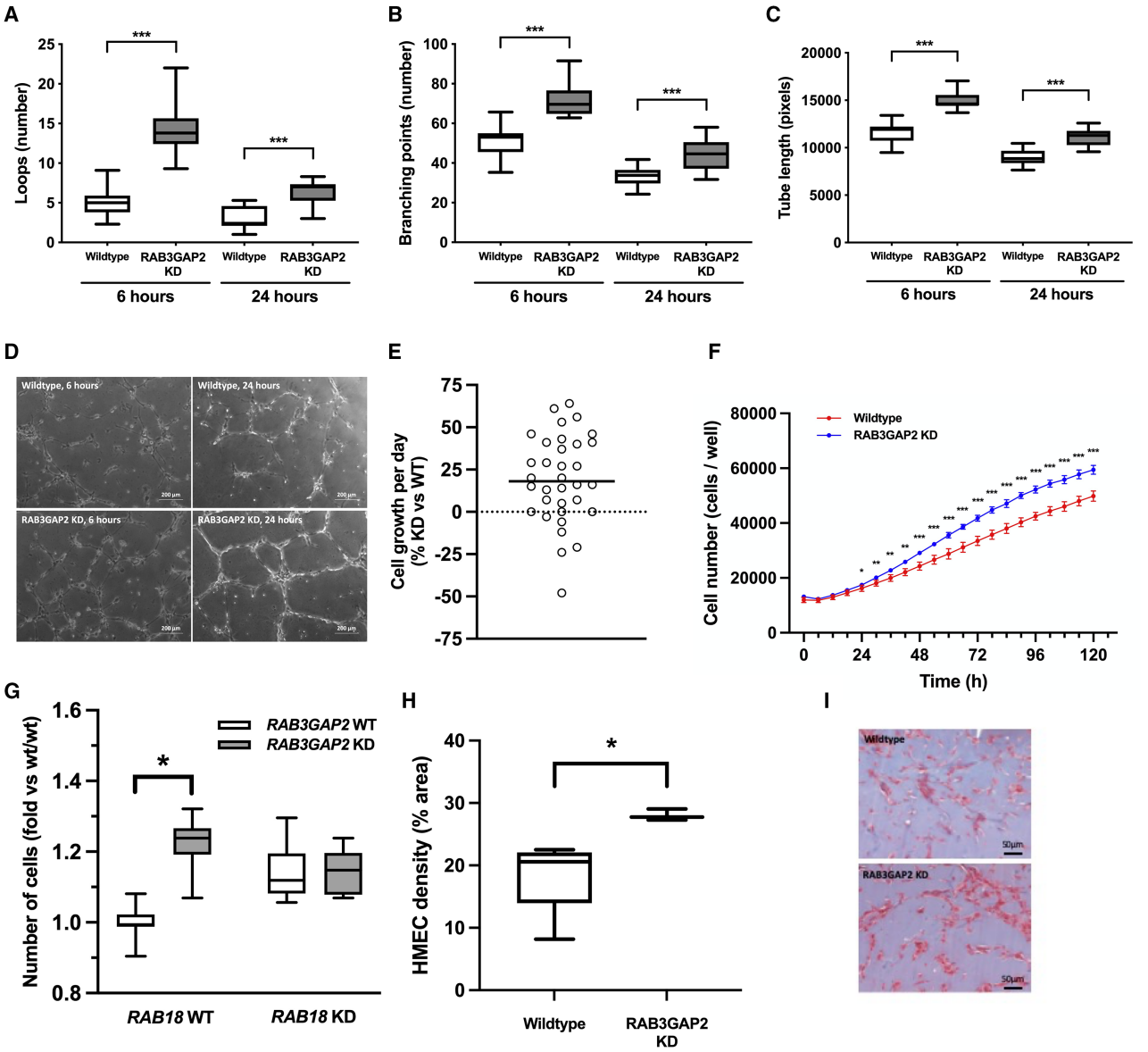

Figure 3. Mechanistic studies investigating the functional consequences of reduced *RAB3GAP2* expression

(A–D) Tube-formation assay using HMECs with or without CRISPR-Cas9-mediated knockdown (KD) of *RAB3GAP2*. $n = 11$ (wild-type) and 13 (*RAB3GAP2* KD) independent experiments at 6 and 24 h. (A) Number of loops, $p_{\text{Mann-Whitney, 6 h}} = 8.0 \times 10^{-7}$ and $p_{\text{Mann-Whitney, 24 h}} = 7.1 \times 10^{-5}$. (B) Number of branching points, $p_{\text{Mann-Whitney, 6 h}} = 8.8 \times 10^{-6}$ and $p_{\text{Mann-Whitney, 24 h}} = 7.6 \times 10^{-4}$. (C) Total tube length, $p_{\text{Mann-Whitney, 6 h}} = 8.0 \times 10^{-7}$ and $p_{\text{Mann-Whitney, 24 h}} = 2.4 \times 10^{-5}$. (D) Representative images of tube formation in HMECs (scale bar, 200 µm).

(E) Growth rate per day expressed as percentage number of *RAB3GAP2*-KD HMECs over wild-type cells, $p_{\text{Wilcoxon}} = 6.0 \times 10^{-4}$, $n = 34$ independent experiments.

(F) Time course of live-cell imaging of HMEC growth, $n_{\text{wt}} = 6$ and $n_{\text{KD}} = 3$ technical replicates in one experiment. Within-experiment significance was tested using multiple Mann-Whitney *U* tests.

(G) Growth rate expressed as fold number of cells vs. control wild-type cells with and without KD of *RAB3GAP2* and *RAB18* in combination ($p_{\text{Mann-Whitney}} = 0.03$).

(H) *In vivo* angiogenesis plug assay in NGS mice using HMECs with or without *RAB3GAP2* KD. Percentage of Masson's trichrome staining of total Matrigel area ($p_{\text{Mann-Whitney}} = 0.036$, $n = 3$–5).

(I) Representative images of Masson's trichrome staining. Scale bars, 50 µm.

*$p < 0.05$, ** <0.01, and ***$p < 0.001$. Data are represented as boxplots showing the median (center line), interquartile range (box), and minimum to maximum values (whiskers).

See also Figures S7 and S8.

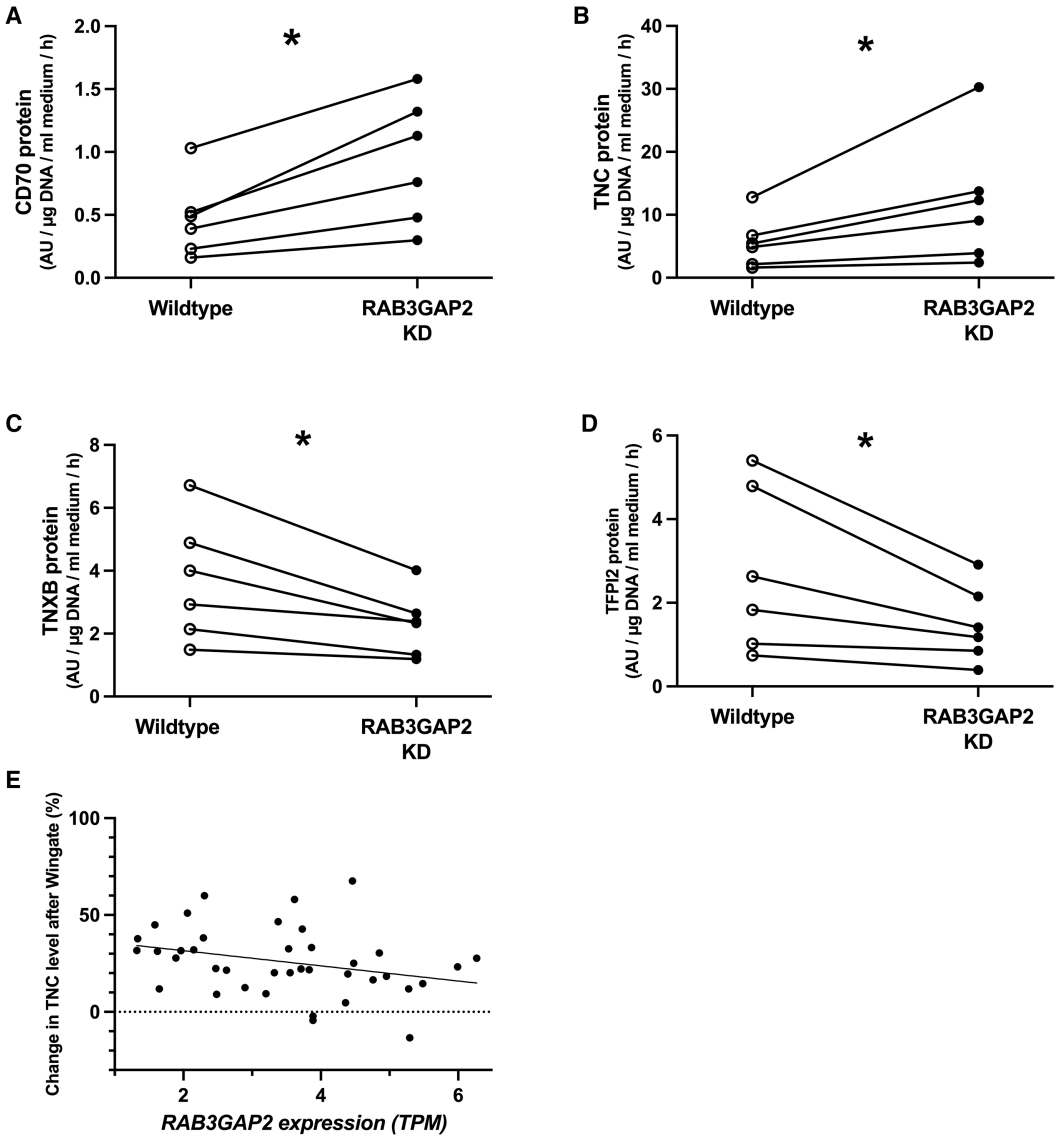

Figure 4. Description of the RAB3GAP2 downstream mechanism regulating angiogenesis identifying tenascin C as one of several effector molecules

The amount of protein in the cell medium after culturing of HMECs using Olink panels with (filled circles) or without (open circles) CRISPR-Cas9-mediated knockdown of *RAB3GAP2*. (A) CD70, (B) TNC, (C) TNXB, and (D) TFPI2 (*$p_{Wilcoxon} < 0.05$, $n = 6$). (E) Correlation between skeletal muscle *RAB3GAP2* mRNA expression and percentage change in circulating TNC concentration before vs. after a 30 s Wingate test. $\rho = -0.37$, $p_{Spearman} < 0.05$, $n = 39$. CD70, cluster of differentiation 70; TNC, tenascin C; TNXB, tenascin X; and TFPI2, tissue factor pathway inhibitor 2.

See also Figures S10 and S11 and Tables S6 and S7.

in vivo, we performed 30 s Wingate tests in healthy male adults (Table S8) and examined basal expression of *RAB3GAP2* in *vastus lateralis* muscle and circulating TNC before and after the exercise. With exercise, circulating TNC increased in 36 of 39 individuals with an average median increase of ~23% ($p_{Wilcoxon} = 1.6 \times 10^{-10}$, $n = 39$).[29] The change in circulating TNC levels with exercise was negatively correlated with skeletal muscle *RAB3GAP2* mRNA levels, with a $\rho = -0.37$, $p_{Spearman} < 0.05$, $n = 39$ (Figure 4E). Furthermore, siRNA-mediated *RAB18* knockdown in HMEC wild-type cells led to 77% increase in TNC secretion compared with control wild-type cells (Figure S11).

TNC is a tissue-remodeling protein associated with both the risk and the recovery of muscle injuries.[30–34] Having established that lower *RAB3GAP2* expression is correlated with an increased release of TNC after exercise, we aimed to explore whether the G allele is also associated with muscle damage. We investigated a cohort of Japanese male athletes[35] with information of non-contact-induced muscle injuries (Table S10). As rs115660502 is not present in the Japanese population and the experimental results show that *RAB3GAP2* likely is the causal gene, we identified an alternative muscle eQTL for *RAB3GAP2* present in the Japanese population using GTEx (rs11547779).

Athletes with muscle injuries had a higher frequency (11%) of the *RAB3GAP2* low-expressing T allele at rs11547779 compared with non-injured controls (6%) and an approximately doubled risk of injury (OR [95% CI] of 1.9 [1.16–3.11], $p_{\text{Cochran-Armitage}} = 9.0 \times 10^{-3}$, $n = 140$ vs. 389, Table S11).

DISCUSSION

Determining the mechanisms linking exercise to beneficial health adaptations may help optimize exercise interventions. Here, we undertook an integrated series of studies to discover, validate, and mechanistically elucidate novel molecular features of skeletal-muscle-related exercise responses.

We began by undertaking a GWAS of the exercise-related C:F phenotype and leveraged this finding to discover novel mechanisms linking exercise to cellular responses. Specifically, we show that a *RAB3GAP2* variant (rs115660502) is associated with C:F ratio and that the frequency of the effect allele (G) varies between elite athletes and population controls. Genetic variation capturing a *RAB3GAP2* low-expressing haplotype is associated with muscle injuries. We determined that *RAB3GAP2* is predominantly expressed in vascular endothelial cells in skeletal muscle and that the G allele is associated with lower *RAB3GAP2* muscle expression and HIIT decreases *RAB3GAP2* muscle expression, which, through either condition, may regulate the secretion of T cell-regulating and angiogenesis-promoting proteins, resulting in an enhanced capillary formation. We demonstrated that *RAB3GAP2* expression is lower in endurance compared with power athletes and is negatively associated with the proportion of type I (oxidative) muscle fibers in both *m. vastus lateralis* and *m. gastrocnemius*. We showed that, by reducing *RAB3GAP2* expression, angiogenesis increases primarily via increased proliferation, both *in vitro* and *in vivo*, possibly via a mechanism including inhibition of RAB18. Finally, we determined that the level of *RAB3GAP2* in muscle is inversely correlated with the exercise-induced secretion of TNC *in vivo*. Taken together, these results show that RAB3GAP2 may play a key role in muscle adaptation to exercise, both acutely by regulating immune and inflammatory pathways and chronically by mediating tissue remodeling and capillary formation (e.g., TNC and CD70 release).

Skeletal muscle is highly vascularized, and muscle capillary density, defined as capillaries per mm^2 (CD), is reported to be highly correlated with whole-body insulin sensitivity.[36] Consistent with the importance of angiogenesis in insulin action and exercise performance, it was recently demonstrated that low expression in muscle of endothelial nitric oxide synthase (eNOS) is a key factor in the early development of insulin resistance.[37]

RAB3GAP2 encodes a regulatory subunit that, together with *RAB3GAP1* (encoding the catalytic subunit), forms the GTPase-activating complex with specificity for the RAB3 Rab-GTPase-activating proteins (RAB3A–D).[24,38] The RAB3 protein family is known to control exocytosis of neurotransmitters and hormones,[24] and mutations in *RAB3GAP2* cause Martsolf syndrome and Warburg micro syndrome 2, diseases characterized by delayed neurodevelopment and cognitive impairments.[39] RAB3A and RAB3B have been suggested as key regulators of vesicle trafficking events, necessary for endothelial cells to form lumens and assemble into capillary networks.[40] Further, it has been demonstrated that RAB3GAP1/2 functions as a GEF for RAB18, a protein that regulates membrane trafficking and lipid droplet metabolism, and that activating RAB18 might be the primary function of RAB3GAP1/2 in most cell types.[41] Importantly, RAB18 is suggested to act as a negative regulator of secretory activity in neuroendocrine cells, likely by impairing secretory granule transport.[42] We show here that by decreasing the levels of RAB18 in endothelial cells, we can mimic the positive effects on cell growth and increased secretion of TNC seen with RAB3GAP2 knockdown. This suggests that the angiogenesis-promoting effect of reducing RAB3GAP2, at least partly, works through inactivation of RAB18. To our knowledge, no previous studies have linked *RAB3GAP2* to exercise-response phenotypes.

The chronic beneficial effects of regular exercise are widespread and well defined.[43] These include improvements in substrate metabolism, vascular health, hormonal homeostasis, longevity, and mood. Both TNC and CD70 are important immune-regulating proteins and play roles in viral response and inflammation.[44,45] As with other inflammatory cytokines, it is possible that exercise improves tolerance to the effects of both TNC and CD70. Our findings suggest that people carrying the rs115660502 G allele may experience more endothelial stress and inflammation. Whether this is associated with longer-term health outcomes cannot be answered through the current study. However, a look-up of the rs115660502 variant (https://hugeamp.org/variant.html?variant=rs115660502, accessed February 21, 2023) indicates that the G allele may convey lower mean platelet volume and monocyte count, but no compelling evidence of association with relevant clinical outcomes such as cardiovascular disease or stroke.

The replicated higher frequency of the effect allele (G) at rs115660502 in endurance athletes supports our initial finding of an association with C:F, as these athletes have a higher proportion of the more-capillary-dense type I fibers. The replicated and to some extent more pronounced lower frequency in power athletes is less evident but may have several explanations. Similar to endurance athletes, power athletes have an extreme fiber type distribution with a higher proportion of the less-capillary-dense type II fibers. High type II fiber proportion has been suggested to be associated with increased risk of muscle injury[46,47] and longer recovery time after exercise.[48] We have not observed a direct association between the rs115660502 variant and fiber type proportions ($p > 0.05$, $n = 663$, data not shown), but higher circulating TNC levels have been reported with increased risk of injury in soccer players.[32] It is possible that RAB3GAP2 low-expressing haplotypes, which stimulate capillary formation, also increase the risk of muscle injuries and that the combination of more injury-prone training and lower benefit of high C:F for their performance may explain the lower frequency in power sport athletes. In support, we observed an approximately doubled risk of injury in carriers of a RAB3GAP2 low-expressing allele (rs11547779). However, this hypothesis should be the aim of future studies.

In summary, naturally occurring genetic perturbation of RAB3GAP2 promotes capillary formation and the release of

TNC and other pro-inflammatory and tissue remodeling proteins, effects resembling those evoked by exercise. However, in untrained individuals, this variant may also predispose to a microvascular endothelium more susceptible to stress with higher risk of endothelial and muscle damage. The higher frequency of the rs115660502 variant allele in highly trained endurance athletes may be ergogenic, by enhancing exercise-induced capillary formation via increased endothelial cell proliferation, inflammatory tolerance, and facilitate muscle repair.

Limitations of the study

Study limitations include the small sample sizes of the cohorts. Here, potentially, advanced computational approaches such as deep learning-based phenotyping (https://doi.org/10.1126/science.adf8009) could help increase the number of individuals with available C:F ratio and improve the power of the association analysis. However, the error of genotype-to-phenotype deep learning prediction may also negatively affect the analysis. Further, the genetic association within each cohort was performed using the SNPTEST frequentist score additive model test. To mitigate potential false-positive associations, adding principal components (PCs) as covariates could help. However, as the samples are from the same group, and thus relatively homogeneous, controlling for PCs is not likely to have a substantial effect on the results. Another limitation is the use of a proxy marker (rs11547779) for rs115660502 in the Japanese cohort. By doing so we acknowledge that neither rs115660502 nor rs11547779 is discernably the functional variant. rs115660502 is associated with a very modest difference in expression level of RAB3GAP2, but as we have not identified the causal variant (or rather haplotype), we don't know the true level of influence on expression. It is also possible that a lifelong exposure of a modest reduction in RAB3GAP2 activity could have pronounced phenotypic effects, and we don't know how environmental exposures could interact with this haplotype. However, this is unlikely to influence the core findings of this study, i.e., that RAB3GAP2 plays a regulatory role in the endothelial cellular response to exercise, as our approach focused on whole-gene manipulation as opposed to single-variant editing. In the current study, we use C:F as a surrogate measure of muscle CD, as we found C:F and CD to be correlated measures, and our access to CD data is limited. However, the relationship between C:F and insulin sensitivity is not as clear as with CD.[36,49] For example, Lillioja et al.[36] report a strong correlation between whole-body insulin sensitivity and CD but a poor relationship with C:F. Further, although Solomon et al.[49] report that CD, C:F, and the mean number of capillary contacts per fiber are all found to be decreased with advancing glucose intolerance in older obese adults, mirrored by lowering amounts of plasma fasting plasma nitric oxide, the trend is less pronounced with C:F. It is worth considering that C:F is generally the golden standard for determining growth of new capillaries, as the number of muscle fibers is not readily changed,[50] whereas CD will be affected by a change in muscle fiber cross-sectional diameter, which is often reported after a period of training. CD is, however, a better indicator of changes in diffusion distance for oxygen from blood to muscle fiber.

RESOURCE AVAILABILITY

Lead contact

Requests for further information, resources, and reagents should be directed to and will be fulfilled by the lead contact, Kristoffer Ström (kristoffer.strom@med.lu.se).

Materials availability

This study did not generate new, unique reagents.

Data and code availability

- RNA-seq data from the Elite Athlete Gene Expression Study and from the RAB3GAP2 knockdown in HMEC cells, as well as microarray data from the Malmö Exercise Intervention Study, have been deposited at the Gene Expression Omnibus. MSAT RNA-seq data have been deposited at the European Genome-Phenome Archive (EGA). All data are publicly available as of the date of publication. Accession numbers are listed in the key resources table.
- This paper does not report original code.
- Any additional information required to reanalyze the data reported in this paper is available from the lead contact upon request.

ACKNOWLEDGMENTS

We thank all the participants from the different studies for their crucial contributions and Professor Tom Carter at University of London for his kind contribution and advice. We thank the LUDC Bioinformatics Unit (https://www.ludc.lu.se/resources/ludc-bioinformatics-unit) for providing bioinformatics, biostatistics, and computational support as well as access to high-performance computing environment. The Lund University Bioimaging Centre (LBIC), Lund University, is gratefully acknowledged for providing experimental resources and staff support. We thank Olga Kotova and Esa Laurila (Lund University Diabetes Center) for technical assistance.

This study was supported by the Swedish Research Council through Strategic Research Area EXODIAB (Dnr 2009-1039), project grants (Dnr 2018-02635, 2018-02837, 2018-03086, and 2020-02191), and a Linnaeus grant (Dnr 349-2006-237); Swedish Foundation for Strategic Research (Dnr IRC15-0067); Swedish Heart-Lung Foundation (Dnr 20190470 and 20220606); Crafoord Foundation; Wallenberg Foundation; Novo Nordisk Foundation (Dnr. NNF21OC0070457); Magn. Bergvall Foundation: Påhlsson Foundation; Diabetes Wellness; Swedish Diabetes Research Foundation; Hjelt Foundation; European Research Council (CoG-2015_681742_NASCENT); and Region Skåne. N.O. is financially supported by the Knut and Alice Wallenberg Foundation as part of the National Bioinformatics Infrastructure Sweden at SciLifeLab. T.K. is supported by a Novo Nordisk Foundation Data Science Investigator grant (NNF20OC0062294). P.W.F. and S.K. were supported by grants from the Novo Nordisk Foundation, Swedish Research Council (#2019-01348), and European Commission (ERC-CoG_NASCENT-681742). M.S.-L. is supported by a Miguel Servet contract from the ISCIII Spanish Health Institute (CPII22/00007) and cofinanced by the European Social Fund. The Pronmed was funded by the SciLifeLab/Knut and Alice Wallenberg National COVID-19 research program (M.H.; KAW 2020.0182 and KAW 2020.0241), the Swedish Heart-Lung Foundation (M.H.; 20210089, 20190639, and 20190637), the Swedish Research Council (R.F.; 2014-02569 and 2014-07606), the Swedish Society of Medicine (M.H.; SLS-938101), and the Swedish Kidney Foundation (R.F.; F2020-0054). The gene expression study in athletes was supported by a grant from the Russian Science Foundation (24-15-00413). Support for the FUSION Tissue Biopsy Study dataset (dbGaP accession phs001048.v2.p1) was contributed by the NHGRI intramural projects ZIAHG000024 and Z1BHG000196; NIDDK grants DK062370, DK072193, and DK099240; NHGRI grant HG003079; American Diabetes Association Pathway to Stop Diabetes Grant 1-14-INI-07; and grants from the Academy of Finland. The Genotype-Tissue Expression (GTEx) Project was supported by the Common Fund of the Office of the Director of the National Institutes of Health and by NCI, NHGRI, NHLBI, NIDA, NIMH, and NINDS. The funders had no role in study design, data collection and analysis, decision to publish, or preparation of the manuscript.

AUTHOR CONTRIBUTIONS

Conceptualization, K.S., N.O., C.M.L., P.W.F., and O.H.; performed experiments, K.S., S.K., B.A.M., O.E., E.K., S.R., A.-M.D.A., E.Z., and K.-F.E.; provided expertise and feedback, S.K., B.A.M., O.E., M.I., E.A.S., A.K.L., R.I.S., K.A.B., A.V.Z., N.A.K., E.V.G., M.H., R.F., H.Z., M. Lipcsey, A. Larsson, A.M., E.A., R.B.P., K. Prüfer, M.S.-L., L.L., K.M., A.P.M., J.P.A.A., M. Lehtovirta, I.I.A., A.S.-L., A. Lucia, N.F., H.-C.H., M.F.G., K.-F.E., K. Pietras, C.M.L., P.W.F., O.H.; validation: E.M.-M., M.I., E.A.S., A.K.L., R.I.S., K.A.B., A.V.Z., N.A.K., E.V.G., M.H., R.F., H.Z., M. Lipcsey, A. Larsson, M.S.-L., N.L.S., A.D., K.M., L.S., A.K., I.I.A., G.W., Y.P., A.S.-L., A. Lucia, N.F., and H.-C.H.; performed formal analysis and curated data, N.O., T.K., C.L., D.K., J.F., M.T., A.M., E.A., R.B.P., K. Pietras, M.F.G., and O.H.; and wrote the manuscript, K.S., N.O., P.W.F., and O.H. All authors reviewed and approved the manuscript.

DECLARATION OF INTERESTS

The authors declare no competing interests.

STAR★METHODS

Detailed methods are provided in the online version of this paper and include the following:

- KEY RESOURCES TABLE
- EXPERIMENTAL MODEL AND STUDY PARTICIPANT DETAILS
  - Human participants in the genome-wide association study
  - Human participants in the eQTL analysis
  - Human participants in the WINGATE study
  - Athlete cohorts
- METHOD DETAILS
  - Assessment of muscle fiber composition in muscle biopsy studies
  - Phenotypes in ULSAM, MM, and MSAT cohorts
  - Genotyping of the ULSAM, MM, and MEI cohorts
  - Genotyping of the replication cohort of athletes
  - Genotyping of the muscle injury cohort (J-HAP)
  - Imputation & meta-analysis
  - Testing allele frequencies in athletes versus population controls
  - eQTL analysis
  - Culture of human microvascular endothelial cells (HMEC-1)
  - Quantitative real-time PCR
  - RNA sequencing
  - HMEC-1 secretion experiments
  - Immunohistochemistry (IHC) and immunofluorescence (IF) of frozen human muscle biopsies
  - IF on HUVEC/HMEC cells
  - Immunoblotting
  - CRISPR/Cas9 genomic editing of HMEC cells
  - Matrigel tube-forming assay
  - Live-cell imaging of HMEC-1
  - *In vivo* angiogenesis plug assay
  - Migration analysis using the wound healing assay
  - Knockdown of RAB18 and RAB3B with siRNA
- QUANTIFICATION AND STATISTICAL ANALYSIS
  - Generally
  - Phenotypes in ULSAM, MM, and MSAT cohorts
  - Genotyping of the ULSAM, MM, and MEI cohorts
  - Genotyping of the replication cohort of athletes
  - Genotyping of the muscle injury cohort (J-HAP)
  - Imputation and meta-analysis
  - Testing allele frequencies in athletes vs. population controls
  - eQTL analysis
  - Quantitative real-time PCR
  - RNA sequencing
  - HMEC-1 secretion experiments
  - Matrigel tube-forming assay
  - Live-cell imaging of HMEC-1 cells

SUPPLEMENTAL INFORMATION

Supplemental information can be found online at https://doi.org/10.1016/j.celrep.2026.116961.

Received: January 20, 2025
Revised: September 19, 2025
Accepted: January 10, 2026

REFERENCES

1. Saltin, B., Henriksson, J., Nygaard, E., Andersen, P., and Jansson, E. (1977). Fiber types and metabolic potentials of skeletal muscles in sedentary man and endurance runners. Ann. N. Y. Acad. Sci. *301*, 3–29.
2. Pillon, N.J., Smith, J.A.B., Alm, P.S., Chibalin, A.V., Alhusen, J., Arner, E., Carninci, P., Fritz, T., Otten, J., Olsson, T., et al. (2022). Distinctive exercise-induced inflammatory response and exerkine induction in skeletal muscle of people with type 2 diabetes. Sci. Adv. *8*, eabo3192. https://doi.org/10.1126/sciadv.abo3192.
3. Golia, E., Limongelli, G., Natale, F., Fimiani, F., Maddaloni, V., Pariggiano, I., Bianchi, R., Crisci, M., D'Acierno, L., Giordano, R., et al. (2014). Inflammation and cardiovascular disease: from pathogenesis to therapeutic target. Curr. Atheroscler. Rep. *16*, 435. https://doi.org/10.1007/s11883-014-0435-z.
4. Donath, M.Y., Meier, D.T., and Böni-Schnetzler, M. (2019). Inflammation in the Pathophysiology and Therapy of Cardiometabolic Disease. Endocr. Rev. *40*, 1080–1091. https://doi.org/10.1210/er.2019-00002.
5. Wu, H., and Ballantyne, C.M. (2020). Metabolic Inflammation and Insulin Resistance in Obesity. Circ. Res. *126*, 1549–1564. https://doi.org/10.1161/CIRCRESAHA.119.315896.
6. Komi, P.V., Viitasalo, J.H., Havu, M., Thorstensson, A., Sjödin, B., and Karlsson, J. (1977). Skeletal muscle fibres and muscle enzyme activities in monozygous and dizygous twins of both sexes. Acta Physiol. Scand. *100*, 385–392.
7. Simoneau, J.A., and Bouchard, C. (1995). Genetic determinism of fiber type proportion in human skeletal muscle. FASEB J. *9*, 1091–1095.
8. Prior, S.J., Roth, S.M., Wang, X., Kammerer, C., Miljkovic-Gacic, I., Bunker, C.H., Wheeler, V.W., Patrick, A.L., and Zmuda, J.M. (2007). Genetic and environmental influences on skeletal muscle phenotypes as a function of age and sex in large, multigenerational families of African heritage. J. Appl. Physiol. *103*, 1121–1127. https://doi.org/10.1152/japplphysiol.00120.2007.
9. Valdivieso, P., Toigo, M., Hoppeler, H., and Flück, M. (2017). T/T homozygosity of the tenascin-C gene polymorphism rs2104772 negatively influences exercise-induced angiogenesis. PLoS One *12*, e0174864. https://doi.org/10.1371/journal.pone.0174864.
10. Valdivieso, P., Vaughan, D., Laczko, E., Brogioli, M., Waldron, S., Rittweger, J., and Flück, M. (2017). The Metabolic Response of Skeletal Muscle to Endurance Exercise Is Modified by the ACE-I/D Gene Polymorphism and Training State. Front. Physiol. *8*, 993. https://doi.org/10.3389/fphys.2017.00993.
11. Vaughan, D., Brogioli, M., Maier, T., White, A., Waldron, S., Rittweger, J., Toigo, M., Wettstein, J., Laczko, E., and Flück, M. (2016). The Angiotensin Converting Enzyme Insertion/Deletion Polymorphism Modifies Exercise-Induced Muscle Metabolism. PLoS One *11*, e0149046. https://doi.org/10.1371/journal.pone.0149046.
12. Nelson, M.R., Tipney, H., Painter, J.L., Shen, J., Nicoletti, P., Shen, Y., Floratos, A., Sham, P.C., Li, M.J., Wang, J., et al. (2015). The support of human genetic evidence for approved drug indications. Nat. Genet. *47*, 856–860. https://doi.org/10.1038/ng.3314.
13. Kanaley, J.A., Colberg, S.R., Corcoran, M.H., Malin, S.K., Rodriguez, N.R., Crespo, C.J., Kirwan, J.P., and Zierath, J.R. (2022). Exercise/Physical Activity in Individuals with Type 2 Diabetes: A Consensus Statement from the

American College of Sports Medicine. Med. Sci. Sports Exerc. *54*, 353–368. https://doi.org/10.1249/MSS.0000000000002800.

14. Costill, D.L., Fink, W.J., and Pollock, M.L. (1976). Muscle fiber composition and enzyme activities of elite distance runners. Med. Sci. Sports *8*, 96–100.
15. Harber, M., and Trappe, S. (2008). Single muscle fiber contractile properties of young competitive distance runners. J. Appl. Physiol. *105*, 629–636. https://doi.org/10.1152/japplphysiol.00995.2007.
16. Widrick, J.J., Trappe, S.W., Costill, D.L., and Fitts, R.H. (1996). Force-velocity and force-power properties of single muscle fibers from elite master runners and sedentary men. Am. J. Physiol. *271*, C676–C683. https://doi.org/10.1152/ajpcell.1996.271.2.C676.
17. Hedstrand, H. (1975). A study of middle-aged men with particular reference to risk factors for cardiovascular disease. Ups. J. Med. Sci. Suppl. *19*, 1–61.
18. Mootha, V.K., Lindgren, C.M., Eriksson, K.F., Subramanian, A., Sihag, S., Lehar, J., Puigserver, P., Carlsson, E., Ridderstråle, M., Laurila, E., et al. (2003). PGC-1alpha-responsive genes involved in oxidative phosphorylation are coordinately downregulated in human diabetes. Nat. Genet. *34*, 267–273. https://doi.org/10.1038/ng1180.
19. Rosenbloom, K.R., Sloan, C.A., Malladi, V.S., Dreszer, T.R., Learned, K., Kirkup, V.M., Wong, M.C., Maddren, M., Fang, R., Heitner, S.G., et al. (2013). ENCODE data in the UCSC Genome Browser: year 5 update. Nucleic Acids Res. *41*, D56–D63. https://doi.org/10.1093/nar/gks1172.
20. Taylor, D.L., Jackson, A.U., Narisu, N., Hemani, G., Erdos, M.R., Chines, P.S., Swift, A., Idol, J., Didion, J.P., Welch, R.P., et al. (2019). Integrative analysis of gene expression, DNA methylation, physiological traits, and genetic variation in human skeletal muscle. Proc. Natl. Acad. Sci. USA *116*, 10883–10888. https://doi.org/10.1073/pnas.1814263116.
21. Miyamoto-Mikami, E., Tsuji, K., Horii, N., Hasegawa, N., Fujie, S., Homma, T., Uchida, M., Hamaoka, T., Kanehisa, H., Tabata, I., and Iemitsu, M. (2018). Gene expression profile of muscle adaptation to high-intensity intermittent exercise training in young men. Sci. Rep. *8*, 16811. https://doi.org/10.1038/s41598-018-35115-x.
22. Pillon, N.J., Gabriel, B.M., Dollet, L., Smith, J.A.B., Sardón Puig, L., Botella, J., Bishop, D.J., Krook, A., and Zierath, J.R. (2020). Transcriptomic profiling of skeletal muscle adaptations to exercise and inactivity. Nat. Commun. *11*, 470. https://doi.org/10.1038/s41467-019-13869-w.
23. Eraslan, G., Drokhlyansky, E., Anand, S., Fiskin, E., Subramanian, A., Slyper, M., Wang, J., Van Wittenberghe, N., Rouhana, J.M., Waldman, J., et al. (2022). Single-nucleus cross-tissue molecular reference maps toward understanding disease gene function. Science *376*, eabl4290. https://doi.org/10.1126/science.abl4290.
24. Sakane, A., Manabe, S., Ishizaki, H., Tanaka-Okamoto, M., Kiyokage, E., Toida, K., Yoshida, T., Miyoshi, J., Kamiya, H., Takai, Y., and Sasaki, T. (2006). Rab3 GTPase-activating protein regulates synaptic transmission and plasticity through the inactivation of Rab3. Proc. Natl. Acad. Sci. USA *103*, 10029–10034. https://doi.org/10.1073/pnas.0600304103.
25. Jakobsen, J.R., Mackey, A.L., Knudsen, A.B., Koch, M., Kjaer, M., and Krogsgaard, M.R. (2017). Composition and adaptation of human myotendinous junction and neighboring muscle fibers to heavy resistance training. Scand. J. Med. Sci. Sports *27*, 1547–1559. https://doi.org/10.1111/sms.12794.
26. Heinemeier, K.M., Bjerrum, S.S., Schjerling, P., and Kjaer, M. (2013). Expression of extracellular matrix components and related growth factors in human tendon and muscle after acute exercise. Scand. J. Med. Sci. Sports *23*, e150–e161. https://doi.org/10.1111/j.1600-0838.2011.01414.x.
27. Raastad, T., Owe, S.G., Paulsen, G., Enns, D., Overgaard, K., Crameri, R., Kiil, S., Belcastro, A., Bergersen, L., and Hallén, J. (2010). Changes in calpain activity, muscle structure, and function after eccentric exercise. Med. Sci. Sports Exerc. *42*, 86–95. https://doi.org/10.1249/MSS.0b013e3181ac7afa.
28. Hyldahl, R.D., Nelson, B., Xin, L., Welling, T., Groscost, L., Hubal, M.J., Chipkin, S., Clarkson, P.M., and Parcell, A.C. (2015). Extracellular matrix remodeling and its contribution to protective adaptation following lengthening contractions in human muscle. FASEB J. *29*, 2894–2904. https://doi.org/10.1096/fj.14-266668.
29. Ekström, O., Ström, K., Mir, B.A., Laurila, E., Wessman, Y., Lehtovirta, M., Eriksson, K.F., and Hansson, O. (2023). Increasing circulating levels of Tenascin C in response to the Wingate Anaerobic test. Clin Physiol Funct Imaging *43*, 271. https://doi.org/10.1111/cpf.12816.
30. Zhang, H., Zhou, L., Wang, H., Gu, W., Li, Z., Sun, J., Wei, X., and Zheng, Y. (2023). Tenascin-C-EGFR activation induces functional human satellite cell proliferation and promotes wound-healing of skeletal muscles via oleanic acid. Dev. Biol. *504*, 86–97. https://doi.org/10.1016/j.ydbio.2023.09.010.
31. Mousley, J.J., Hill-Buxton, L.M., Gill, S.D., McGee, S.L., and Page, R.S. (2021). Polymorphisms and alterations in gene expression associated with rotator cuff tear and healing following surgical repair: a systematic review. J. Shoulder Elb. Surg. *30*, 200–215. https://doi.org/10.1016/j.jse.2020.07.045.
32. Larruskain, J., Celorrio, D., Barrio, I., Odriozola, A., Gil, S.M., Fernandez-Lopez, J.R., Nozal, R., Ortuzar, I., Lekue, J.A., and Aznar, J.M. (2018). Genetic Variants and Hamstring Injury in Soccer: An Association and Validation Study. Med. Sci. Sports Exerc. *50*, 361–368. https://doi.org/10.1249/MSS.0000000000001434.
33. Vaughn, N.H., Stepanyan, H., Gallo, R.A., and Dhawan, A. (2017). Genetic Factors in Tendon Injury: A Systematic Review of the Literature. Orthop. J. Sports Med. *5*, 2325967117724416. https://doi.org/10.1177/2325967117724416.
34. Mackey, A.L., Brandstetter, S., Schjerling, P., Bojsen-Moller, J., Qvortrup, K., Pedersen, M.M., Doessing, S., Kjaer, M., Magnusson, S.P., and Langberg, H. (2011). Sequenced response of extracellular matrix deadhesion and fibrotic regulators after muscle damage is involved in protection against future injury in human skeletal muscle. FASEB J. *25*, 1943–1959. https://doi.org/10.1096/fj.10-176487.
35. Pitsiladis, Y.P., Tanaka, M., Eynon, N., Bouchard, C., North, K.N., Williams, A.G., Collins, M., Moran, C.N., Britton, S.L., Fuku, N., et al. (2016). Athlome Project Consortium: a concerted effort to discover genomic and other "omic" markers of athletic performance. Physiol. Genomics *48*, 183–190. https://doi.org/10.1152/physiolgenomics.00105.2015.
36. Lillioja, S., Young, A.A., Culter, C.L., Ivy, J.L., Abbott, W.G., Zawadzki, J.K., Yki-Järvinen, H., Christin, L., Secomb, T.W., and Bogardus, C. (1987). Skeletal muscle capillary density and fiber type are possible determinants of in vivo insulin resistance in man. J. Clin. Investig. *80*, 415–424. https://doi.org/10.1172/JCI113088.
37. Blackwood, S.J., Tischer, D., van de Ven, M.P.F., Pontén, M., Edman, S., Horwath, O., Apró, W., Röja, J., Ekblom, M.M., Moberg, M., and Katz, A. (2024). Elevated heart rate and decreased muscle endothelial nitric oxide synthase in early development of insulin resistance. Am. J. Physiol. Endocrinol. Metab. *327*, E172–E182. https://doi.org/10.1152/ajpendo.00148.2024.
38. Nagano, F., Sasaki, T., Fukui, K., Asakura, T., Imazumi, K., and Takai, Y. (1998). Molecular cloning and characterization of the noncatalytic subunit of the Rab3 subfamily-specific GTPase-activating protein. J. Biol. Chem. *273*, 24781–24785.
39. Abdel-Hamid, M.S., Abdel-Ghafar, S.F., Ismail, S.R., Desouky, L.M., Issa, M.Y., Effat, L.K., and Zaki, M.S. (2020). Micro and Martsolf syndromes in 34 new patients: Refining the phenotypic spectrum and further molecular insights. Clin. Genet. *98*, 445–456. https://doi.org/10.1111/cge.13825.
40. Norden, P.R., Sun, Z., and Davis, G.E. (2020). Control of endothelial tubulogenesis by Rab and Ral GTPases, and apical targeting of caveolin-1-labeled vacuoles. PLoS One *15*, e0235116. https://doi.org/10.1371/journal.pone.0235116.
41. Fairlie, G.M.J., Nguyen, K.M., Nam, S.E., Shaw, A.L., Parson, M.A.H., Shariati, H.R., Wang, X., Jenkins, M.L., Gong, M., Burke, J.E., and Yip, C.K. (2025). Biochemical and structural characterization of Rab3GAP reveals insights into Rab18 nucleotide exchange activity. Nat. Commun. *16*, 479. https://doi.org/10.1038/s41467-025-55828-8.

42. Vazquez-Martinez, R., Cruz-Garcia, D., Duran-Prado, M., Peinado, J.R., Castaño, J.P., and Malagon, M.M. (2007). Rab18 inhibits secretory activity in neuroendocrine cells by interacting with secretory granules. Traffic *8*, 867–882. https://doi.org/10.1111/j.1600-0854.2007.00570.x.

43. Febbraio, M.A. (2017). Exercise metabolism in 2016: Health benefits of exercise - more than meets the eye. Nat. Rev. Endocrinol. *13*, 72–74. https://doi.org/10.1038/nrendo.2016.218.

44. Udalova, I.A., Ruhmann, M., Thomson, S.J.P., and Midwood, K.S. (2011). Expression and immune function of tenascin-C. Crit. Rev. Immunol. *31*, 115–145. https://doi.org/10.1615/critrevimmunol.v31.i2.30.

45. Han, B.K., Olsen, N.J., and Bottaro, A. (2016). The CD27-CD70 pathway and pathogenesis of autoimmune disease. Semin. Arthritis Rheum. *45*, 496–501. https://doi.org/10.1016/j.semarthrit.2015.08.001.

46. Macaluso, F., Isaacs, A.W., and Myburgh, K.H. (2012). Preferential type II muscle fiber damage from plyometric exercise. J. Athl. Train. *47*, 414–420. https://doi.org/10.4085/1062-6050-47.4.13.

47. Friden, J., Sjostrom, M., and Ekblom, B. (1983). Myofibrillar damage following intense eccentric exercise in man. Int. J. Sports Med. *4*, 170–176. https://doi.org/10.1055/s-2008-1026030.

48. Lievens, E., Klass, M., Bex, T., and Derave, W. (2020). Muscle fiber typology substantially influences time to recover from high-intensity exercise. J. Appl. Physiol. *128*, 648–659. https://doi.org/10.1152/japplphysiol.00636.2019.

49. Solomon, T.P.J., Haus, J.M., Li, Y., and Kirwan, J.P. (2011). Progressive hyperglycemia across the glucose tolerance continuum in older obese adults is related to skeletal muscle capillarization and nitric oxide bioavailability. J. Clin. Endocrinol. Metab. *96*, 1377–1384. https://doi.org/10.1210/jc.2010-2069.

50. Olfert, I.M., Baum, O., Hellsten, Y., and Egginton, S. (2016). Advances and challenges in skeletal muscle angiogenesis. Am. J. Physiol. Heart Circ. Physiol. *310*, H326–H336. https://doi.org/10.1152/ajpheart.00635.2015.

51. Patro, R., Duggal, G., Love, M.I., Irizarry, R.A., and Kingsford, C. (2017). Salmon provides fast and bias-aware quantification of transcript expression. Nat. Methods *14*, 417–419. https://doi.org/10.1038/nmeth.4197.

52. Love, M.I., Huber, W., and Anders, S. (2014). Moderated estimation of fold change and dispersion for RNA-seq data with DESeq2. Genome Biol. *15*, 550. https://doi.org/10.1186/s13059-014-0550-8.

53. Bray, N.L., Pimentel, H., Melsted, P., and Pachter, L. (2016). Near-optimal probabilistic RNA-seq quantification. Nat. Biotechnol. *34*, 525–527. https://doi.org/10.1038/nbt.3519.

54. Soneson, C., Love, M.I., and Robinson, M.D. (2015). Differential analyses for RNA-seq: transcript-level estimates improve gene-level inferences. F1000Res. *4*, 1521. https://doi.org/10.12688/f1000research.7563.2.

55. GTEx Consortium (2020). The GTEx Consortium atlas of genetic regulatory effects across human tissues. Science *369*, 1318–1330. https://doi.org/10.1126/science.aaz1776.

56. Miyamoto-Mikami, E., Kumagai, H., Tanisawa, K., Taga, Y., Hirata, K., Kikuchi, N., Kamiya, N., Kawakami, R., Midorikawa, T., Kawamura, T., et al. (2021). Female Athletes Genetically Susceptible to Fatigue Fracture Are Resistant to Muscle Injury: Potential Role of COL1A1 Variant. Med. Sci. Sports Exerc. *53*, 1855–1864. https://doi.org/10.1249/MSS.0000000000002658.

57. Qu, Z., Andersen, J.L., and Zhou, S. (1997). Visualisation of capillaries in human skeletal muscle. Histochem. Cell Biol. *107*, 169–174.

58. Brooke, M.H., and Kaiser, K.K. (1970). Three "myosin adenosine triphosphatase" systems: the nature of their pH lability and sulfhydryl dependence. J. Histochem. Cytochem. *18*, 670–672.

59. Keildson, S., Fadista, J., Ladenvall, C., Hedman, Å.K., Elgzyri, T., Small, K.S., Grundberg, E., Nica, A.C., Glass, D., Richards, J.B., et al. (2014). Expression of Phosphofructokinase in Skeletal Muscle Is Influenced by Genetic Variation and Associated With Insulin Sensitivity. Diabetes *63*, 1154–1165.

60. Delaneau, O., and Zagury, J.F. (2012). Haplotype inference. Methods Mol. Biol. *888*, 177–196. https://doi.org/10.1007/978-1-61779-870-2_11.

61. Howie, B.N., Donnelly, P., and Marchini, J. (2009). A flexible and accurate genotype imputation method for the next generation of genome-wide association studies. PLoS Genet. *5*, e1000529. https://doi.org/10.1371/journal.pgen.1000529.

62. Marchini, J., Howie, B., Myers, S., McVean, G., and Donnelly, P. (2007). A new multipoint method for genome-wide association studies by imputation of genotypes. Nat. Genet. *39*, 906–913. https://doi.org/10.1038/ng2088.

63. Mägi, R., and Morris, A.P. (2010). GWAMA: software for genome-wide association meta-analysis. BMC Bioinf. *11*, 288. https://doi.org/10.1186/1471-2105-11-288.

64. Viechtbauer, W. (2010). Conducting Meta-Analyses in*R*with the**metafor**-Package. J. Stat. Softw. *36*, 48. https://doi.org/10.18637/jss.v036.i03.

65. Pruim, R.J., Welch, R.P., Sanna, S., Teslovich, T.M., Chines, P.S., Gliedt, T.P., Boehnke, M., Abecasis, G.R., and Willer, C.J. (2010). LocusZoom: regional visualization of genome-wide association scan results. Bioinformatics *26*, 2336–2337. https://doi.org/10.1093/bioinformatics/btq419.

66. McGawley, K., Juudas, E., Kazior, Z., Ström, K., Blomstrand, E., Hansson, O., and Holmberg, H.-C. (2017). No additional benefits of block- over evenly-distributed high-intensity interval training within a polarized microcycle. Front. Physiol. *8*, 413. https://doi.org/10.3389/fphys.2017.00413.

67. Rankinen, T., Fuku, N., Wolfarth, B., Wang, G., Sarzynski, M.A., Alexeev, D.G., Ahmetov, I.I., Boulay, M.R., Cieszczyk, P., Eynon, N., et al. (2016). No Evidence of a Common DNA Variant Profile Specific to World Class Endurance Athletes. PLoS One *11*, e0147330. https://doi.org/10.1371/journal.pone.0147330.

68. Scott, R.A., Irving, R., Irwin, L., Morrison, E., Charlton, V., Austin, K., Tladi, D., Deason, M., Headley, S.A., Kolkhorst, F.W., et al. (2010). ACTN3 and ACE genotypes in elite Jamaican and US sprinters. Med. Sci. Sports Exerc. *42*, 107–112. https://doi.org/10.1249/MSS.0b013e3181ae2bc0.

69. Elgzyri, T., Parikh, H., Zhou, Y., Dekker Nitert, M., Rönn, T., Segerström, Å.B., Ling, C., Franks, P.W., Wollmer, P., Eriksson, K.F., et al. (2012). First-Degree Relatives of Type 2 Diabetic Patients Have Reduced Expression of Genes Involved in Fatty Acid Metabolism in Skeletal Muscle. J. Clin. Endocrinol. Metab. *97*, E1332–E1337. https://doi.org/10.1210/jc.2011-3037.

70. Ekman, C., Elgzyri, T., Ström, K., Almgren, P., Parikh, H., Dekker Nitert, M., Rönn, T., Manderson Koivula, F., Ling, C., Tornberg, Å.B., et al. (2015). Less pronounced response to exercise in healthy relatives to type 2 diabetic subjects compared with controls. J. Appl. Physiol. *119*, 953–960. https://doi.org/10.1152/japplphysiol.01067.2014.

71. Shabalin, A.A. (2012). Matrix eQTL: ultra fast eQTL analysis via large matrix operations. Bioinformatics (Oxford, England) *28*, 1353–1358. https://doi.org/10.1093/bioinformatics/bts163.

72. Balduzzi, S., Rücker, G., and Schwarzer, G. (2019). How to perform a meta-analysis with R: a practical tutorial. Evid. Based. Ment. Health *22*, 153–160. https://doi.org/10.1136/ebmental-2019-300117.

73. Vandesompele, J., De Preter, K., Pattyn, F., Poppe, B., Van Roy, N., De Paepe, A., and Speleman, F. (2002). Accurate normalization of real-time quantitative RT-PCR data by geometric averaging of multiple internal control genes. Genome Biol. *3*, RESEARCH0034.

74. Brown, R.M., Meah, C.J., Heath, V.L., Styles, I.B., and Bicknell, R. (2016). Tube-Forming Assays. Methods Mol. Biol. *1430*, 149–157. https://doi.org/10.1007/978-1-4939-3628-1_9.

75. Nowak-Sliwinska, P., Alitalo, K., Allen, E., Anisimov, A., Aplin, A.C., Auerbach, R., Augustin, H.G., Bates, D.O., van Beijnum, J.R., Bender, R.H.F., et al. (2018). Consensus guidelines for the use and interpretation of angiogenesis assays. Angiogenesis *21*, 425–532. https://doi.org/10.1007/s10456-018-9613-x.

STAR★METHODS

KEY RESOURCES TABLE

REAGENT or RESOURCE	SOURCE	IDENTIFIER
Antibodies		
Rabbit polyclonal anti-RAB3GAP2 (for IHC and IF)	Atlas Antibodies	Cat#HPA026273; RRID: AB_1856007
Biotinylated goat anti-rabbit IgG	Vector Laboratories	Cat#BA-1000; RRID: AB_2313606
Cy™5 AffiniPure® Donkey Anti-Rabbit IgG	Jackson Immuno Research	Cat#711-175-152; RRID: AB_2340607
Non-immune polyclonal rabbit IgG	Abcam	Cat#ab27478; RRID: AB_2616600
Mouse monoclonal anti-CD31	Dako/Agilent	Cat# M0823; RRID: AB_2114471
Goat Anti-Mouse IgG H&L (Alexa Fluor® 488	Agilent	Cat# ab150113; RRID: AB_2576208
Rabbit polyclonal anti-RAB3GAP2 (for immunoblotting)	Thermo Fisher Scientific	Cat# PA555296; RRID: RRID: AB_2646245
Mouse monoclonal anti-alpha-tubulin	Abcam	Cat#ab7291; RRID: AB_2241126
Rabbit monoclonal anti-GAPDH	Abcam	Cat# ab181602; RRID: AB_2630358
Goat Anti-Rabbit Secondary Antibody Conjugated to HRP	BIO-RAD	Cat# 1662408; RRID: AB_11125345
Goat Anti-Mouse Secondary Antibody Conjugated to HRP	BIO-RAD	Cat# 1706516; RRID: AB_2921252
Chemicals, peptides, and recombinant proteins		
Trichrome	Abcam	ab150686
Lipofectamine™ RNAiMAX Transfection Reagent	Thermo Fisher Scientific	Cat# 13778075
Matrigel		
Human EGF Recombinant Protein	Thermo Fisher Scientific	Cat# PHG0314
GlutaMAX™ Supplement	Thermo Fisher Scientific	Cat# 35050038
Hydrocortisone	Merck	Cat# H0888
Fetal Bovine Serum	Merck	Cat# 7524
MCDB 131 Medium, no glutamine	Thermo Fisher Scientific	Cat# 10372019
Antibiotic-Antimycotic	Thermo Fisher Scientific	Cat# 15240062
TrypLE™ Express Enzyme	Thermo Fisher Scientific	Cat#12604013
VECTASHIELD® Antifade Mounting Medium with DAPI	Vector Laboratories	Cat# H-1200
Ulex Europaeus Agglutinin I (UEA I), Rhodamine	Vector Laboratories	Cat# RL-1062
SYTOX™ Green Nucleic Acid Stain	Thermo Fisher Scientific	Cat# S7020
SuperSignal™ West Pico PLUS Chemiluminescent Substrate	Thermo Fisher Scientific	Cat# 34579
AmpliTaq Gold™ 360 Master Mix	Thermo Fisher Scientific	Cat# 4398876
Avertin (2,2,2-Tribromoethanol)	Merck	Cat# T48402
Critical commercial assays		
RNeasy Plus Mini Kit	Qiagen	Cat# 74136
RNeasy Fibrous Tissue Mini Kit	Qiagen	Cat# 74704
DNeasy Blood & Tissue Kit	Qiagen	Cat# 69504
QuantiTect Reverse Transcription Kit	Qiagen	Cat# 205311
TaqMan™ Gene Expression Master Mix	Thermo Fisher Scientific	Cat# 4369016
TURBO DNA-free™ Kit	Thermo Fisher Scientific	Cat# AM1907
NEBNext® Ultra™ II Directional RNA Library Prep Kit for Illumina®	New England Biolabs	Cat# E7760L
NEBNext Globin & rRNA Depletion kit	New England Biolabs	Cat# E7750X
VECTASTAIN® Elite® ABC-HRP Kit	Vector Laboratories	Cat# PK-6100
ImmPACT® DAB Substrate Kit	Vector Laboratories	Cat# SK-4105
INSTA-Blot Human Tissues PVDF membrane	Novus Biologicals	Cat# NBP2-31378
Invitrogen™ Human Tenascin C ELISA Kit	Thermo Fisher Scientific	Cat# EH446RB
QIAshredder minispin columns	Qiagen	Cat# 79654

(*Continued on next page*)

Continued

REAGENT or RESOURCE	SOURCE	IDENTIFIER
Cell Line Nucleofector® Kit V	Lonza	Cat# VCA-1003
GeneJET PCR Purification Kit	Thermo Fisher Scientific	Cat# K0701
Alt-R™ Genome Editing Detection Kit	Integrated DNA Technologies	Cat# 1075931
Deposited data		
RNAseq data from the ELITE ATHLETE GENE EXPRESSION STUDY	–	GEO: GSE200398
RNAseq data from the MSAT study	–	EGAD00001008984
Microarray data from the Malmö Exercise Intervention study	–	GEO: GSE161719
RNAseq data from the RAB3GAP2 knockdown in HMEC cells	–	GEO: GSE314190
Experimental models: Cell lines		
Human Microvascular Endothelial Cells (HMEC-1)	ATCC	Cat#CRL-3243
HUVEC/TERT2	ATCC	Cat#CRL-4053
Experimental models: Organisms/strains		
NOD.Cg-Prkdcscid Il2rgtm1Wjl/SzJ mice	The Jackson Laboratory	Cat#JAX#005557
Oligonucleotides		
Silencer™ Select siRNA targeting RAB18	Thermo Fisher Scientific	Cat#4390824; Assay ID: s22703
Silencer™ Select siRNA targeting RAB3B	Thermo Fisher Scientific	Cat#4390824; Assay ID: s11669
Silencer™ Select Negative Control No. 1 siRNA	Thermo Fisher Scientific	Cat#4390843
Synthetic sgRNA containing the sequence ATCTCCAACCAATGATCTTA complementary to the protein-encoding sequence in RAB3GAP2 exon 3 (cut site at Leu-88)	Integrated DNA Technologies	Custom made
RAB3GAP2 (exon 24-25 boundary) Gene Expression Assay	Thermo Fisher Scientific	Cat#4331182; Assay ID: Hs00202700_m1
RAB3GAP2 (exon 3-4 boundary) Gene Expression Assay	Thermo Fisher Scientific	Cat#4351372; Assay ID: Hs01073425_m1
RAB3B Gene Expression Assay	Thermo Fisher Scientific	Cat#4331182; Assay ID: Hs01001137_m1
RAB18 Gene Expression Assay	Thermo Fisher Scientific	Cat#4331182; Assay ID: Hs00222021_m1
POLR2A Gene Expression Assay	Thermo Fisher Scientific	Cat#4331182; Assay ID: Hs00172187_m1
Human HPRT1 (HGPRT) Endogenous Control	Thermo Fisher Scientific	Cat#4326321E
Human PPIA (Cyclophilin A) Endogenous Control	Thermo Fisher Scientific	Cat#4326316E
Software and algorithms		
Salmon v1.3.0 (transcript expression quantification)	Patro et al.[51]	–
DESeq2 v1.26.0 (differential gene expression analysis)	Love et al.[52]	–
Kallisto v0.48.0 (pseudoalignment)	Bray et al.[53]	–
tximport Bioconductor package (gene expression)	Soneson et al.[54]	–
Other		
Viia 7 real-time PCR system	Thermo Fisher Scientific	Cat# 4453536
2200 TapeStation system	Agilent	–
BioAnalyzer electrophoresis system	Agilent	–
TruSeq Stranded mRNA LT Sample Prep Kit-Set A	Illumina	Cat# RS-122-2101
NextSeq® 500/550 High Output Kit v2.5	Illumina	Cat# 20024906
NextSeq® 500 Instrument	Illumina	–
HiSeq system	Illumina	–
TissueLyser II system	Qiagen	–
Qubit spectrophotometer	Thermo Fisher Scientific	–
NanoDrop ND-1000 spectrophotometer	NanoDrop Technologies	–

(*Continued on next page*)

Continued

REAGENT or RESOURCE	SOURCE	IDENTIFIER
Olink Target 96 immunoassay panels (Cardiometabolic, Oncology II, Cardiovascular III and the Immuno-Oncology panels)	OLINK	https://www.olink.com/products/target/)
Zeiss LSM800 laser scanning confocal microscope	Zeiss	–
Image analysis platform myWim	Wimasis	www.wimasis.com
ZEISS Celldiscoverer 7 system	Zeiss	www.zeiss.com/microscopy/en/products/imaging-systems/celldiscoverer-7
Culture-Insert 4-Well in μ-Dish 35 mm	Micromedic (Ibidi)	Cat#80466

EXPERIMENTAL MODEL AND STUDY PARTICIPANT DETAILS

Human participants in the genome-wide association study

Genome-wide association study (GWAS) (ULSAM and MM): We conducted a GWAS in 610 men from two cohorts of Swedish ancestry. These cohorts were the *Uppsala Longitudinal Study of Adult Men* (ULSAM, *n* = 482, Table S7)[17] and the *Malmö Men study* (MM, *n* = 128, Table S8)[18] . The ULSAM cohort consisted of men aged 71.0 ± 0.6 years [mean ± SD] with BMI of 26.3 ± 3.4 kg/m^2 [mean ± SD]. All participants in the ULSAM study gave written informed consent and the study was approved by the Regional Ethical Review Board in Uppsala. The MM cohort consisted of men aged 65.9 ± 2.0 years [mean ± SD] with BMI of 26.4 ± 3.4 kg/m^2 [mean ± SD], including 50 participants with diagnosed type 2 diabetes (T2D) at enrollment. All participants in the MM cohort provided written informed consent and the study was approved by the local Ethics committee, Lund University (Dnr LU238-99, 2001).

Human participants in the eQTL analysis

The eQTL analysis was done in three cohorts of Swedish ancestry, i.e. the *Malmö Exercise Intervention study* (MEI, *n*=46, Table S9) , the Malmö Men MSAT study

The MEI cohort consisted of men aged 37.7 ± 4.3 years [mean ± SD] and BMI = 28.0 ± 3.1 kg/m2 [mean ± SD], including 22 participants with and 24 without a first-degree family member with T2D. All participants provided written informed consent and the study was approved by the local Ethics committee, Lund University (Dnr 2006/13).

Human participants in the WINGATE study

Subjects in the *Muscle SATellite cell study* (MSAT) were 39 healthy men aged 36.5±8.3 years, with BMI of 24.1±2.5 kg/m^2, VO_{2max} 52.0±8.1 ml/kg/min [mean ± SD]) that were recruited to the study by advertising in social media and through local cycling clubs. Inclusion criteria were as follows: (1) male (2) healthy, no medications (3) age range between 20 and 55 years. Participants were given both verbal and written information about the experimental procedures before giving their written informed consent. Each participant completed three visits at different time points. The first visit involved a medical examination with blood samples and anthropometric measurements. The second visit consisted, after an overnight fast, of a Wingate test followed by a muscle biopsy. During the third and final visit, VO_{2max} was measured. All participants provided written informed consent and the study was approved by the local Ethics committee, Lund University (Dnr 2015/593). For a more detailed description see Ekström *et al*[29]

Athlete cohorts

Discovery cohorts

Cohort 1. Swedish cross-country skiers (n = 15). Here, 14 junior cross-country skiers (8 males: age and VO_{2max} were 18-20 years and 65.7 ± 2.6 [mean ± SD] ml/kg/min, respectively; 6 females: age and VO_{2max} were 18-20 years and 54.7 ± 4.7 [mean ± SD] ml/kg/min, respectively) were recruited from two specialist Swedish ski high schools. In addition, one senior male cross-country skier was recruited (age and VO_{2max} were 38 years and 69.5 ml/kg/min). All junior athletes competed at a national level and six were members of national junior development teams; the one senior skier was a World championship medalist. All participants provided written informed consent, and the study protocol was approved by the Regional Ethical Review Board, Umeå University.

Cohort 2. Spanish athletes from different disciplines (total n = 141), including triathletes (n = 16). All athletes were Caucasian men with expertise in international competitions. Blood/saliva samples were collected over 10 years in different locations in Spain from runners (mostly 5,000 m and longer), professional road cyclists, rowers, canoeists, and triathletes. Except for the professional cyclists, inclusion criteria for this group were: having been a finalist in $\geq$1 Olympic Games or World/European championships (as a senior or under-23). Their age and VO^{V} were 19–32 years and 74.0 ± 5.5 ml/kg/min [mean ± SD], respectively. Saliva samples were also collected from Spanish (Caucasian) male control, disease-free participants, who were either inactive undergraduate students living in Madrid or recreational runners (n = 6). Their age and VO^{2max} were 19–32 years and 45.0 ± 5.5 ml/kg/min [mean ± SD], respectively. In

addition, MAF from Iberian (IBS) population from 1000G was used as a Spanish population reference. All participants provided written informed consent, and the study protocol was approved by the Ethical Review Board of Universidad Pablo Olavide.

Cohort 3. Elite Polish short track speed skaters (n = 18). Participants were members of the Polish national team who at least once had reached the final of the Winter Olympic Games or World/European championships. Their age were 18-28 years, and VO_{2max} was 68.5 ± 4.2 ml/kg/min) [mean ± SD]. Polish non-athlete controls were also included (n = 24; 15 males and 9 females, ages 19-33 years; VO_{2max} was not measured). For DNA isolation purposes, whole blood samples were collected. All subjects provided written informed consent ,and the study protocol was approved by the Ethics committee of the Medical University of Bialystok (Poland), approval number: R-I-002/286/2013.

Cohort 4. Jamaican sprinters (n = 116) comprising national- and international-level athletes. Jamaican controls comprised 311 participants (male = 156, female = 155) from throughout the island. The athletes (male = 60, female = 56) had participated in sprint events up to 400 m, jump events and throw events (100-200 m, n = 71; 400 m, n = 35; jump and throw, n = 10), and could be subdivided further into national-level athletes (n = 28), who were competitive at national-level competitions in Jamaica and the Caribbean, and international-level athletes (n = 86), who had competed at major international competitions for Jamaica. Forty-six of these international athletes had won medals at major international competitions or held sprint world records. All subjects provided written informed consent to participate in the study, which was approved by the Ethics Committee of University of West Indies.

Genotyping of the variants achieving genome-wide significance was performed and the allele frequencies were compared to the corresponding non-athlete controls of Swedish, Spanish, Polish and Jamaican population allele frequencies.

Replication cohort

The cohort consisted of 143 athletes from Russia (75 males, 68 females) who were prospectively stratified into two groups (endurance and power athletes). The endurance group (n = 71; 33 males, 38 females; age 25.1 ± 3.5 years) included athletes competing in biathlon (n = 21), cross-country skiing (n = 35), 5-25 km swimming (n = 8) and race walking (n = 7). The power group (n = 72; 42 males, 30 females; age 24.0 ± 3.3 years) included athletes competing in short-distance races, including 100-400 m running (n = 12), sprint cycling (n = 11), 200-500 m canoeing/kayaking (n = 17), 50-100 m swimming (n = 20) and 500-1000 m speed skating (n = 12). All athletes were classified as 'highly elite' (participants of Olympic games, prize winners in international competitions) and none had ever tested positive for doping by a WADA-accredited laboratory. Controls were 150 healthy, unrelated Russians (96 males and 54 females; age: 42.1 ± 3.8 years) without any competitive sport experience (explored by survey). The athletes and controls were all Caucasians. All subjects provided written informed consent to participate in the study, which was approved by the Ethics Committee of the Federal Research and Clinical Center of Physical-chemical Medicine. The elite athlete gene expression study (analysis of RAB3GAP2 gene expression in the vastus lateralis) involved 7 strength (mean age ± SD: 32.6 ± 8.0 years; mean height: 178.4 ± 5.3 cm; mean body mass: 87.7 ± 14.2 kg) and 12 endurance (mean age ± SD: 34.9 ± 10.1 years; mean height: 181.9 ± 6.3 cm; mean body mass: 75.6 ± 10.2 kg) male athletes.

Muscle biopsy studies. The *FUSION muscle biopsy study* involved 291 Finnish individuals (166 men, age 59.5 ± 8.1 years; 125 women, age 60.3 ± 8.1 years), as previously described.[20] The study was approved by the Hospital District of Helsinki and Uusimaa (this data was used with permission; Database of Genotypes and Phenotypes (dbGaP) Study Accession: phs001048.v2.p1). The *GTEx muscle biopsy study* involved 791 individuals (535 men, age 20-79 years; 256 women, age 20-79 years), as previously described.[55]

Muscle injury cohort (J-HAP): The Japanese cohort consisted of 529 male athletes from the Japanese Human Athlome Project (J-HAP).[35] In J-HAP, the history of sports-related injuries was assessed using a questionnaire as described previously.[56] The muscle injury group (n = 140) included only athletes with non-contact muscle injuries diagnosed by medical practitioners (i.e., athletes with contact muscle injury or muscle injury not diagnosed by medical practitioners were excluded from the analysis). Description of the cohort are shown in Table S11. Written informed consent was obtained from each participant. The study procedure was approved by the Ethics Committees of Juntendo University and performed in accordance with the Declaration of Helsinki.

Human microvascular endothelial cells (HMEC-1)

HMEC-1 cells (CRL-3243 (Lot: 64334159), ATCC, VA, USA) were grown at 37°C and 5% CO_2 in growth medium (MCDB131 medium (Thermo Fischer Scientific, Waltham, MA, USA)) supplemented with 10 ng/ml EGF (Thermo Fischer Scientific), 1 μg/ml hydrocortisone (Sigma, Merck, Darmstadt, Germany), 10 mM GlutaMAX (Thermo Fischer Scientific), 10% FBS (Sigma) and Antibiotic-Antimycotic solution (Thermo Fisher Scientific, Gibco) on tissue culture plates precoated with Attachment Factor (Thermo Fisher Scientific). Cells were passaged at around 70-80% confluence. Testing for mycoplasma infection was done routinely.

In vivo *angiogenesis plug assay*

For the *in vivo* angiogenesis plug assay, eight- to eighteen-weeks-old female NSG mice were used. The mice were anaesthetized with isoflurane, the groin was shaved and cleaned before injection of cold Matrigel solution. All animal experiments were approved by the local ethical committee for animal care in Lund (M167-15)

METHOD DETAILS

Assessment of muscle fiber composition in muscle biopsy studies

In the *FUSION study*, muscle samples were obtained from the *m. vastus lateralis* using a conchotome, under local anesthesia, with 20 mg·ml−1 lidocaine hydrochloride without epinephrine. Muscle fiber composition in 291 individuals was estimated based on the

expression of the myosin heavy chain 1 (MYH1; highly expressed in type IIx muscle fibers), myosin heavy chain 2 (MYH2; highly expressed in type IIa muscle fibers), and myosin heavy chain 7 (MYH7; highly expressed in type I muscle fibers) genes, as previously described[20]. Expression of the RAB3GAP2 gene was determined as previously described[20] and presented in transcripts per kilobase million (TPM). In the *GTEx muscle biopsy study*, muscle fiber composition of *m. gastrocnemius* (2 cm below the patella) in 791 individuals was estimated based on the expression of the MYH1, MYH2 and MYH7 genes, as previously described.[55] The data used for the analyses described in this manuscript were obtained from the GTEx Portal on 05/23/2023.

Phenotypes in ULSAM, MM, and MSAT cohorts

In the ULSAM, MM and Muscle SATellite cell (MSAT) cohorts, muscle biopsies were taken with a 6 mm Bergström needle and frozen in liquid nitrogen, and serial sections (10 or 16 μm) were cut using a cryostat at -20 °C. Capillaries were stained using the double staining method.[57] calculated as the number of capillaries divided by the number of fibers observed within a given section. Myofibrillar ATPase histochemistry was performed by preincubation at pH 4.4, 4.6, and 10.3 to identify muscle fiber types.[58] the proportion of fiber types (i.e. type I, IIa or IIx) were calculated as the number of each fiber type, divided by the total number of fibers in the section, multiplied by 100. Computer image analysis was performed using image analysis equipment, for ULSAM (Multisync II, BIO-RAD SA, Richmond, CA, USA) and for MM, MEI and MSAT (BioPix IQ 2.0.16 software, BioPix AB, Sweden). The phenotypes and sample sizes for each phenotype are reported in Tables S6, S7, S8 and S9. Spearman correlation matrices for C:F and fiber type, stratified by cohort, are presented in Tables S1 and S2. Within each cohort, all phenotypes were pre-adjusted for age and BMI, and inverse rank-normal transformed using the Rankit equation to provide normal data distributions. C:F was not measured in the MSAT cohort.

Genotyping of the ULSAM, MM, and MEI cohorts

Genotyping of the ULSAM cohort was done using the Illumina Omni 2.5M array and Illumina CardioMetabochip (Illumina, California, USA) and for the MM and MEI cohorts using the HumanOmniExpress 12v1 C chips (Illumina, California, USA).Genotypes were called using the Illumina Genome studio software, as described in detail elsewhere.[59] Individuals were excluded on the basis of: call rate <95%; gender mismatch; relatedness; and non-European ancestry. Variants were excluded on the basis of: call rate <95% (>99% for MAF <5%); exact p-value for Hardy-Weinberg equilibrium $<10^{-6}$; and MAF <1%. Genotyping of the different cohorts of imputed genome-wide significant variants from the meta-analysis were done using either TaqMan PCR or Sequenom platforms according to the manufacturer's instructions. For TaqMan an ABI Prism Sequence Detection System ABI 7900HT (Applied Biosystems) was used for post-PCR allelic discrimination by measuring allele-specific fluorescence. The results were in Hardy-Weinberg equilibrium ($p<1x10^{-4}$).

Genotyping of the replication cohort of athletes

DNA samples were obtained from leukocytes (venous blood). Four milliliters of venous blood were collected in tubes containing EDTA (Vacuette EDTA tubes; Greiner Bio-One, Kremsmünster, Austria). Blood samples were transported to the laboratory at 4°C and DNA was extracted on the same day. DNA extraction and purification were performed using a commercial kit (Techno-Sorb, Moscow, Russia) according to the manufacturer's instructions (Technoclon, Moscow, Russia), which included chemical lysis, selective DNA binding on silica spin columns, and ethanol washing. The extracted DNA quality was assessed by means of agarose gel electrophoresis.). Genotyping was performed using HumanOm-ni1-Quad BeadChips or HumanOmniExpress BeadChips (Illumina, San Diego, CA, USA) to genotype > 900,000 SNPs. The assay required 200 ng of DNA sample as input with a concentration of at least 50 ng/μL. Exact concentrations of DNA in each sample were measured using a Qubit Fluorometer (Invitrogen, Waltham, MA, USA). All further procedures were performed according to the instructions of the Infinium High-Density Assay. Ten percent of samples were genotyped twice with a 100% success rate of reproducibility. Bcftools was used for vcf files conversion. Phasing and imputation of genotypes were done using shapeit2 and impute2 programs.

Genotyping of the muscle injury cohort (J-HAP)

Total DNA was extracted from the saliva using Oragene® DNA Collection Kit (DNA Genotekk, ON, Canada). The concentration and purity of the extracted DNA was assessed using a NanoDrop 8000 spectrophotometer (Thermo Fisher Scientific, MA, USA). Genome-wide SNP genotypes were determined by the Japonica Array ver. 1 (Toshiba, Tokyo, Japan). Standard quality control (QC), imputation with IMPUTE2 using 3.5KJPN haplotype reference panel, and post imputation QC (Imputation quality r2 > 0.3; SNP Call rate > 0.97; Hardy–Weinberg equilibrium, P > 1E-6; Minor Allele Frequency > 0.05) were performed. Genotype data of the rs11547779 was extracted from the imputed genotype data. Association analysis of the rs11547779 polymorphism with muscle injury was conducted using the Cochran-Armitage trend test. The odds ratio (OR) and 95% confidence interval (CI) were calculated under the additive genetic model. Written informed consent was obtained from each participant. The study procedure was approved by the Ethics Committees of Juntendo University and performed in accordance with the Declaration of Helsinki.

Imputation & meta-analysis

Genotype data in each cohort were imputed up to 35 million variants from the 1000 Genomes reference panel (all ancestries, March 2012). Prephasing of haplotypes and imputation were performed using ShapeIT[60] and IMPUTE2,[61] respectively. The association within each cohort was performed using the SNPTEST frequentist score additive model test.[62] Genetic variants that had poor

imputation quality inferred by an info score ≤0.4 and/or had high standard error (SE>10) were excluded from meta-analyses. A conservative filtering of genetic variants with respect to strand inconsistencies was performed prior to meta-analysis. Fixed effects meta-analyses were undertaken on the summary statistics obtained from the two cohorts using GWAMA,[63] with phenotypes inverse rank-normal transformed and pre-adjusted for age and BMI. Post-meta-analysis QC included removing variants that: a) were detectable only in one cohort and b) had a total minor allele count <10. To validate the quality of imputation, all imputed genome-wide significant SNPs were directly typed in the MM cohort. The imputation error rates vary from variant to variant (i.e., from 0-4% for common homozygotes, 0-86% for heterozygotes), and these error rates were inversely related to the imputation info score. To ensure that findings were not biased by factors related to genotype imputation, genetic association analyses were re-run using directly genotyped data, which did not indicate any major influence of imputation on the results. Results from the directly genotyped, rather than imputed, data are generally presented in the manuscript. Analyses conditioning on variants associated with the index traits at a level of genome-wide significance ($P<5x10^{-8}$) were undertaken to discover possible secondary association signals in corresponding regions. The conditional analyses were conducted on individual-level data and performed separately for ULSAM and Malmö Men datasets. In case more than one variant located on the same haplotype was found to be associated at the genome-wide significance level, and the associated variants were not in a strong linkage disequilibrium (LD) with each other, we tested for secondary / independent association. For this purpose, an analysis was performed, where association analysis of all genetic variants from the haplotype region was re-run adjusting for the genome-wide significant variants sequentially one-by-one. If the association with $P<5x10^{-8}$ remained after adjusting for another neighboring genome-wide significant variant, we concluded that the two genome-wide significant variants represented independent genetic signals. Otherwise, their association was capturing the same genetic signal. The 'Metafor' command in R software[64] was used to make Forest plots, and the LocusZoom browser was used for creating regional association plots.[65]

Testing allele frequencies in athletes versus population controls

The genome-wide significant index variants were genotyped in the four cohorts of elite athletes from different disciplines and populations, i.e. Swedish cross-country skiers.[66] Spanish athletes from different disciplines,[67] Polish speed skaters, and Jamaican sprinters (up to 400 m and in jump and throw events)[68] and in corresponding population-matched controls of non-athlete status. Since the athletes originated from different world populations (Sweden, Spain, Poland, and Jamaica) we normalized the G-allele frequency at rs115660502 in the athletes by G-allele frequency in the control (non-athletes) group from the corresponding population. For example, the ratio of the G-allele frequency in Swedish skiers to the G-allele frequency in Swedish controls was ∼2.5, while the corresponding ratio for Jamaican sprinters was ∼0.5, suggesting that the G-allele of rs115660502 is over-represented in endurance sports (skiing) and under-represented in power sports (sprinting). To test for significance, resampling with replacement by randomly drawing an equal number of controls as athletes and calculating ratios 100 000 times was done to build confidence intervals. The same resampling procedure was repeated for building the empirical distribution of G-allele frequencies in all populations. Next, statistical significance was tested by counting the number of times the re-sampled G-allele frequency of the controls was different or equal to the respective athletes. We defined athletes competing in cross-country skiing and triathlon as extreme endurance athletes (i.e., disciplines with > 1.5 h of total uninterrupted physically demanding performance time) and athletes competing in sprint running as extreme power athletes (i.e., disciplines with < 60 s of total performance time). Other disciplines were defined as not being extreme in their physical profile, e.g., skating, basketball, and judo.

eQTL analysis

The eQTL analysis was done in three cohorts of Swedish ancestry, i.e. the Malmö Exercise Intervention study (MEI, n=46, Table S9),[69,70] the Malmö Men study (MM, n=128, Table S2)[18] and the MSAT study (MSAT, n=39, Table S8). The MEI cohort consisted of men aged 37.7 ± 4.3 years [mean ± SD] and BMI = 28.0 ± 3.1 kg/m^2 [mean ± SD], including 22 participants with and 24 without a first-degree family member with T2D. eQTL analyses were done using Affymetrix microarray expression data from the MEI (n = 39; 23,941 probe sets) and MM (n = 38; 22,283 probe sets) cohorts. Genome-wide significant variants from the meta-analysis for each phenotype were tested for linear associations with gene expression levels using the 'Matrix_eQTL' command in R.[71] Cis-eQTL (within a 1 Mb window) was performed separately for MEI, MM and MSAT with the corresponding False Discovery Rate (FDR) correction for multiple testing (FDR<5%). To be consistent with the primary GWAS analyses, we used age and BMI as covariates for eQTL analysis. The results of the eQTL analysis were meta-analyzed with Stouffer's z-score method. The R commands "hgu133a.db" and "nugohs1a520180.db" were used for probeset-gene annotation. We conducted an eQTL analysis in the MM, MEI, and MSAT datasets using the MatrixEQTL[71] package to estimate beta coefficients and standard errors. In addition, we extracted beta and standard error estimates for muscle tissues from the public FUSION and GTEx v7 data. To integrate these estimates, we performed a meta-analysis using the meta package in R,[72] employing a random effects model to account for the heterogeneity of microarray and RNA-Seq expression data combination.

Culture of human microvascular endothelial cells (HMEC-1)

HMEC-1 cells (ATCC, VA, USA) were grown at 37°C and 5% CO_2 in growth medium (MCDB131 medium (Thermo Fischer Scientific) supplemented with 10 ng/ml EGF (Thermo Fischer Scientific), 1 μg/ml hydrocortisone (Merck), 10 mM GlutaMAX (Thermo Fischer Scientific, 10% FBS (Sigma) and Antibiotic-Antimycotic solution (Thermo Fisher Scientific) on tissue culture plates precoated with

Attachment Factor (Thermo Fisher Scientific). Cells were passaged at around 70-80% confluence. At every subculturing, number of cells were estimated using a Bürker Chamber (VWR). Testing for mycoplasma infection was done routinely.

Quantitative real-time PCR

Verification of a sustained CRISPR/Cas9-mediated knockdown of RAB3GAP2 and verification of knockdown of RAB3B and RAB18 with siRNA in HMEC cells, as well as analysis of the expression of RAB3GAP2 mRNA in human skeletal muscle was done using quantitative real-time PCR. RNA was isolated with the RNeasy Plus Mini Kit (Qiagen, Hilden, Germany) and concentration and purity were measured using a NanoDrop ND-1000 spectrophotometer (A260 / A280 > 1.8 and A260 / A230 > 1.0) (NanoDrop Technologies, Wilmington, DE, USA). Reverse transcription of 500 ng RNA was performed using the QuantiTect Reverse Transcription kit (Qiagen). quantitative real-time PCR was run on a Viia 7 real-time PCR system (Thermo Fisher Scientific, MA, USA) with 2 ng cDNA in 10 μl reactions and TaqMan Gene Expression Master Mix according to the manufacturer's instructions (Applied Biosystems, Thermo Fisher Scientific). Samples for each gene were analyzed in triplicates on the same 384 well plate with 3 endogenous controls (POL2A, HPRT1 and PPIA). The expression levels were calculated and normalized by geometric averaging of the endogenous controls as previously described.[73] TaqMan Assays used: RAB3GAP2 (exon 24-25 boundary) (Hs00202700_m1), RAB3GAP2 (exon 3-4 boundary) (Hs01073425_m1), RAB3B (Hs01001137_m1) and RAB18 (Hs00222021_m1) (Thermo Fisher Scientific). Endogenous control assays: POLR2A (Hs00172187_m1), HPRT1 (4326321E, VIC-MGB) and PPIA (4326316E, VIC-MGB).

RNA sequencing

HMEC-1 cells grown at a confluence of ~70-80%, were washed in PBS, detached using TrypLE (Thermo Fisher Scientific, Waltham, MA, USA) and counted. RNA was extracted from ~500k cells lysed in RLT plus lysis buffer (Qiagen, Hilden, Germany), using the RNeasy Plus Mini Kit (Qiagen). RNA concentration was determined using a NanoDrop ND-1000 spectrophotometer (A260 / A280 > 1.8 and A260 / A230 > 1.0) (NanoDrop Technologies, Wilmington, DE, USA) and RNA integrity was verified using the 2200 TapeStation instrument (Agilent Technologies, CA, US). RNA sequencing was performed on 500 ng input RNA. Library preparation was made using the TruSeq Stranded Total RNA Library Prep Kit with Ribo-Zero Human/Mouse/Rat Set A (Illumina, San Diego, CA, USA) and sequencing was performed on a NextSeq 500 instrument using the NextSeq® 500/550 High Output Kit v2 (150 cycles) (Illumina). Transcript expression quantification was performed with Salmon v1.3.0.[51] Differential gene expression analysis was carried out using DESeq2 v1.26.0.[52]

ELITE ATHLETE GENE EXPRESSION STUDY. Prior to taking a muscle biopsy from the vastus lateralis of the left leg (in the morning), athletes were asked not to train for one day to analyze their gene expression profiles in a resting state. RNeasy Mini Fibrous Tissue Kit (Qiagen, Hilden, Germany) was used to isolate RNA from 19 muscle tissue samples of Russian athletes (7 strength and 12 endurance athletes). Frozen tissue samples were placed in a box submerged in liquid nitrogen. Each sample was transferred without thawing on a sterile Petri dish placed on a frozen plastic ice pack. A piece of tissue with a weight of 10 mg was separated with a sterile scalpel and immediately placed in a 2 mL safe-lock microcentrifuge tube containing 300 μL of lysis buffer and one sterile stainless-steel bead with a diameter of 4 mm. Samples were homogenized using the TissueLyser II system (Qiagen, Hilden, Germany) shaking twice for 2 min at 25 Hz. RNA samples were isolated according to the manufacturer's guidelines. RNA concentration was measured using the Qubit spectrophotometer (Thermo Fisher Scientific, Waltham, MA, USA). RNA quality was assessed using the BioAnalyzer electrophoresis system and BioAnalyzer RNA Nano assay (Agilent Technologies, Santa Clara, CA, USA). RNA integrity number (RIN) was calculated for each RNA sample. Only RNA samples with RIN > 7 were included in the study. Samples were stored at −80°C until sequencing libraries were prepared. Total RNA samples were treated with DNAse I using a Turbo DNA-free Kit (Thermo Fisher Scientific) according to the kit guidelines. Libraries for RNA sequencing were prepared using NEBNext Ultra II Directional RNA Library Prep Kit for Illumina with the NEBNext rRNA Depletion Module (New England Biolabs, Ipswich, MA, USA). RNA libraries were sequenced on the HiSeq system (Illumina, San Diego, CA, USA) with 250 cycles. Sequenced reads were pseudoaligned to hg38 gencode (v37) transcriptome using kallisto v0.48.0[53] with default settings. Gene level expression abundances were calculated using the tximport Bioconductor package.[54] Expression of the RAB3GAP2 gene was presented in transcripts per kilobase million (TPM). Data Availability Statement: RNA-seq data of 19 athletes reported in this paper have been deposited in GEO with accession number GSE200398.

HMEC-1 secretion experiments

HMEC-1 cells seeded at a confluence of ~ 60-70% were allowed to grow for 24 h at 37°C and 5% CO_2. Cells were then washed in growth medium (GM) and new GM was added after which the cells were allowed to incubate for an additional 2-3h at 37oC and 5 % CO2. Cell medium was collected and centrifuged at 200 g for 5 min, and the supernatant was frozen at -20°C. Cells were washed in PBS, detached using TrypLE (Thermo Fisher Scientific) and centrifuged at 200 g for 5 min and the pellet was frozen at -20°C. Total DNA was extracted from the cells using the DNeasy Blood & Tissue Kit (Qiagen, Hilden, Germany) and DNA concentration was determined using a NanoDrop ND-1000 spectrophotometer (NanoDrop Technologies, Wilmington, DE, USA). Secreted factors were measured in 40 μl of supernatant using the Olink Target 96 immunoassay panels for protein biomarker discovery (Olink, Uppsala, Sweden). Panels used in the analysis were the Cardiometabolic, Oncology II, Cardiovascular III and the Immuno-Oncology panel where each panel offers the simultaneous detection of 92 biomarkers (for a full list see: https://www.olink.com/products/target/). Relative quantification of biomarkers is made by generating normalized protein expression (NPX) values in arbitrary units. Results are then divided by cell DNA content to adjust for cell density.

Immunohistochemistry (IHC) and immunofluorescence (IF) of frozen human muscle biopsies

5 μm thick sections of human skeletal muscle tissue were fixed in ice-cold acetone, rinsed in PBS and permeabilized in 0,5% TritonX-100. Sections for IHC, were incubated with 0,3% hydrogen peroxide solution. Sections were blocked with 10% normal goat serum or 10% bovine serum albumin followed by incubation with 0,1 μg/ml or 0.5 μg/ml rabbit anti-RAB3GAP2 antibody (Atlas antibodies, Bromma, Sweden), for IHC and IF respectively. Sections were washed in PBS and incubated with biotinylated goat anti-rabbit IgG (1:1000, Vector Laboratories, Burlingame, CA, USA) or with Cy-5 conjugated donkey anti-rabbit IgG (1:400, Jackson Immuno Research, Cambridge, UK) for IHC and IF respectively. Non-immune rabbit IgG (Abcam, Cambridge, UK) was used as a negative control. For the IHC sections, an ABC kit (Vectastain Elite, Standard, Vector Laboratories, Burlingame, CA) and immPACT-DAB (Vector Laboratories) were used. After counter staining with Mayers hematoxylin, sections were mounted and imaged using an Aperio ScanScope CS scanner. For endothelial cell identification, sections for IF were counterstained either with 2.0 μg/ml mouse anti-CD31 (Dako, Glostrup, Denmark) and Alexa488 conjugated goat anti-mouse IgG (1:400; Abcam) and DAPI (4',6-diamidino-2-phenylindole) for nuclear identification (Vector Laboratories, Burlingame, CA, US); or with Rhodamine labeled Ulex Europaeus Agglutinin I (UEA I) (Vector Laboratories) (10 μg/ml). Sections were mounted and imaged in a Zeiss LSM800 laser scanning confocal microscope (Zeiss, Germany). DAPI (4',6-diamidino-2-phenylindole) was used for nuclear identification. For each individual (n = 11), 2 slides were prepared with 2 sections per slide, one section for the actual staining and the other used as negative control. Depending on the size of the biopsy, between 2 and 7 images per section were acquired and inspected.

IF on HUVEC/HMEC cells

HUVEC or HMEC cells grown on coverslips in 24-well plates were fixed in ice-cold acetone, rinsed in PBS, permeabilized in 0.5% TritonX-100 and blocked with 10% normal bovine serum followed by incubation with 0.5 μg/ml rabbit anti-RAB3GAP2 antibody or 0.5 μg/ml non-immune rabbit IgG followed by incubation with a Cy-5 conjugated donkey anti-rabbit IgG diluted 1:400. SYTOX Green nuclear stain (Thermo Fisher Scientific) diluted 1:3000, was used as a counterstain. After rinsing with PBS, the coverslips were mounted and imaged using a Zeiss LSM 5 laser scanning confocal microscope (Zeiss, Germany).

Immunoblotting

The following antibodies were used for immunoblotting: rabbit anti-RAB3GAP2 (Thermo Fisher Scientific), mouse anti-alpha-tubulin (Abcam, Cambridge, UK), rabbit anti-GAPDH (Abcam). Secondary HRP-conjugated antibodies (goat anti-rabbit, goat anti-mouse) were from Bio-Rad (Hercules, CA, USA). For tissue lysate blots, a pre-blotted membrane with different human tissue lysates was used (INSTA-Blot, Novusbio, Bio-Techne Ltd, Abingdon, UK). For analyses of CRISPR/Cas9 knockdown efficiency on RAB3GAP2, cells were lysed in 2% SDS in PBS with protease inhibitor cocktail (Roche, Basel, Switzerland), passed through QIAshredder minispin columns (Qiagen, Hilden, Germany) to reduce the viscosity, and the protein content was quantified using a BCA Protein Assay Kit (Thermo Fisher Scientific). 20 μg of protein was run on a 4-20% Mini-Protean TGX SDS-PAGE gel (Bio-Rad) and electroblotted onto a nitrocellulose membrane (Bio-Rad). From this point, for both human tissue lysate blots and the CRISPR knockdown analysis, the same blotting protocol was used. The membrane was rinsed in TBS, blocked in 5% bovine serum albumin in TBS for 1 h at room temperature, then transferred to antibody incubation buffer (1% bovine serum albumin in TBS with 0.05% Tween-20) with anti-RAB3GAP2 diluted 1:2000, and incubated overnight at 4°C. Next, the membrane was washed for 4 x 5 min in wash buffer (TBS with 0.05% Tween-20) and incubated with HRP-conjugated anti-rabbit diluted 1:10000 in antibody incubation buffer for 1 h at room temperature. The membrane was washed for 4 x 5 min in wash buffer and developed using SuperSignal West Pico PLUS Chemiluminescent Substrate (Thermo Fisher Scientific) and a CCD camera (Bio-Rad). For the second blotting step the membrane was stripped in Restore Western Blot Stripping Buffer (Thermo Fisher Scientific), then the previously described blotting protocol was followed, but using mouse anti-tubulin (diluted 1:5000) or rabbit anti-GAPDH (diluted 1:10000) antibodies, and species-specific secondary HRP-conjugated antibodies.

CRISPR/Cas9 genomic editing of HMEC cells

Synthetic sgRNA containing the sequence ATCTCCAACCAATGATCTTA complementary to the protein-encoding sequence in RAB3GAP2 exon 3 (cut site at Leu-88) was obtained from Integrated DNA Technologies (IDT, Coralville, IO, USA). A non-targeting negative control sgRNA designed to have no genomic homology in human cells (IDT) was complexed and transfected into cells in parallel with the target sgRNA (these cells are here named wildtype). Electroporation of CRISPR/Cas9-sgRNA complex into HMEC cells: 135 pmol Cas9 protein (IDT) was combined with 150 pmol sgRNA in a total volume of 5 μl and incubated for 15 min. Next, the ribonucleoprotein complex was combined with 1 million HMEC cells suspended in 100 μl nucleofection buffer kit V (Lonza, Basel, Switzerland), electroporated using T-020 program on Amaxa nucleofector IIb (Lonza), and the cells were seeded in 6-well plates. To evaluate the CRISPR/Cas9 editing efficiency, genomic DNA was extracted from the cells five days post-nucleofection using a DNeasy Blood & Tissue Kit (Qiagen, Hilden, Germany) and used to PCR amplify the genomic region surrounding the sgRNA-targeted locus. The primers used were: GGAGAAAGAGGGAAATGGAGAG and CCCACAGGAAGAAGAAGGAAATA. PCR was performed using an AmpliTaq Gold 360 Master Mix (Thermo Fisher Scientific) following the manufacturer's protocol, but with an annealing temperature of 58°C. PCR amplicons were then purified using a GeneJET PCR Purification Kit (Thermo Fisher Scientific) and submitted for Sanger sequencing (Eurofins Genomics, Ebersberg, Germany) using the primer AAACTTCCTGGGCTCCAAGATTG. Additionally, the CRISPR/Cas9 editing efficiency was evaluated using an Alt-R Genome Editing Detection Kit (IDT) that employs T7 endonuclease to detect indel-caused heteroduplexes in re-hybridized PCR amplicons. The edited cells were then expanded

and RAB3GAP2 protein content was detected using immunoblotting. To detect possible off-targeting effects caused by CRISPR/Cas9 editing, we PCR-amplified five loci with the highest off-targeting potential, as assessed by the IDT CRISPR-Cas9 guide RNA design checker. AmpliTaq Gold 360 Master Mix (Thermo Fisher Scientific) was used for the PCR, according to the manufacturer's protocol. The amplicons were purified using a GeneJET PCR Purification Kit (Thermo Fisher Scientific) and submitted for Sanger sequencing (Eurofins Genomics). No traces of Cas9-induced indels were detected in the sequencing files. The selected genomic loci (hg38) and the corresponding primers were: chr16:61669411 (TCAGGCAAGCCACCAAAT and TGTATGGGAGCAGAG ACTAGAA); chr14:40316144 (GTTCTGTGAAGGCTAAGAGAGG and CCTTCGGGCTTTGTTGTTTC); chr6:66820388 (ATTCACTC CGGCCTTCTAAAC and AGCCCATATAGCCAAGACAATC); chr13:107837835: (CATTCATACCACCTCCCACTATC and CACAGG GAAACCTCCATCAA); chr2:220422562: (AGGTTTACCCACCCAGTTTC and TGAATCCTCATCACCCATCTTC).

Matrigel tube-forming assay

The Matrigel tube-forming assay is a specific and extensively used tool for studying angiogenesis *in vitro*, and a detailed experimental protocol has been previously described.[74] Briefly, HMEC-1 cells, cultured to 80-90% confluence in growth medium, were seeded on 12-well plates precoated with Matrigel at a density of 50k cells/well, and were allowed to incubate for 24 h at 37°C in 5% CO_2. Images of the tubular network formation (between 3-4 images/well) were captured using a brightfield microscope at regular time intervals during the 24 h period. Network formation was analyzed and quantified using the online automated image analysis platform myWim (Wimasis Image Analysis, Cordoba, Spain). The identity of the different images was not disclosed during the analysis.

Live-cell imaging of HMEC-1

HMEC-1 wildtype and RAB3GAP2 knockdown cells were seeded on a 12-well plate precoated with Matrigel at a density of 30 or 40 k cells/well and were allowed to grow overnight at 37°C in 5% CO_2. The following day, fresh growth medium was added to the well, and the plate was transferred to a ZEISS Celldiscoverer 7 system (Zeiss, Germany) for live cell imaging, where cell growth was monitored using transmitted light (phase-gradient contrast) for 72-120 h. An initial image was captured in each well at timepoint zero, then images were acquired every 6 h throughout the experiment. Cells were counted in Arivis Vision4D, v4.0.0 using the "Machine learning segmentation" tool, with the "Fluorescence and EM robust" feature selected. To train the segmentation tool, 20 cells and 6 background segments were manually classified in a randomly chosen image and area. Smoothing was set to sigma 1 and threshold to 72%. This training set was then applied to the entire dataset.

In vivo angiogenesis plug assay

All animal experiments were approved by the local ethical committee for animal care in Lund (M167-15). Matrigel plugs were prepared according to Nowak Sliwinska et al.[75] Harvested HMECs in PBS were mixed with ice cold overnight thawed Matrigel (GFR, Phenol Red-free, BD Biosciences, Franklin Lakes, NJ, USA), at a final concentration of 5 mg/ml, without additional supplements and kept on ice prior to injection. Eight- to eighteen-week-old female NSG mice were anaesthetized with isoflurane, the groin was shaved and cleaned before injection of 100µl of cold Matrigel solution containing 1 x 10^6 HMECs per plug into the groin area. After 30 s gelling time the needle was removed, and the mice were removed from anesthesia. After 7 days, mice were anesthetized with 2.5% Avertin (12.5 mg/kg body weight; Sigma-Aldrich, Merck, Darmstadt, Germany), plugs were removed and fixed overnight before paraffin embedding. Sections were stained with the connective tissue stain, Trichrome (Abcam, Cambridge, UK).

Migration analysis using the wound healing assay

A cell-free gap was created using 2-well cell culture inserts placed in a 35mm µ-dish (Ibidi GmbH, Germany). Briefly, wildtype and RAB3GAP2 knockdown HMEC cells were seeded on both wells of a 2-well cell culture insert. After a 24 h incubation, the inserts were removed, and the optically confluent cells were allowed to migrate over the 500µm cell-free gap created by the inserts. Images were captured at regular time intervals.

Knockdown of RAB18 and RAB3B with siRNA

HMEC-1 cells (50 000 / well) were seeded on 6-well plates. After 24h, cells were transfected with 10nM siRNA targeting RAB18 or RAB3B (Thermo Fisher Scientific), or a scrambled negative control siRNA using lipofectamine (Lipofectamine™ RNAiMAX, Thermo Fisher Scientific). After 24 h, transfection medium was replaced with growth medium in which the cells were allowed to grow for another 24-48 h before cells were detached and quantified using a Bürker Chamber (VWR). Knockdown was confirmed with qPCR (see qPCR section for information on TaqMan assays). To analyze secretion of tenascin-C (TNC) into the medium, growth medium was collected 48h after transfection medium was removed. Amount of TNC protein was estimated using the Invitrogen™ Human Tenascin C ELISA Kit (Thermo Fisher Scientific).

QUANTIFICATION AND STATISTICAL ANALYSIS

Generally

All statistical details can be found in the results section, included in text, figures, tables and supplemental materials. Results are expressed as median with range or as individual level data. All statistical tests used are given together with the p-values in the text and

figures. Non-parametric tests have been used, e.g. Mann-Whitney U and Wilcoxon. The number of n in experiments reflects the number of independent experiments (i.e. technical replicates are not used as n). Further details of selected experiments can be found below.

Phenotypes in ULSAM, MM, and MSAT cohorts

Computer image analysis was performed using image analysis equipment, for ULSAM (Multisync II, BIO-RAD SA, Richmond, CA, USA) and for MM, MEI and MSAT (BioPix IQ 2.0.16 software, BioPix AB, Sweden). The phenotypes and sample sizes for each phenotype are reported in Tables S6, S7, S8 and S9. Spearman correlation matrices for C:F and fiber type, stratified by cohort, are presented in Tables S1 and S2. Within each cohort, all phenotypes were pre-adjusted for age and BMI, and inverse rank-normal transformed using the Rankit equation to provide normal data distributions. C:F was not measured in the MSAT and MEI cohorts.

Genotyping of the ULSAM, MM, and MEI cohorts

Genotypes were called using the Illumina Genome studio software, as described in detail elsewhere.[59] Individuals were excluded on the basis of: call rate <95%; gender mismatch; relatedness; and non-European ancestry. Variants were excluded on the basis of: call rate <95% (>99% for MAF <5%); exact p-value for Hardy-Weinberg equilibrium $<10^{-6}$; and MAF <1%. Genotyping of the different cohorts of imputed genome-wide significant variants from the meta-analysis were done using either TaqMan PCR or Sequenom platforms according to the manufacturer's instructions. For TaqMan an ABI Prism Sequence Detection System ABI 7900HT (Applied Biosystems) was used for post-PCR allelic discrimination by measuring allele-specific fluorescence. The results were in Hardy-Weinberg equilibrium ($p<1x10^{-4}$).

Genotyping of the replication cohort of athletes

Ten percent of samples were genotyped twice with a 100% success rate of reproducibility. Bcftools was used for vcf files conversion. Phasing and imputation of genotypes were done using shapeit2 and impute2 programs.

Genotyping of the muscle injury cohort (J-HAP)

Genome-wide SNP genotypes were determined by the Japonica Array ver. 1 (Toshiba, Tokyo, Japan). Standard quality control (QC), imputation with IMPUTE2 using 3.5KJPN haplotype reference panel, and post imputation QC (Imputation quality r2 > 0.3; SNP Call rate > 0.97; Hardy–Weinberg equilibrium, P > 1E-6; Minor Allele Frequency > 0.05) were performed. Genotype data of the rs11547779 was extracted from the imputed genotype data. Association analysis of the rs11547779 polymorphism with muscle injury was conducted using the Cochran-Armitage trend test. The odds ratio (OR) and 95% confidence interval (CI) were calculated under the additive genetic model.

Imputation and meta-analysis

Genotype data in each cohort were imputed up to 35 million variants from the 1000 Genomes reference panel (all ancestries, March 2012). Prephasing of haplotypes and imputation were performed using ShapeIT[60] and IMPUTE2,[61] respectively. The association within each cohort was performed using the SNPTEST frequentist score additive model test.[62] Genetic variants that had poor imputation quality inferred by an info score $\leq$0.4 and/or had high standard error (SE>10) were excluded from meta-analyses. A conservative filtering of genetic variants with respect to strand inconsistencies was performed prior to meta-analysis. Fixed effects meta-analyses were undertaken on the summary statistics obtained from the two cohorts using GWAMA,[63] with phenotypes inverse rank-normal transformed and pre-adjusted for age and BMI. Post-meta-analysis QC included removing variants that: a) were detectable only in one cohort and b) had a total minor allele count <10. To validate the quality of imputation, all imputed genome-wide significant SNPs were directly typed in the MM cohort. The imputation error rates vary from variant to variant (i.e., from 0-4% for common homozygotes, 0-86% for heterozygotes), and these error rates were inversely related to the imputation info score. To ensure that findings were not biased by factors related to genotype imputation, genetic association analyses were re-run using directly genotyped data, which did not indicate any major influence of imputation on the results. Results from the directly genotyped, rather than imputed, data are generally presented in the manuscript. Analyses conditioning on variants associated with the index traits at a level of genome-wide significance ($P<5x10^{-8}$) were undertaken to discover possible secondary association signals in corresponding regions. The conditional analyses were conducted on individual-level data and performed separately for ULSAM and Malmö Men datasets. In case more than one variant located on the same haplotype was found to be associated at the genome-wide significance level, and the associated variants were not in a strong linkage disequilibrium (LD) with each other, we tested for secondary / independent association. For this purpose, an analysis was performed, where association analysis of all genetic variants from the haplotype region was re-run adjusting for the genome-wide significant variants sequentially one-by-one. If the association with $P<5x10^{-8}$ remained after adjusting for another neighboring genome-wide significant variant, we concluded that the two genome-wide significant variants represented independent genetic signals. Otherwise, their association was capturing the same genetic signal. The 'Metafor' command in R software[64] was used to make Forest plots, and the LocusZoom browser was used for creating regional association plots.[65]

Testing allele frequencies in athletes vs. population controls

The genome-wide significant index variants were genotyped in the four cohorts of elite athletes from different disciplines and populations, and in corresponding population-matched controls of non-athlete status. Since the athletes originated from different world populations (Sweden, Spain, Poland, and Jamaica) we normalized the G-allele frequency at rs115660502 in the athletes by G-allele frequency in the control (non-athletes) group from the corresponding population. For example, the ratio of the G-allele frequency in Swedish skiers to the G-allele frequency in Swedish controls was ~2.5, while the corresponding ratio for Jamaican sprinters was ~0.5, suggesting that the G-allele of rs115660502 is over-represented in endurance sports (skiing) and under-represented in power sports (sprinting). To test for significance, resampling with replacement by randomly drawing an equal number of controls as athletes and calculating ratios 100 000 times was done to build confidence intervals. The same resampling procedure was repeated for building the empirical distribution of G-allele frequencies in all populations. Next, statistical significance was tested by counting the number of times the re-sampled G-allele frequency of the controls was different or equal to the respective athletes. We defined athletes competing in cross-country skiing and triathlon as extreme endurance athletes (i.e., disciplines with > 1.5 h of total uninterrupted physically demanding performance time) and athletes competing in sprint running as extreme power athletes (i.e., disciplines with < 60 s of total performance time). Other disciplines were defined as not being extreme in their physical profile, e.g., skating, basketball, and judo.

eQTL analysis

Genome-wide significant variants from the meta-analysis for each phenotype were tested for linear associations with gene expression levels using the 'Matrix_eQTL' command in R.[71] Cis-eQTL (within a 1 Mb window) was performed separately for MEI, MM and MSAT with the corresponding False Discovery Rate (FDR) correction for multiple testing (FDR<5%). To be consistent with the primary GWAS analyses, we used age and BMI as covariates for eQTL analysis. The results of the eQTL analysis were meta-analyzed with Stouffer's z-score method. The R commands "hgu133a.db" and "nugohs1a520180.db" were used for probeset-gene annotation. We conducted an eQTL analysis in the MM, MEI, and MSAT datasets using the MatrixEQTL[71] package to estimate beta coefficients and standard errors. In addition, we extracted beta and standard error estimates for muscle tissues from the public FUSION and GTEx v7 data. To integrate these estimates, we performed a meta-analysis using the meta package in R,[72] employing a random effects model to account for the heterogeneity of microarray and RNA-Seq expression data combination.

Quantitative real-time PCR

The expression levels were calculated and normalized by geometric averaging of the endogenous controls as previously described.[73]

RNA sequencing

For the RNA sequencing screen in HMECs with or without CRISPR-Cas9-mediated knockdown of RAB3GAP2 expression, transcript expression quantification was performed with Salmon v1.3.0.[51] Differential gene expression analysis was carried out using DESeq2 v1.26.0.[52]

For the elite athlete gene expression study, sequenced reads were pseudoaligned to hg38 gencode (v37) transcriptome using kallisto v0.48.0[53] with default settings. Gene level expression abundances were calculated using the tximport Bioconductor package.[54] Expression of the RAB3GAP2 gene was presented in transcripts per kilobase million (TPM). Data Availability Statement: RNA-seq data of 19 athletes reported in this paper have been deposited in GEO with accession number GSE200398.

HMEC-1 secretion experiments

Secreted factors were measured in supernatant using the Olink Target 96 immunoassay panels for protein biomarker discovery (Olink, Uppsala, Sweden). Panels used in the analysis were the Cardiometabolic, Oncology II, Cardiovascular III and the Immuno-Oncology panel where each panel offers the simultaneous detection of 92 biomarkers (for a full list see: https://www.olink.com/products/target/). Relative quantification of biomarkers was made by generating normalized protein expression (NPX) values in arbitrary units. Results were then divided by cell DNA content to adjust for cell density.

Matrigel tube-forming assay

Images of the tubular network formation were analyzed and quantified using the online automated image analysis platform myWim (Wimasis Image Analysis, Cordoba, Spain). The identity of the different images was not disclosed during the analysis.

Live-cell imaging of HMEC-1 cells

Cells were counted in Arivis Vision4D, v4.0.0 using the "Machine learning segmentation" tool, with the "Fluorescence and EM robust" feature selected. To train the segmentation tool, 20 cells and 6 background segments were manually classified in a randomly chosen image and area. Smoothing was set to sigma 1 and threshold to 72%. This training set was then applied to the entire dataset.

Cell Reports, Volume *45*

Supplemental information

RAB3GAP2 is a regulator of skeletal muscle endothelial cell proliferation and associated with capillary-to-fiber ratio

Kristoffer Ström, Nikolay Oskolkov, Tugce Karaderi, Sebastian Kalamajski, Bilal A. Mir, Ola Ekström, Eri Miyamoto-Mikami, Claes Ladenvall, Ellen Kakulidis, Steven Reid, Anna-Maria Dutius Andersson, Dmytro Kryvokhyzha, Enming Zhang, Joao Fadista, Manonanthini Thangam, Motoyuki Iemitsu, Ekaterina A. Semenova, Andrey K. Larin, Rinat I. Sultanov, Konstantin A. Babalyan, Andrey V. Zhelankin, Nikolay A. Kulemin, Edward V. Generozov, Michael Hultström, Robert Frithiof, Hugo Zeberg, Miklos Lipcsey, Anders Larsson, Anubha Mahajan, Emma Ahlqvist, Rashmi B. Prasad, Kay Prüfer, CHARGE Hemostasis Working Group, Maria Sabater-Lleal, Nicholas L. Smith, Abbas Dehghan, Lars Lind, Kerry McGawley, Andrew P. Morris, Johan P.A. Andersson, Mikko Lehtovirta, Łukasz Szczerbiński, Adam Kretowski, Ildus I. Ahmetov, Guan Wang, Yannis Pitsiladis, Alejandro Santos-Lozano, Alejandro Lucia, Noriyuki Fuku, Hans-Christer Holmberg, Maria F. Gomez, Karl-Fredrik Eriksson, Kristian Pietras, Cecilia M. Lindgren, Paul W. Franks, and Ola Hansson

Supplemental Figures

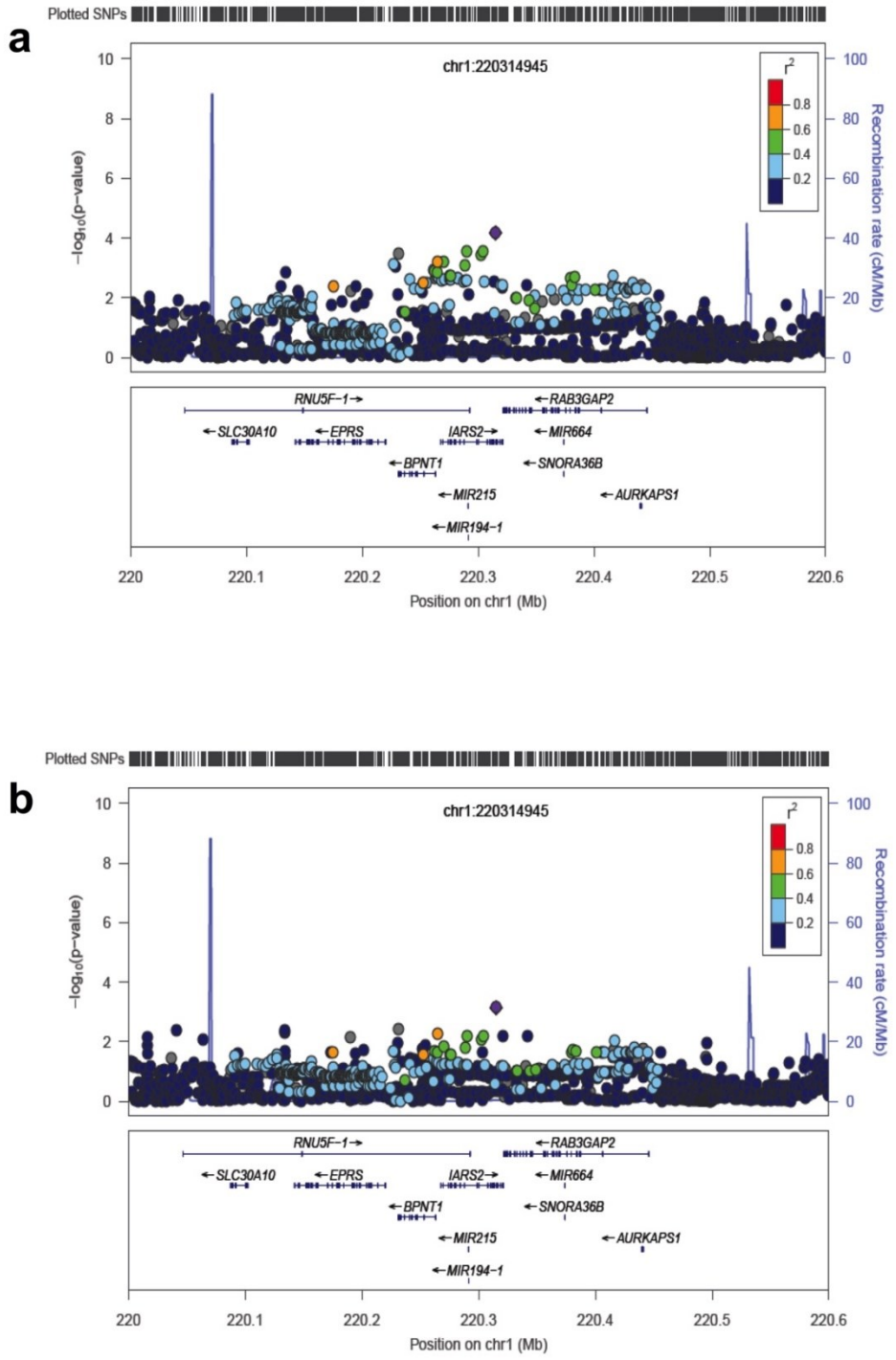

Supplemental Figure S1. Enlarged view of genetic locus (LocusZoom) plots of the region on chromosome 1 associated with capillary density. The purple diamond represents the genetic variant with the lowest p-value (left y-axis) in the region. Other variants (circles) are colored according to their linkage disequilibrium with this variant, *i.e.,* from highest (red) to lowest (dark blue). Estimated recombination rates are shown on the right y-axis. (**a**) Conditioning on the rs115660502 and (**b**) conditioning on the rs191465330.

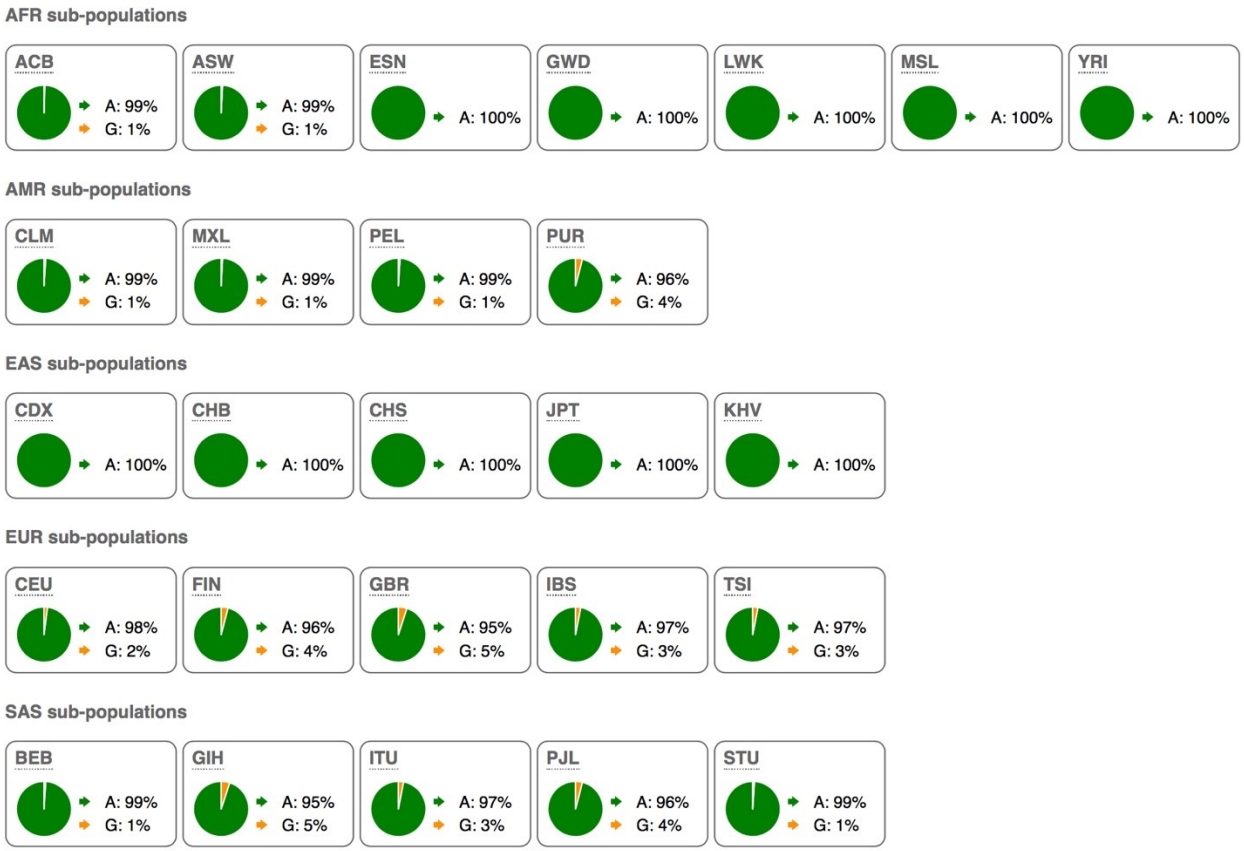

Supplemental Figure S2. Allele frequencies of the rs115660502 in different populations from the 1000G. The geographic distribution of the C:F increasing G-allele indicates that it is a fairly young allele (< 50,000 years) as it is present only in non-African populations or at a low frequency in European-admixed African populations. AFR = African, AMR = Ad Mixed American, EAS = East Asian, EUR = European, SAS = South Asian.

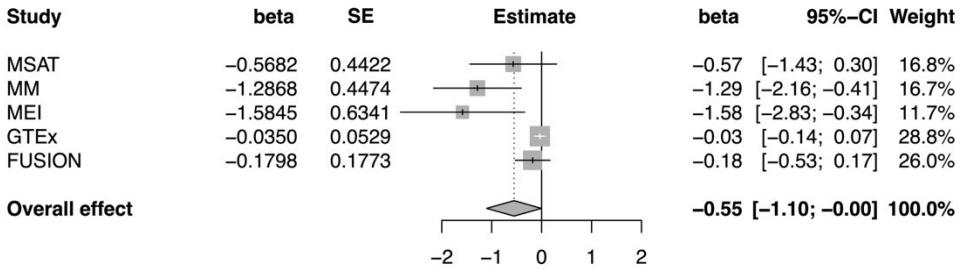

Supplemental Figure S3 Forest plot displaying the results of a meta-analysis of rs115660502 on the beta estimates from five eQTL studies: the Malmö Satellite Cell (MSAT), Malmö Men study (MM), Malmö Exercise Intervention (MEI), GTEx public database, and FUSION Skeletal Muscle Study. Test for overall effect: $z = -1.97$, $P < 0.05$. Heterogeneity: $I^2 = 74\%$, $\tau^2 = 0.27$, $P < 0.01$, $n_{tot} = 1123$.

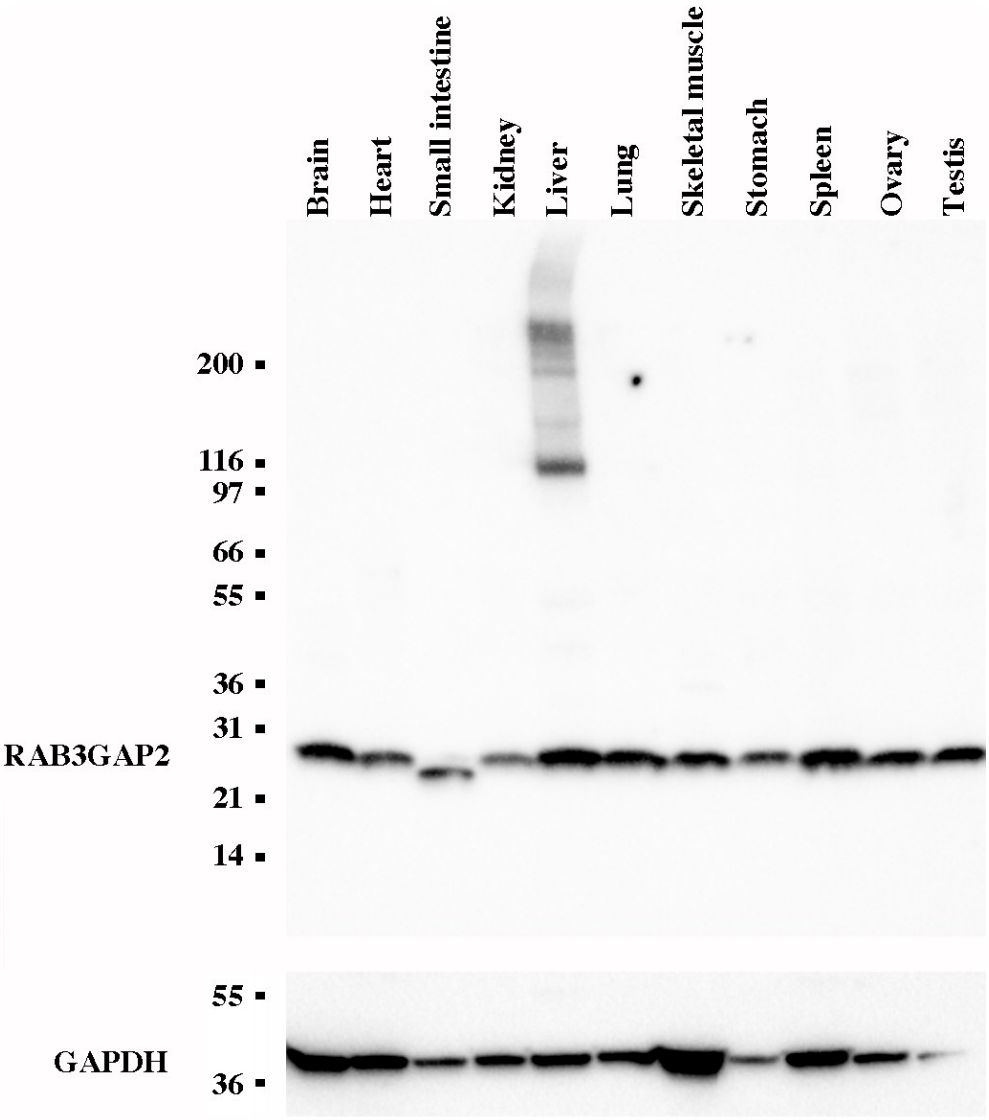

Supplemental Figure S4. The RAB3GAP2 protein is widely expressed in human tissues seen with western blot of RAB3GAP2 with a pre-blotted membrane with different human tissue lysates (Novusbio).

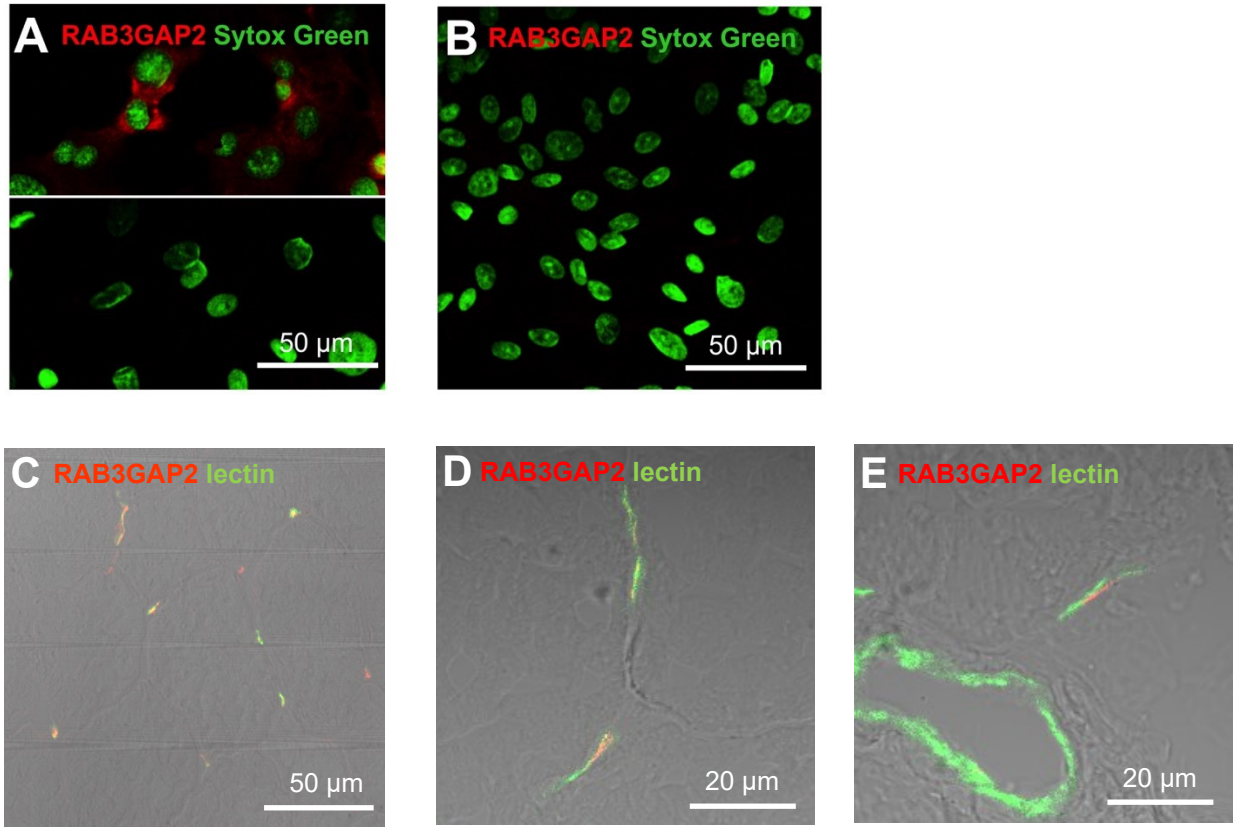

Supplemental Figure S5. (**a**) Representative confocal immunofluorescence images showing staining of human microvascular endothelial cells (HMECs) with rabbit anti-RAB3GAP2 (red; upper panel), or with non-immune isotype control (lower panel). (**b**) Confocal immunofluorescence image of human umbilical vein endothelial cells (HUVECs) showing no detection of RAB3GAP2 (red) when cells are stained as in the upper panel in (**a**). Nuclei were stained with the DNA-binding dye SYTOX Green. The calculated percentage of RAB3GAP2 positive cells was 46% (164 out of 355 cells). Experiments using cultured cells were repeated 3 times. (**c**) Lower and (**d-e**) higher magnification of confocal immunofluorescence images showing RAB3GAP2 expression (red) and the endothelial marker lectin (green) in human skeletal muscle, demonstrating RAB3GAP2 localization to the endothelium in capillaries (**c-d**), but not in the wall of large vessels (**e**). Experiments using sections from skeletal muscle were repeated twice.

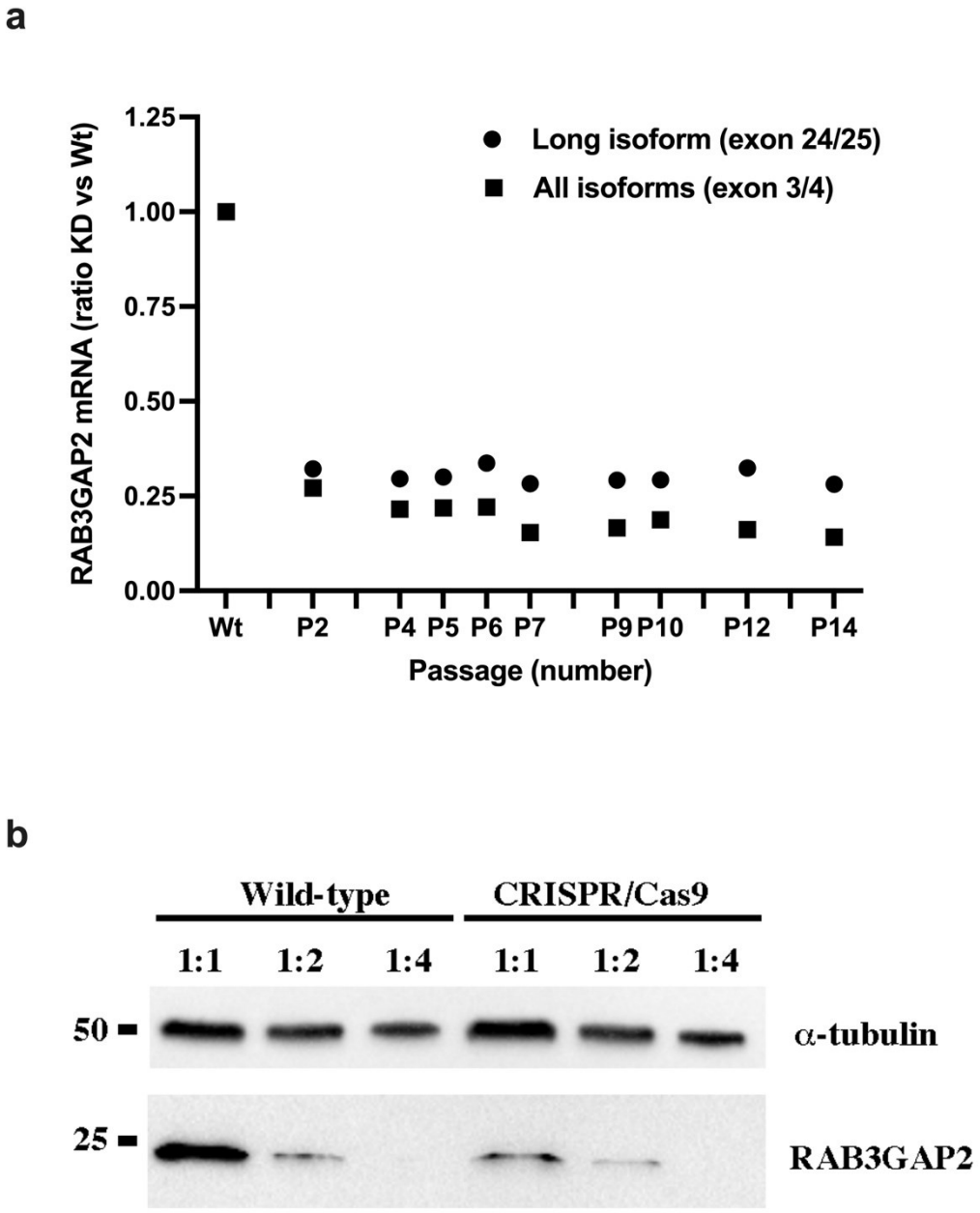

Supplemental Figure S6. (**a**) Sustained CRISPR-Cas9-mediated *RAB3GAP2* mRNA knockdown (KD) in human microvascular endothelial cells (HMEC) in different passages estimated with quantitative real-time PCR. Dots and squares show *RAB3GAP2* KD ratio vs Wildtype of long isoform and all isoforms, respectively. (**b**) Western blot for RAB3GAP2 and alpha-tubulin (reference) on protein lysates obtained from wild-type and *RAB3GAP2* CRISPR/Cas9-mediated knockdown HMEC cells. Different dilutions of protein lysates (1:1, 1:2, 1:4) were loaded on the gel to assess linearity between protein quantity and band intensity.

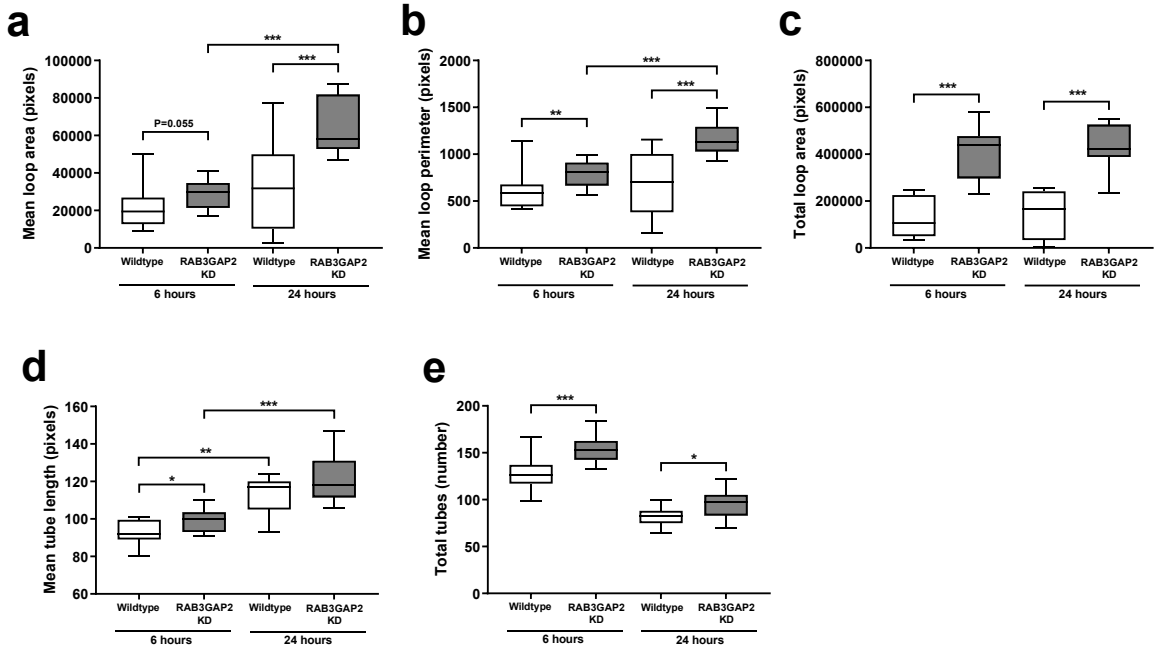

Supplemental Figure S7. Tube formation assay using human microvascular endothelial cells (HMECs) with or without CRISPR-Cas9-mediated knockdown (KD) of *RAB3GAP2*. n = 11 (wildtype) and 13 (*RAB3GAP2* KD) independent experiments at 6 and 24 hours. (**a**) Mean loop area, $p_{\text{Mann-Whitney, 6 h}} = 0.055$, $p_{\text{Mann-Whitney, 24 h}} = 7.0 \times 10^{-4}$ and $p_{\text{Wilcoxon, RAB3GAP2 6h vs 24 h}} = 2.0 \times 10^{-4}$. (**b**) Mean loop perimeter, $p_{\text{Mann-Whitney, 6 h}} = 7.3 \times 10^{-3}$, $p_{\text{Mann-Whitney, 24 h}} = 5.0 \times 10^{-4}$and $p_{\text{Wilcoxon, RAB3GAP2 6h vs 24 h}} = 2.0 \times 10^{-4}$. (**c**) Total loop area, $p_{\text{Mann-Whitney, 6 h}} < 1.0 \times 10^{-4}$ and $p_{\text{Mann-Whitney, 24 h}} < 1.0 \times 10^{-4}$. (**d**) Mean tube length, $p_{\text{Mann-Whitney, 6 h}} = 0.017$, $p_{\text{Mann-Whitney, 24 h}} = 0.257$, $p_{\text{Wilcoxon, wildtype 6h vs 24 h}} = 2.9 \times 10^{-3}$and $p_{\text{Wilcoxon, RAB3GAP2 6h vs 24 h}} = 2.0 \times 10^{-4}$. (**e**) Total tubes, $p_{\text{Mann-Whitney, 6 h}} < 1.0 \times 10^{-3}$ and $p_{\text{Mann-Whitney, 24 h}} = 2.0 \times 10^{-4}$. * $p_{\text{Mann-Whitney}} < 0.05$, ** $p_{\text{Mann-Whitney}}$, $p_{\text{Wilcoxon}} < 0.01$, *** $p_{\text{Mann-Whitney}}$, $p_{\text{Wilcoxon}} < 0.001$.

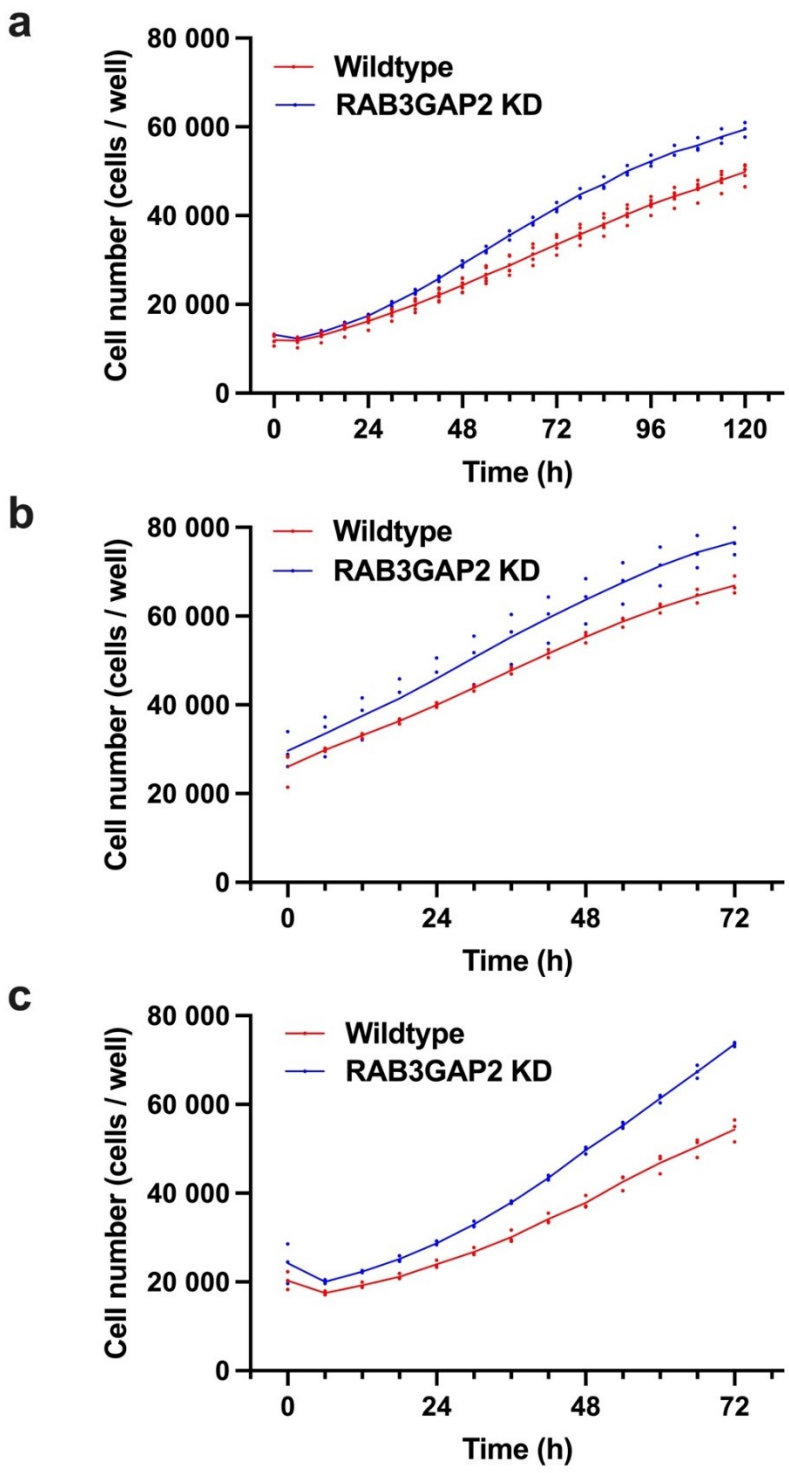

Supplemental Figure S8. (**a-c**) Independent replicates of time-course live cell imaging of human microvascular endothelial cell (HMEC) growth (n = 3) in wildtype (red) and CRISPR-Cas9-mediated *RAB3GAP2* knockdown (blue). Individual replicates are shown, n = 3 per experiment, except for wildtype in (**a**) where n = 6. The data shown in (**a**) is identical to data presented in the main figure 3f.

Wildtype

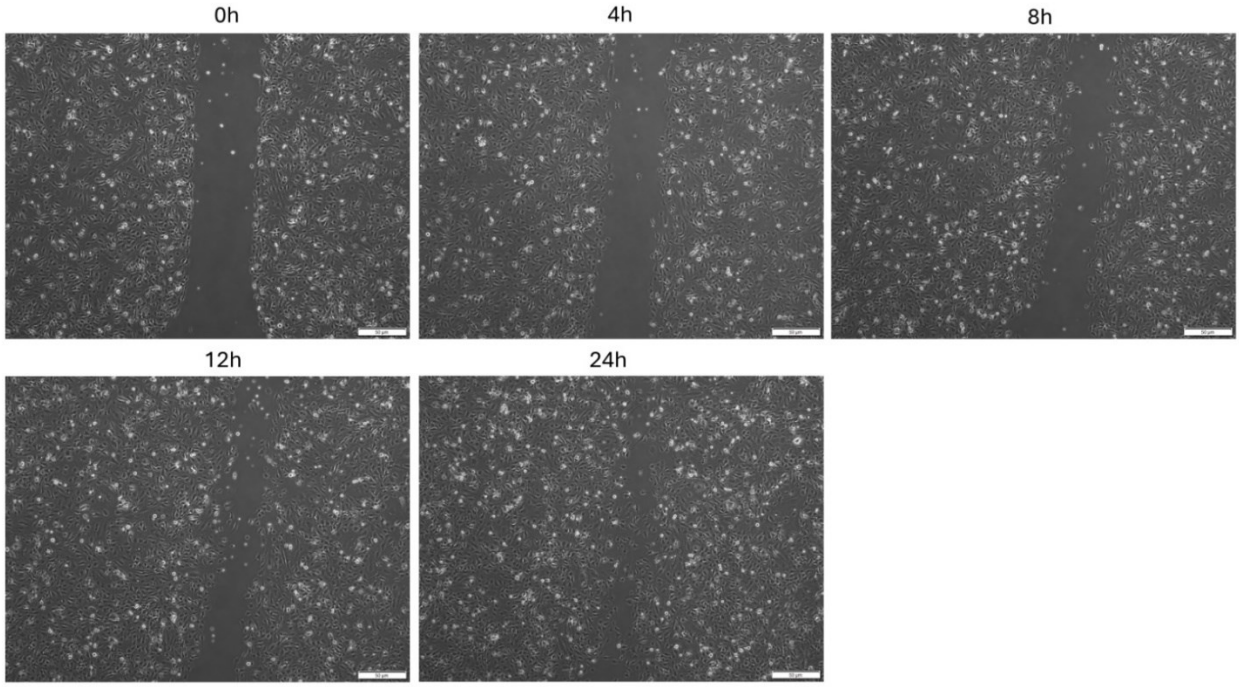

RAB3GAP2 Knockdown

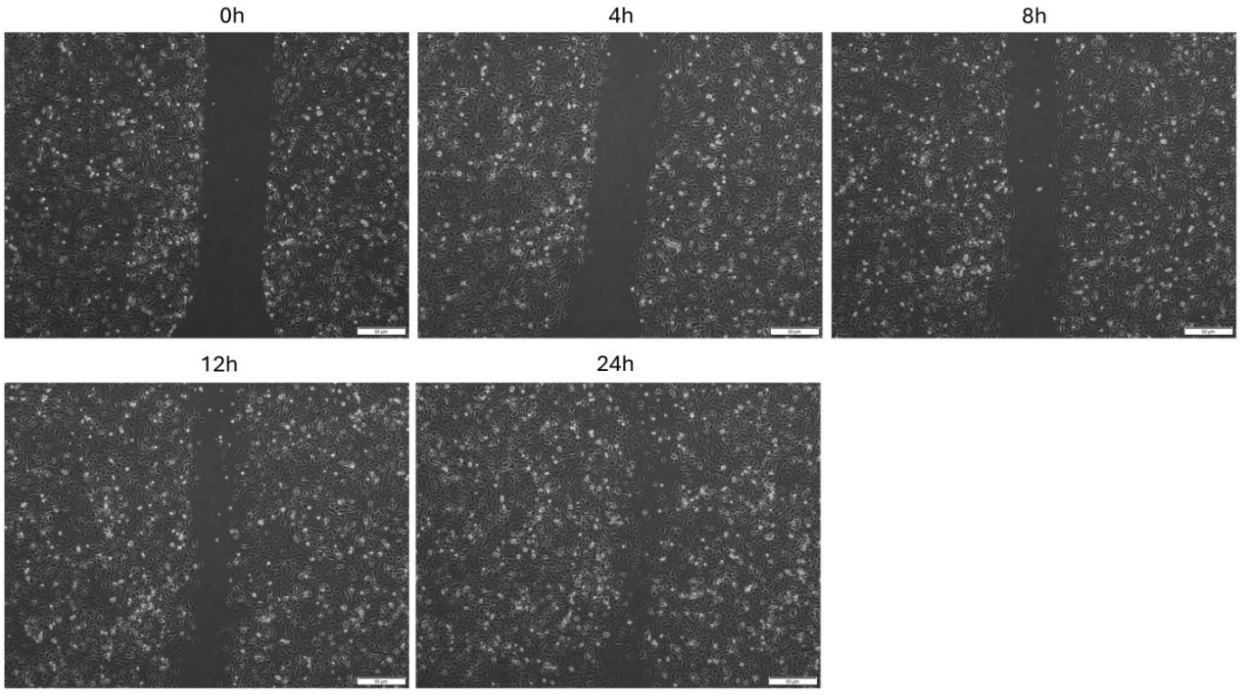

Supplemental Figure S9. Characterization of migratory activity in HMEC Wildtype and *RAB3GAP2* knockdown cells using the basic cell culture wound healing assay. Representative images from five time points (0h, 4h, 8h, 12h and 24h) are shown (n=3).

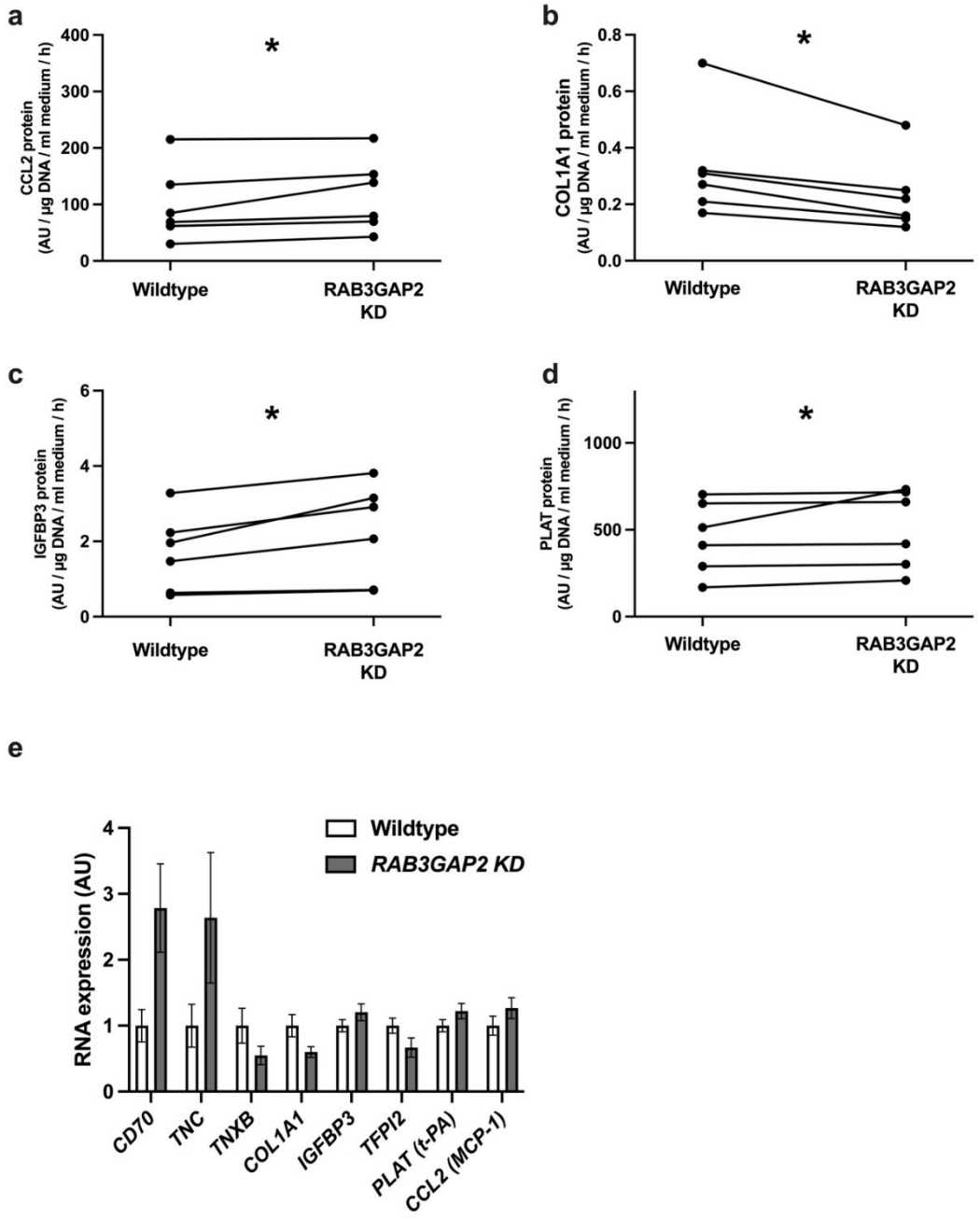

Supplemental Figure S10. (**a-d**) Amount of protein in the cell medium after culturing of human microvascular endothelial cells (HMECs) using Olink panels with or without CRISPR-Cas9-mediated knockdown of *RAB3GAP2*. (**a**) PLAT (**b**) COL1A1, (**c**) IGFBP3, (**d**) CCL2 (* $p_{\text{Wilcoxon}} < 0.05$, n = 6). (**e**) Corresponding RNA expression by RNA sequencing in HMECs from independent experiments, n = 8. CD70 (cluster of differentiation 70), TNC (tenascin C), TNXB (tenascin X), TFPI2 (tissue factor pathway inhibitor 2), PLAT (plasminogen activator, tissue-type) (aka, t-PA), COL1A1 (collagen, type I, alpha 1), IGFBP3 (insulin-like growth factor-binding protein 3), CCL2 (chemokine (C-C motif) ligand 2) (aka, MCP-1 (monocyte chemoattractant protein 1).

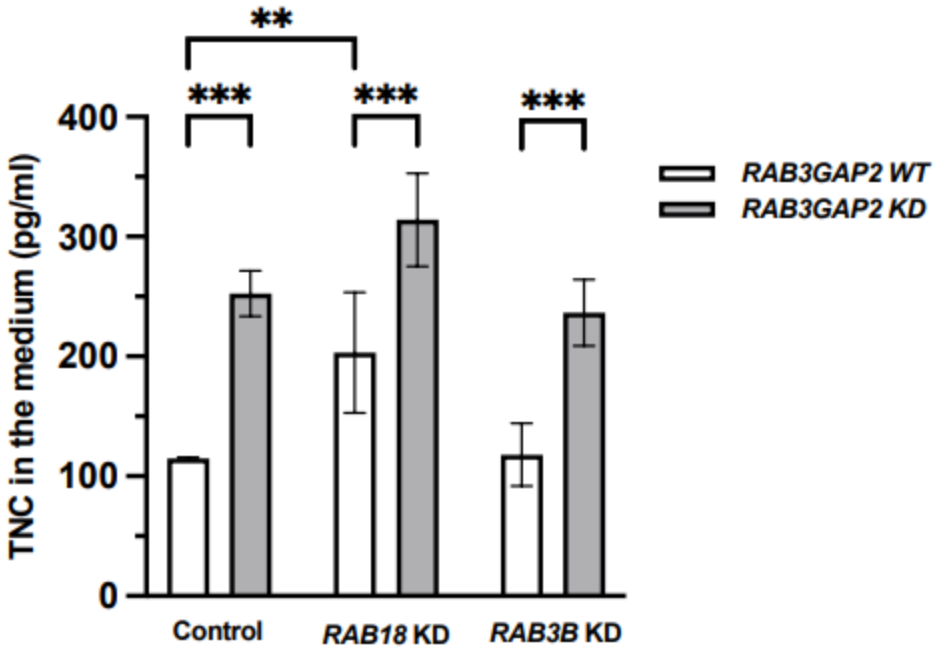

Supplemental Figure S11. Amount of Tenascin C (TNC) protein in the cell medium after culturing of human microvascular endothelial cells (HMECs) with (grey bars) or without (white bars) CRISPR-Cas9-mediated knockdown of *RAB3GAP2*, and with or without siRNA mediated knockdown of *RAB18* or *RAB3B*. Control cells are transfected with negative control siRNA. Data is presented as median ± range. (** $p_{\text{Anova}} < 0.01$, *** $p_{\text{Anova}} < 0.001$, n = 3).

Supplemental Tables

Supplemental Table S1. Description of the Uppsala Longitudinal Study of Adult Men (ULSAM) cohort					
	N	**Minimum**	**Maximum**	**Mean**	**SD**
Age (yrs)	482	69	74	71	1
Body weight (kg^{BW})	482	46	138	80	11
BMI (kg^{BW} / m^2)	482	17	40	26	3
Waist-to-hip ratio	482	0.78	1.12	0.95	0.05
VO_{2peak} (ml / kg^{BW} / min)	N/A	N/A	N/A	N/A	N/A
Type I (%)	482	3	90	49	16
Type IIa (%)	482	5	69	31	13
Type IIX (%)	482	0	59	21	12
Capillary Density (nr / fiber)	482	0.8	3	1.5	0.3

Supplemental Table S2. Description of the Malmö Men (MM) cohort					
	N	**Minimum**	**Maximum**	**Mean**	**SD**
Age (yrs)	128	56	70	66	2
Body weight (kg^{BW})	127	54	114	82	12
BMI (kg^{BW} / m^2)	127	19	36	26	3
Waist-to-hip ratio	125	0.84	1.14	0.97	0.05
VO_{2peak} (ml / kg^{BW} / min)	116	15	51	28	6
Type I (%)	128	10	79	39	13
Type IIa (%)	128	3	73	31	13
Type IIX (%)	126	1	68	29	15
Capillary Density (nr / fiber)	121	0.91	5.35	2.10	0.92

Supplemental Table S3. Spearman correlations between phenotypes in the Uppsala Longitudinal Study of Adult Men (ULSAM) cohort

		Type I	**Type IIA**	**Type IIX**	**Capillary density**
Type I	Correlation coefficient	1.00	-0.66	-0.60	0.35
	p-value	0.000	0.000	0.000	0.000
	n	515	515	515	515
Type IIA	Correlation coefficient	-0.66	1.00	-0.22	-0.22
	p-value	0.000	0.000	0.000	0.000
	n	515	515	515	515
Type IIX	Correlation coefficient	-0.60	-0.22	1.00	-0.22
	p-value	0.000	0.000	0.000	0.000
	n	515	515	515	515
Capillary density	Correlation coefficient	0.35	-0.22	-0.22	1.00
	p-value	0.000	0.000	0.000	0.000
	n	515	515	515	515

Supplemental Table S4. Spearman correlations between phenotypes in the Malmö Men (MM) cohort					
		Type I	**Type IIA**	**Type IIX**	**Capillary density**
Type I	Correlation coefficient	1.00	-0.29	-0.61	0.32
	p-value	0.000	0.001	0.000	0.000
	n	128	128	128	121
Type IIA	Correlation coefficient	-0.29	1.00	-0.52	-0.04
	p-value	0.001	0.000	0.000	0.695
	n	128	128	128	121
Type IIX	Correlation coefficient	-0.61	-0.52	1.00	-0.27
	p-value	0.000	0.000	0.000	0.006
	n	128	128	128	121
Capillary density	Correlation coefficient	0.32	-0.04	-0.27	1.00
	p-value	0.000	0.695	0.006	0.0000
	n	121	121	121	121

Supplemental Table S5. Skeletal muscle eQTLs from the meta-analysis of the Malmö Men (MM) and Malmö Exercise Intervention (MEI) cohorts.

SNP	Gene symbol	Effect Allele	t-stat (MEI)	p-value (MEI)	t-stat (MM)	p-value (MM)	p-value (meta-analysis)	FDR (meta-analysis)
rs115660502	*RAB3GAP2*	G	-3.4	0.002	-2.9	0.006	6.04E-05	0.007
rs191465330	*RAB3GAP2*	A	1.9	0.069	-1.7	0.098	0.025	0.547

Supplemental Table S6. RNAseq of human microvascular endothelial cells (HMEC) with or without knockdown of *RAB3GAP2*. Please see provided Excel file.

Supplemental Table S7. Concentration of secreted proteins in the medium of human microvascular endothelial cells (HMECs) with or without knockdown of *RAB3GAP2*

Gene symbol	Uniprot ID	Olink Assay	mean fold change	SD	p-value
CD70	P32970	CD70	2.05	0.38	0.03
TNC	P24821	TNC	1.97	0.32	0.03
TNXB	P22105	TNXB	0.53	0.11	0.03
TFPI2	P48307	TFPI-2	0.59	0.13	0.03
TNFRSF10C	O14798	TNFRSF10C	0.62	0.19	0.03
VIM	P08670	VIM	1.76	0.73	0.03
PLXNB2	O15031	PLXNB2	1.67	0.55	0.03
TFF3	Q07654	TFF3	0.66	0.12	0.03
NPPB	P16860	NT-proBNP	0.66	0.11	0.03
IL1RL1	Q01638	ST2	0.71	0.15	0.03
COL1A1	P02452	COL1A1	0.70	0.07	0.03
IL17R	Q96F46	IL-17RA	1.43	0.36	0.03
PAM	P19021	PAM	1.30	0.15	0.03
IGFBP3	P17936	IGFBP3	1.30	0.18	0.03
TNFRSF11B	O00300	OPG	0.80	0.09	0.03
TREML2	Q5T2D2	TLT-2	1.26	0.27	0.03
CCL2	P13500	MCP-1	1.25	0.23	0.03
SPP1	P10451	OPN	0.82	0.10	0.03
TNFRSF6B	O95407	TNFRSF6B	0.81	0.08	0.03
PTPRS	Q13332	PTPRS	1.23	0.16	0.03
PLAT	P00750	t-PA	1.13	0.17	0.03
TNFSF10	P50591	TRAIL	0.68	0.22	0.06
MMP12	P39900	MMP12	0.69	0.21	0.06
IGFBP1	P08833	IGFBP-1	0.72	0.16	0.06
PRCP	P42785	PRCP	1.44	0.58	0.06
KIT	P10721	KIT	1.36	0.34	0.06
VEGFA	P15692	VEGFA	1.35	0.28	0.06
CXCL5	P42830	CXCL5	1.30	0.26	0.06
CXCL16	Q9H2A7	CXCL16	1.29	0.26	0.06
PLAU	P00749	uPA	1.28	0.22	0.06
NRP1	O14786	NRP1	1.27	0.26	0.06
ANG	P03950	ANG	1.21	0.19	0.06
MMP2	P08253	MMP-2	0.84	0.12	0.06
CTSZ	Q9UBR2	CTSZ	1.20	0.21	0.06
TGFA	P01135	TGF-alpha	0.91	0.12	0.06
NID1	P14543	NID1	1.10	0.12	0.06
LYVE1	Q9Y5Y7	LYVE1	0.95	0.03	0.06
ICAM1	P05362	ICAM1	1.95	1.03	0.09
CD46	P15529	CD46	1.51	0.52	0.09

NOTCH1	P46531	NOTCH1	1.46	0.50	0.09
ENG	P17813	ENG	1.45	0.61	0.09
GDF15	Q99988	GDF-15	1.41	0.51	0.09
GAS6	Q14393	GAS6	1.32	0.36	0.09
AREG	P15514	AREG	0.83	0.18	0.09
CTSV	O60911	CTSV	1.22	0.18	0.09
TNFRSF1B	P20333	TNF-R2	0.88	0.14	0.09
LTBP2	Q14767	LTBP2	1.11	0.16	0.09
LDLR	P01130	LDL receptor	1.29	0.36	0.13
FGF2	P09038	FGF2	1.21	0.31	0.13
SDC1	P18827	SYND1	1.10	0.14	0.13
MEGF9	Q9H1U4	MEGF9	1.51	0.51	0.16
DPP4	P27487	DPP4	1.43	0.57	0.16
TXLNA	P40222	TXLNA	1.38	0.57	0.16
CD274	Q9NZQ7	PD-L1	1.24	0.51	0.16
TGFBR3	Q03167	TGFBR3	1.21	0.34	0.16
C1QTNF1	Q9BXJ1	C1QTNF1	0.87	0.22	0.16
ITGAV	P06756	ITGAV	1.19	0.24	0.16
TNFSF12	O43508	TWEAK	0.86	0.13	0.16
SIRPA	P78324	SHPS-1	1.17	0.28	0.16
ICAM2	P13598	ICAM-2	0.89	0.15	0.16
TNFRSF1A	P19438	TNF-R1	0.88	0.11	0.16
TGFB1	P01137	LAP TGF-beta-1	1.12	0.21	0.16
FABP4	P15090	FABP4	1.33	0.36	0.19
ABL1	P00519	ABL1	1.27	0.40	0.19
MICA / MICB	Q29983.Q29980	MIC-A/B	0.90	0.17	0.19
FAS	P25445	FAS	1.67	0.85	0.22
F11R	Q9Y624	JAM-A	1.47	0.69	0.22
LTBR	P36941	LTBR	1.35	0.51	0.22
EPCAM	P16422	Ep-CAM	1.32	0.44	0.22
LGALS3	P17931	GAL-3	1.30	0.49	0.22
EPHA2	P29317	EPHA2	1.20	0.29	0.22
CCL5	P13501	CCL5	1.18	0.27	0.22
MET	P08581	MET	1.15	0.28	0.22
CCL15	Q16663	CCL15	0.92	0.11	0.22
PLAUR	Q03405	U-PAR	1.11	0.17	0.22
ANPEP	P15144	AP-N	1.37	0.63	0.25
CDKN1A	P38936	CDKN1A	1.26	0.41	0.25
IGF1R	P08069	IGF1R	1.19	0.26	0.25
GPC1	P35052	GPC1	1.16	0.22	0.25
FOLR3	P41439	FR-gamma	0.91	0.13	0.25
TNFRSF14	Q92956	TNFRSF14	0.96	0.13	0.25
SCAMP3	O14828	SCAMP3	1.45	0.69	0.31
CD40	P25942	CD40	1.30	0.69	0.31
CSTB	P04080	CSTB	1.25	0.49	0.31
CXCL8	P10145	IL8	1.21	0.26	0.31

CCL20	P78556	CCL20	1.18	0.26	0.31
ST6GAL1	P15907	ST6GAL1	1.17	0.35	0.31
METAP2	P50579	MetAP 2	1.15	0.26	0.31
OSMR	Q99650	OSMR	1.13	0.17	0.31
PDGFA	P04085	PDGF subunit A	0.94	0.15	0.31
CDH5	P33151	CDH5	0.93	0.09	0.31
IGFBP6	P24592	IGFBP6	0.96	0.18	0.31
HSPG2	P98160	PLC	1.06	0.14	0.31
IL18BP	O95998	IL-18BP	1.07	0.12	0.34
TNFRSF9	Q07011	TNFRSF9	1.17	0.30	0.38
EGFR	P00533	EGFR	1.17	0.25	0.38
COMP	P49747	COMP	0.80	0.16	0.44
CTSD	P07339	CTSD	1.24	0.35	0.44
ITGB5	P18084	ITGB5	1.21	0.30	0.44
ESM1	Q9NQ30	ESM-1	1.19	0.28	0.44
CD163	Q86VB7	CD163	1.15	0.35	0.44
IFNGR1	P15260	IFN-gamma-R1	1.14	0.30	0.44
CCL14	Q16627	CCL14	1.11	0.29	0.44
IL6R	P08887	IL-6RA	1.11	0.20	0.44
CD59	P13987	CD59	0.95	0.15	0.44
TIMP1	P01033	TIMP1	0.97	0.07	0.44
TGFBI	Q15582	TGFBI	1.02	0.06	0.44
NOTCH3	Q9UM47	Notch 3	1.15	0.37	0.50
TNFRSF19	Q9NS68	TNFRSF19	0.94	0.23	0.50
AXL	P30530	AXL	1.03	0.19	0.56
PECAM1	P16284	PECAM-1	1.22	0.51	0.56
TFRC	P02786	TR	1.26	0.48	0.56
TLR3	O15455	TLR3	1.17	0.30	0.56
LGALS1	P09382	GAL-1	1.12	0.23	0.56
CD93	Q9NPY3	CD93	1.10	0.22	0.56
TFPI	P10646	TFPI	1.08	0.16	0.56
ALCAM	Q13740	ALCAM	1.05	0.19	0.56
SOD1	P00441	SOD1	1.01	0.06	0.56
IL7R	P16871	IL7R	1.00	0.35	0.56
ADA	P00813	ADA	1.03	0.28	0.59
CASP8	Q14790	CASP-8	1.24	0.51	0.63
PDGFB	P01127	PDGF subunit B	1.06	0.14	0.63
TIMP4	Q99727	TIMP4	1.05	0.13	0.63
PCSK9	Q8NBP7	PCSK9	0.97	0.11	0.63
PCOLCE	Q15113	PCOLCE	1.04	0.09	0.63
TEK	Q02763	TIE2	1.02	0.24	0.63
NT5E	P21589	5'-NT	0.97	1.09	0.66
CASP3	P42574	CASP-3	1.20	0.40	0.69
BLMH	Q13867	BLM hydrolase	1.11	0.31	0.69
IGFBP2	P18065	IGFBP-2	1.08	0.15	0.69
GRN	P28799	GRN	1.08	0.23	0.69

CCL7	P80098	MCP-3	0.98	0.20	0.69
TNFRSF12A	Q9NP84	TNFRSF12A	1.03	0.12	0.69
CCN1	O00622	CYR61	1.01	0.10	0.69
PGF	P49763	PGF	1.00	0.23	0.69
ANXA1	P04083	ANXA1	1.10		0.72
LYN	P07948	LYN	1.02	0.14	0.75
COL18A1	P39060	COL18A1	1.08	0.27	0.84
EFEMP1	Q12805	EFEMP1	1.07	0.20	0.84
CSF1	P09603	CSF-1	1.06	0.28	0.84
S100A11	P31949	S100A11	1.06	0.34	0.84
CXCL1	P09341	CXCL1	1.05	0.23	0.84
IGFBP7	Q16270	IGFBP-7	1.01	0.15	0.84
SERPINE1	P05121	PAI	1.00	0.11	0.84
TCN2	P20062	TCN2	1.01	0.18	0.84
MMP9	P14780	MMP-9	1.05	0.16	0.88
VASN	Q6EMK4	VASN	1.08	0.24	0.91
SERPINA5	P05154	SERPINA5	1.06	0.20	1.00
MMP7	P09237	MMP7	1.06	0.35	1.00
FCRLB	Q6BAA4	FCRLB	0.98	0.12	1.00
TIE1	P35590	TIE1	1.03	0.15	1.00
EPHB4	P54760	EPHB4	1.03	0.19	1.00
IL6	P05231	IL6	1.02	0.21	1.00
CST3	P01034	CST3	1.01	0.06	1.00

Supplemental Table S8. Description of the Wingate test cohort. Muscle SATellite cell study (MSAT)					
	N	**Minimum**	**Maximum**	**Mean**	**SD**
Age (yrs)	39	21	54	36	8
Body weight (kg^{BW})	39	70	97	79	6
BMI (kg^{BW} / m^2)	39	19	31	24	3
VO_{2peak} (ml / kg^{BW} / min)	39	31	70	52	8
Peak power (W / kg^{BW})	39	11	16	13	1
Average power (W / kg^{BW})	39	8	10	9	1
Type I (%)	35	40	81	62	10
Type II (%)	35	19	60	38	10
Capillary Density (nr / fiber)	N/A	N/A	N/A	N/A	N/A
Note: Type II fiber types were not separated and are given as Type II = Type IIa + Type IIx					

Supplemental Table S9. Description of the Malmö Exercise Intervention (MEI) cohort					
	N	**Minimum**	**Maximum**	**Mean**	**SD**
Age (yrs)	46	30	46	38	4
Body weight (kg^{BW})	46	64	129	91	13
BMI (kg^{BW} / m^2)	46	23	35	28	3
Waist-to-hip ratio	46	0.78	1.03	0.93	0.05
VO_{2peak} (ml / kg^{BW} per min)	46	21	44	32	5
Type I (%)	46	7	73	40	13
Type IIa (%)	43	7	48	28	10
Type IIX (%)	43	8	64	33	14

Supplemental Table S10. Description of the muscle injury cohort of Japanese athletes			
	Muscle injury N = 140	**No muscle injury N = 389**	***P*-value**
Age (yrs)	20.3 ± 1.8	20.2 ± 1.9	0.67 [a]
Body weight (kg^{BW})	68.8 ± 10.2	68.2 ± 10.0	0.58 [a]
BMI (kg^{BW} / m^2)	22.7 ± 2.7	22.6 ± 2.7	0.61 [a]
Competitive level			0.48 [b]
International, n (%)	14 (10.0)	45 (11.6)	
National, n (%)	77 (55.0)	192 (49.4)	
Regional, n (%)	27 (19.3)	97 (24.9)	
Others, n (%)	22 (15.7)	55 (14.1)	
Main Sport			0.0001 [b]
Track & field, n (%)	28 (20.0)	139 (35.7)	
Soccer, n (%)	55 (39.3)	157 (40.4)	
Others, n (%)	57 (40.7)	93 (23.9)	
Playing years in main sport (yrs)	10.8 ± 3.9	11.0 ± 3.9	0.55 [a]

Values are presented as the means ± SD unless noted otherwise. [a] P value by the unpaired t-test. [b] P value by the $\chi 2$ test.

Supplemental Table S11. Incidence of non-contact skeletal muscle injuries in a cohort of Japanese athletes stratified by the alternative muscle eQTL (rs11547779). The T-allele is the *RAB3GAP2* low-expressing allele and is associated with increased risk of skeletal muscle injury.

	Skeletal muscle injury, n (%)	**No skeletal muscle injury, n (%)**
CC	111 (79.3)	343 (88.2)
CT	28 (20.0)	45 (11.6)
TT	1 (0.7)	1 (0.3)